In vivo characterization of histone modifications in *Drosophila melanogaster*

Dissertation

to obtain the academic degree

Doctor rerum naturalium (Dr. rer. nat.)

submitted to the Department of Biology, Chemistry and Pharmacy

of Freie Universität Berlin

by

Katharina Kawall

Berlin 2016

Erstgutachter: Prof. Dr. S. Sigrist

Zweitgutachter: Prof. Dr. A. Zychlinsky

Tag der Disputation: 12.9.2016

We are the music makers,
And we are the dreamers of dreams,
Wandering by lone sea-breakers,
And sitting by desolate streams;
World-losers and world-forsakers,
On whom the pale moon gleams:
Yet we are the movers and shakers
Of the world for ever, it seems.

James O' Shaughnessy

Index

Zusammenfassung

Das Ziel dieser Arbeit war es epigenetische Histonmodifikationen, die an der Regulation zellulärer Differenzierung beteiligt sind, zu identifizieren und zu charakterisieren. Dafür nutzte ich *Drosophila melanogaster* als Modellsystem, da es sich hierfür hervorragend mit zahlreichen Stammzellsystemen wie zum Beispiel der Keimbahnstammzellen der Ovare eignet. Zur Identifizierung von Histonmodifikationen, die in Keimbahnstammzellen angereichert sind, wurden Antikörperfärbungen durchgeführt, die zeigten, dass die Modifikationen von Histon H3, H3K27me3 und H3T11Ph, Kandidaten mit einer potentiellen Funktion in Keimbahnstammzellen sind. Ich konnte zeigen dass der Methyltransferase Komplex namens Polycomb Repressive Complex 2 (PRC2), der für die Trimethylierung von H3K27 verantwortlich ist, notwendig für den Stammzellerhalt von Keimbahn- und somatischen Stammzellen im Ovar von *D. melanogaster* ist. Interessanterweise ist die Phosphorylierung von H3T11 auch abhängig von der enzymatischen Aktivität der PRC2 Untereinheit Enhancer of zeste (E(z)), aber nicht von anderen Untereinheiten des PRC2 Komplexes oder der Modifikation H3K27me3. Die Phosphorylierung H3T11 ist daher von einer bislang unbekannten Funktion von E(z) abhängig. Um die Bedeutung von H3T11ph *in vivo* zu charakterisieren, stellte ich Fliegen her, die mutant für H3T11 (H3T11A) sind. Diese Tiere sterben während der Embryogenese, weswegen ich genetische Mosaike in somatischen Zellen des Ovars und in Flügelimaginalscheiben analysierte. Die H3T11A Mutation alleine war nicht ausreichend, um das H3T11ph Signal in diesen Zellen zu entfernen. Ein signifikanter Anteil der H3T11ph findet auf dem Histonvariant H3.3 statt. Das steht im Kontrast zur H3K27 Trimethylierung, welche exklusiv auf dem kanonischen H3 zu finden ist. Das Entfernen von H3T11ph sowohl vom kanonischen H3 als auch vom varianten Histon H3.3, führte zu einem Proliferationsdefekt und einem erhöhten Level an H3K27me3. Genomweite Analysen von H3T11ph zeigten, dass H3T11ph an Grenzen von H3K27me3 Chromatin Domänen stark angereichert ist und dass diese Stellen mit Insulatorproteinen überlappen. Die H3T11 Phosphorylierung könnte daher dafür nötig sein, die Ausbreitung von H3K27me3 über Chromatinregionen durch einen negativen Feedback Mechanismus der H3K27 Methyltransferase E(z) zu limitieren.

Summary

The aim of this study was to identify and characterize ‘epigenetic’ histone modifications that contribute to the regulation of cellular differentiation. In order to address this aim I used *Drosophila melanogaster* as a model system as it provides extensively characterized stem cell systems such as germline stem cells (GSCs) of the ovary. Screening for histone modifications that are enriched in GSCs, identified two modifications of histone H3, methylation at lysine 27 (H3K27me3) and phosphorylation at threonine 11 (H3T11ph), as canidates with a potential function in GSCs. I could then show that the methyl transferase complex that is resposible for H3K27 trimethylation, the Polycomb Repressive Complex 2 (PRC2), is necessary for the maintenance of germline and somatic stem cells in the ovary of *D. melanogaster*. Interestingly, the phosphorylation of H3T11 was also found to be dependent on the enzymatic activity of the PRC2 methyltransferase subunit Enhancer of zeste (E(z)) but not on the other subunits of the PRC2 complex or the modification H3K27me3. Hence, the phosphorylation of H3T11 is dependent on a previously not anticipated function of E(z) independent of the PRC2 complex. In order to further characterize the relevance of H3T11 phosphorylation *in vivo* I generated flies that are mutant for H3T11 (H3T11A). These individuals die during embryogenesis, therefore I analysed genetic mosaics in somatic cells of the ovary and wing imaginal disc cells. I found that introducing the H3T11A mutation in the canonical histone H3 alone was not sufficient to eliminate the H3T11ph signal from cells and that a significant portion of the H3T11 phosphorylation infact takes place on the closely related variant histone H3.3. This is in striking contrast to the methylation of H3K27, which is almost exclusively found on the canonical histone H3. Abolishing H3T11 phosphorylation from both, the canonical and the variant histone led to a significant proliferation defect and elevated levels of H3K27 methylation. Genome wide analysis of the H3T11ph modification revealed a peak like enrichment of H3T11ph at boundaries of chromatin domains that are enriched for H3K27me3 and a significant overlap of these peaks with sites that direct the assembly of chromatin insulator elements. H3T11 phosphorylation might therefore be required to limit the spread of the H3K27me3 modification across chromatin by a negative feedback mechanism involving the H3K27 methyltransferase E(z).

1 Introduction

A central aspect of multicellular development is that cells become at some point determined to adopt a specific cell fate. The developmental decision that allows cells to become a certain part of the body is orchestrated by various levels of regulation. Epigenetics is one major regulatory mechanism, which refers to covalent modifications of DNA, proteins and RNA, thereby regulating gene expression (Waddington, 2012). These modifications do not change the underlying DNA sequence but they affect how cells „read“ genes and thereby decide which cell type they become. In my work I focused on the characterization of covalent histone modifications in different cell types of the fruit fly, *Drosophila melanogaster* (*D. melanogaster*). The main experimental system in my work was the germline of *D. melanogaster* in which I investigated the crosstalk of epigenetic regulators and modifications that control the transition between undifferentiated and differentiated cell types.

1.1 Function of canonical histones

The genetic information of an eukaryotic cell is packaged as chromatin into the cell nucleus. Chromatin in its most basic form is composed of DNA and histone proteins. The repeating structural (and functional) unit of chromatin is the nucleosome, which contains eight histone proteins and about 146 base pairs (bp) of DNA. Histones are a family of small, positively charged proteins: H1, H2A, H2B, H3, and H4 (Kornberg, 1974; Luger, Rechsteiner, Flaus, Waye, & Richmond, 1997). DNA is negatively charged due to the phosphate groups in its phosphate-sugar backbone, therefore histones bind DNA tightly. Two of each of the histones H2A, H2B, H3, and H4 come together to form a histone octamer, around which DNA is wraped in approximately two turns (Van Holde, Sahasrabuddhe, & Shaw, 1974). Multiple nucleosomes form in a linear fashion along the DNA molecule. This produces the so-called 10 nm fiber, which is traditionally described, based on its appearance, as “beads on a string“ (Olins & Olins, 2003). Nucleosomes are connected with each other via DNA segments of variable length which are termed linker DNA (Finch & Klug, 1976; Ramakrishnan, Finch, Graziano, Lee, & Sweet, 1993). Histone H1 is associated both with linker DNA and with nucleosomes (Simpson, 1978). This interaction is necessary for higher order folding of the nucleosomal chain into the 30

nm fiber establishing the second structural packaging unit of chromatin (Thoma, Koller, & Klug, 1979; Zhou, Gerchman, Ramakrishnan, Travers, & Muyldermans, 1998). It still remains to be shown how the 30 nm fiber is further compacted. Some models predict that the 30 nm fiber exists as loops which can be further compacted to finally generate the structure of a chromosome (Felsenfeld & Groudine, 2003). The extent of chromatin condensation varies during the cell cycle. When eukaryotic cells divide, genomic information must be equally partitioned into both daughter cells. To accomplish this, the chromatin becomes highly compacted into metaphase chromosomes (G. Li, Sudlow, & Belmont, 1998). Once a cell has divided its chromosomes uncoil again. During DNA replication in S phase of the cell cycle new nucleosomes are assembled to package the newly synthesized DNA into chromatin. At the beginning of S phase canonical histones are produced in large quantities (Heintz, Sive, & Roeder, 1983; Plumb, Stein, & Stein, 1983; Robbins & Borun, 1967). After S phase excessive histone molecules and histone mRNAs are degraded as a surplus of canonical histones can be toxic for the cell (Gunjan & Verreault, 2003; Kaygun & Marzluff, 2005). Beside their function in compaction of DNA, histones also have a key function in the regulation of various processes like gene transcription or DNA repair.

1.2 Posttranslational modifications of histones

Histones are proteins that undergo multiple types of posttranslational modifications (PTMs) to regulate chromatin condensation, DNA accessibility and bona fide gene expression. The amino acids of the N- and C- terminal tails of histones, which protrude from the surface of the nucleosome, are the main targets for modifications (Kouzarides, 2007). These modifications include methylation, acetylation, phosphorylation, ubiquitylation, sumoylation, prolin isomerization, ADP ribosylation and deimination (Bannister & Kouzarides, 2011). Furthermore, lysine residues can be mono-, di- and tri-methylated and arginine residues can be mono- and di-methylated (Kouzarides, 2007). Typically, a particular histone modification is abbreviated by the histone name, the type and the position of the residue followed by the modification and the quantity of the modification added to the residue. For example, H3K4me3 indicates that there are three methyl groups attached to the lysine at position four in the histone tail of histone H3. Histone modifications exert their effects via two basic

mechanisms. The first one involves the modification directly influencing the overall structure of chromatin. Histone modifications can thereby disrupt or weaken the contacts between nucleosomes in order to unfold higher order chromatin structure (Bannister & Kouzarides, 2011). Histone acetylation for example reduces the positive charge of histones leading to a disruption of the electrostatic interactions between histones and DNA. This leads to a less compacted chromatin structure which facilitates the access of proteins, for example involved in transcription (Shogren-Knaak et al., 2006). This is consistent with the finding that histone acetylation is frequently enriched in promoters of active genes, where it possibly facilitates binding of transcription factors to the promoter (Z. Wang et al., 2008). The second mechanism by which histone modifications modulate gene transcription involves the recruitment of proteins and protein complexes with specific enzymatic activities to the modification sites. For example, methylation of lysine at position 9 of histone H3 leads to the binding of Heterochromatin Protein 1 (HP1) (Bannister et al., 2001; Lachner, O'Carroll, Rea, Mechtler, & Jenuwein, 2001), which leads subsequently to the condensation of chromatin and the formation of heterochromatin. The combination of various histone modifications and proteins enriched on chromatin is thought to be one of the main determinants in a cell that leads to different cell fate decisions and their maintenance in multicellular organisms.

1.3 Chromatin states

The local chromatin environment, termed chromatin state, depends on the cell cycle stage and the transcriptional state of a particular genomic region. It is critical for the cell to tightly regulate the particular chromatin state at each genomic location. Historically, chromatin was classified into two states (Allis, 2007). Euchromatin refers to transcriptionally active regions of loosely packed chromatin, where the DNA is accessible to sequence specific transcription factors and the basic transcriptional machinery. In contrast, heterochromatin refers to tightly packed domains and is associated with transcriptionally silent regions. In heterochromatin, much of the chromatin exists as dense nucleosome clusters preventing access of the transcription machinery to the DNA. The particular packaging state is highly flexible, such that if the appropriate signals and proteins are present or absent a euchromatic region can turn into heterochromatin or *vice versa*. The broad classification of chromatin states into

euchromatin and heterochromatin can be further separated by the presence of distinct sets of histone modifications and their binding proteins (Filion et al., 2010; Kharchenko et al., 2011). One heterochromatic state is classified by the presence of the histone modification H3K9me2 and its binding protein, HP1, which is prominent in pericentric chromatin regions. Another heterochromatic type of chromatin is characterized by the binding of Polycomb group (PcG) proteins and the presence of the histone modification H3K27me3. In *D. melanogaster* euchromatin is also further subdivided depending on whether it harbors actively transcribed genes or not. Along the sequence of actively transcribed genes, histone modifications further specify transcriptional start sites (TSS) by the precence of H3K4 di- and trimethylation, regions of active transcript elongation by H3K36 and H3K79 methylation, as well as enhancer regions by the presence of H3K27 acetylation and H3K4 monomethylation. (MacAlpine, Gordan, Powell, Hartemink, & MacAlpine, 2010). Thus, the eukaryotic genome is organized into functionally and structurally distinct domains, representing regulatory units for gene expression and chromosome behavior. It is important that boundaries between certain chromatin domains ensure the proper maintenance of these regions by prohibiting unwanted spread of distinct PTMs in flanking domains. DNA sequences that mark the borders between adjacent domains are called insulators or boundary elements, which are required for the maintenance of different chromatin states. Insulators act as a barrier to prevent the spreading of repressive heterochromatin from one domain into euchromatic regions (Sun & Elgin, 1999). Moreover they can also prevent the communication between distant elements such as enhancers to influence gene expression, a function known as enhancer-blocking activity (Capelson & Corces, 2004).

1.4 The histone code hypothesis

Molecular events that define the cellular commitment to various differentiation programs are not yet fully understood. A wide range and combination of chromatin modifications may be used to establish novel patterns of gene expression thereby orchestrating cell fate decisions (Berger, 2007; Margueron & Reinberg, 2010). The discovery that certain modifications are correlated with changes in DNA transcription, and that these modifications occur in a regulated and nonrandom manner led to the hypothesis that histone modifications constitute a distinct “histone code“

(Jenuwein & Allis, 2001; Turner, 2000). The histone code hypothesis states that ”multiple histone modifications, acting in a combinatorial or sequential fashion on one or multiple histone tails, specify unique downstream functions” (Jenuwein & Allis, 2001). With regard to the histone code, histones are not only considered as packing elements to build a particular chromatin structure but rather as signaling molecules. As such, they recruit particular chromatin-modifying enzymes and would trigger a particular downstream event.

1.5 The Polycomb system

Polycomb group (PcG) genes were discovered in *D. melanogaster* as repressors of Hox genes, a set of transcription factors that specify cell identity along the anteroposterior axis of segmented animals (Schuettengruber, Chourrout, Vervoort, Leblanc, & Cavalli, 2007). Polycomb (Pc) and a number of other PcG genes were originally identified because of specific mutant phenotypes that suggested that the products of these genes are needed for repression of multiple Hox genes (Duncan, 1982; Ingham, 1984; Lewis, 1978; Struhl, 1981). Subsequent molecular studies showed that Hox genes are indeed misexpressed in Pc mutant embryos (Beachy, Helfand, & Hogness, 1985; Struhl & Akam, 1985; Wedeen, Harding, & Levine, 1986; White & Wilcox, 1985). Because mutations in several different *D. melanogaster* genes caused the same phenotype as mutations in Pc, this set of Hox gene repressors was named the “Polycomb group” and the phenotype was termed „Polycomb phenotype“ (Casanova, Sanchez-Herrero, & Morata, 1985; Duncan, 1982). PcG proteins act through cis-acting DNA elements called Polycomb response elements (PREs) (Muller & Bienz, 1991; J. Simon, Chiang, Bender, Shimell, & O'Connor, 1993). PREs are recognized by a complex called Pho repressive complex (PhoRC) which is composed of the subunits Pho and dSfmbt. Pho contains a sequence-specific DNA binding activity and dSfmbt contains MBT (malignant brain tumor) repeats which selectively bind to monomethylated or dimethylated H3K9 or H4K20 (Klymenko et al., 2006). The PRE bound PhoRC recruits another complex which is called the Polycomb Repressive Complex 2 (PRC2). The PRC2 is a multimeric complex composed of four subunits: Enhancer of zeste (E(z)), Supressor of zeste 12 (Su(z)12), Extra sex combs (ESC) and Nurf55 (O'Meara & Simon, 2012). This complex functions as a histone methyltransferase (HMTase) that specifically methylates lysine 27 of histone H3

(H3K27) in nucleosomes *in vitro* (Cao & Zhang, 2004a; Czermin et al., 2002). The enzymatically active subunit of this complex is the methyltransferase E(z) which contains a SET domain and thereby catalyzes successive trimethylation of H3K27 (Dillon, Zhang, Trievel, & Cheng, 2005; Joshi et al., 2008; Rea et al., 2000). Su(z)12 contains a VEFS domain and binds to E(z) to promote the complex assembly. Via its N-terminus Su(z)12 also binds to Nurf55. Nurf55 is structurally important for the complex assembly and furthermore binds the N-terminus of histone H3. In case H3K4 is trimethylated the Nurf55 subunit senses this and PRC2 is prevented from binding (Nekrasov, Wild, & Muller, 2005; Tie, Furuyama, Prasad-Sinha, Jane, & Harte, 2001). The subunit ESC was shown to bind already existing H3K27me3 which leads to an allosteric stimulation of the PRC2 and propagation of the H3K27me3 mark (Hansen et al., 2008; Margueron et al., 2009). The exact mechanism of H3K27me3 spreading is still unclear, but it has been suggested that spreading is achieved by local diffusion of PRC2 or by the formation of chromosome loops (Y. B. Schwartz & Pirrotta, 2007; Talbert & Henikoff, 2006). Loss or impairment of any of the three PRC2 subunits E(z), Su(z)12 and ESC leads to a dramatic reduction of the HMTase activity of the PRC2 and thus to a reduction of H3K27me3 (Cao & Zhang, 2004b; Ketel et al., 2005; Nekrasov et al., 2005; Pasini, Bracken, Jensen, Lazzerini Denchi, & Helin, 2004). Su(z)12 and Nurf55 are both essential for nucleosome binding of the PRC2 (Nekrasov et al., 2005). In mammals the PRC2 also has four subunits that are orthologous to the PRC2 components in *D. melanogaster*: Suppressor of zeste 12 homolog (Suz12), Embryonic ectoderm development (Eed, homolog to ESC), Enhancer of zeste (EZH1/EZH2) and RbAp48 (homolog to Nurf55) (Cao et al., 2002; Kuzmichev, Nishioka, Erdjument-Bromage, Tempst, & Reinberg, 2002). After trimethylation of H3K27 by the PRC2 complex this modification is then bound by the chromo-domain containing protein Polycomb (Pc), a subunit of the Polycomb Repressive Complex 1 (PRC1) (Cao & Zhang, 2004a). In addition to Pc, the PRC1 complex contains the proteins Polyhomeotic (Ph), Posterior sex combs (Psc) and dRing (Saurin, Shao, Erdjument-Bromage, Tempst, & Kingston, 2001). Once bound to H3K27me3, the PRC1 mediates the ubiquitination of H2AK119 (Lagarou et al., 2008; Martin & Zhang, 2005; H. Wang et al., 2004) which leads then to the subsequent compaction of the chromatin and silencing of target genes (Hu et al., 2012).

1.6 Genomic organisation of histone genes in *D. melanogaster*

In all higher eukaryotes canonical histone genes are present in high copy numbers that are often distributed over several chromosomes (Marzluff, Wagner, & Duronio, 2008). For example, in the haploid genome of *Caenorhabditis elegans* (*C.elegans*) approximately 70 histone genes are present (Pettitt, Crombie, Schumperli, & Muller, 2002) and the human genome has 64 histone genes (Marzluff, Gongidi, Woods, Jin, & Maltais, 2002). In many organisms the arrangement of the histone genes seems to be random across the genome as there is no regular gene order. For example, in *C.elegans* the histone genes are distributed along five of six chromosomes without any regular arrangement (Pettitt et al., 2002) and in humans histone genes are clustered at three different loci (Marzluff et al., 2002). The high number of histone genes and their distribution along the genome prevent straightforward functional genetics (Kouzarides, 2007). Genetic analysis has been limited to lower eukaryotes, such as the yeast *Saccharomyces cerevisiae* (*S. cerevisiae*), in which histone genes are encoded by tandem repeats (Marzluff et al., 2008). Systematic mutagenesis of histone genes in *S. cerevisiae* has identified histone residues essential for viability and for response to environmental challenges (Nakanishi et al., 2008). However, there are likely to be additional roles for histone residues in multicellular organisms, which exhibit a more diverse regulation of genome activity across different cell types and developmental stages. *D. melanogaster* is an ideal model organism in which to investigate histone functions as there are many advanced genetic techniques available and the development of the fly is well characterized. Most importantly, in *D. melanogaster* all canonical histone genes are clustered in a single chromosomal locus of chromosome 2L, containing 23 copies of each histone gene (Gunesdogan, Jackle, & Herzig, 2010, 2014). The genes of the canonical histones are arranged in gene clusters. One gene cluster, termed hereafter gene unit (GU), contains one copy of the genes for histone H1, H2B, H2A, H3 and H4 each. A deletion of the whole histone complex was established defining a histone null mutation (His^C) in *D. melanogaster* (Gunesdogan et al., 2010). Homozygous His^C mutant embryos die during embryogenesis as the maternally derived histones are only sufficient to drive the first 14 embryonic cell cycles. In the absence of zygotic histone expression, embryos fail to complete cell cycle 15 and die. This lethality can be rescued in a dose-dependent manner

by introducing wildtype histone gene unit (His-GU) transgenes. Twelve transgenes resulted in a complete rescue as viable and fertile adults are able to develop. This experimental system can be used to specifically generate transgenic flies that carry histones with altered modification sites and address the relevance of this site for the development and homeostasis of a multicellular organism. This system was already applied in many publications using His-GUs carrying a H3K4R, H3K27R and H3S28A mutation respectively (Gunesdogan et al., 2014; Hodl & Basler, 2012; Pengelly, Copur, Jackle, Herzig, & Muller, 2013; Yung, Stuetzer, Fischle, Martinez, & Cavalli, 2015). Thus this system is a very useful tool to decipher the „histone code“, to investigate the crosstalk between various histone modifications and to estimate the impact a distinct histone modification has on the development of a multicellular organism.

1.7 Histone variants

Adding another layer of complexity to chromatin regulation, for almost all histones there are variant proteins encoded in the genomes of multicelluar eukaryotes. These histone variants take over specific regulatory functions, are expressed outside of S-phase and can be incorporated into chromatin to replace canonical histones (Henikoff, Furuyama, & Ahmad, 2004; Sittman, Graves, & Marzluff, 1983; Wu & Bonner, 1985). The genes for histone variants normally exist as single copies in the genome (Sarma & Reinberg, 2005). The amino acid sequence of some histone variants are almost identical to their canonical counterparts, whereas other show bigger differences in their sequences (Malik & Henikoff, 2003). Histone variants exist in all higher eukaryotes. Variants for histone H1, H2A and H3 are well characterized and each of them have different functions (Kamakaka & Biggins, 2005). A histone H3 variant in *D. melanogaster*, Centromeric Histone H3 (CenH3) in mammals and Centromere identifier (Cid), becomes incorporated into nucleosomes located at centromeric regions of chromosomes (Bischoff, Maier, Tilz, & Ponstingl, 1990; Palmer, O'Day, Trong, Charbonneau, & Margolis, 1991). Another histone H3 variant, H3.3, differs from canonical H3 in only four amino acid residues (Akhmanova et al., 1995; Fretzin, Allan, van Daal, & Elgin, 1991). H3.3 is found primarily in euchromatin and is enriched for active histone modifications such as H3K4me2/3, H3K9Ac, and H3K14Ac (Chow et al., 2005; McKittrick, Gafken, Ahmad, & Henikoff, 2004). H3.3 is thought to be incorporated into chromatin after transcription mediated nucleosome displacement

via its chaperone HIRA (Tagami, Ray-Gallet, Almouzni, & Nakatani, 2004). Nevertheless, H3.3 is not exclusively coupled to transcription, nor does it appear to be essential for normal transcription since transcriptional outputs from flies lacking H3.3 were indistinguishable from wild-type animals (Hodl & Basler, 2009). When H3.3 is mutated in *D. melanogaster*, canonical H3 expression is up-regulated, suggesting that canonical H3 is capable of fulfilling the role of H3.3 in transcription (Sakai, Schwartz, Goldstein, & Ahmad, 2009). However, H3.3 plays a key role in the germline as flies lacking H3.3 are sterile (Hodl & Basler, 2009). This sterility cannot be rescued by canonical H3 or a H3.3 mutant where lysine four is mutated into alanine.

1.8 The female germline of *D. melanogaster* as an experimental system

The production of functional gametes is essential for the maintenance of all sexually reproducing metazoan species. The oogenesis of *D. melanogaster* as a model system has been widely used to investigate many aspects of developmental and cellular biology. Each wildtype female fly has a pair of ovaries which is composed of 16 to 20 ovarioles each. Each ovariole contains a chain of maturing egg chambers in different developmental stages (Figure 1 A). New egg chambers are generated at the anterior tip of the ovariole in a region called the germarium. The germarium can be further divided into four regions according to the developmental stage of the germline cells, which can be either still dividing (region 1), early postmitotic (region 2A), stretched out over the entire width of the germarium (region 2B), or encapsulated by somatic cells (region 3). A germarium is schematically shown in figure 1 B. In region 1 of the germarium, the germline stem cells (GSCs) are situated. The germline of female fruit flies is one of the best studied stem cell systems (Fuller & Spradling, 2007). The GSCs are situated right next to their stem cell niche consisting of so called cap cells (CCs) and a group of approximately 6 to 10 disc shaped cells termed the terminal filament cells (TFs). GSCs divide asymmetrically to give rise to a self-renewed GSC which remains attached to the neighboring niche and a cystoblast that is displaced to the posterior. The cystoblast divides four more times with incomplete cytokinesis to form a 16 cell cyst. The cells in these cysts are interconnected by cytoplasmic bridges called ring canals. The fusome is a large cytoplasmic structure that connects individual cells in a cyst through these ring canals (Lin, Yue, & Spradling, 1994). One

of the 16 cells later becomes the oocyte and enters meiosis. The other 15 cells become nurse cells. The nurse cells become polyploid due to endoreplication and produce huge amounts of ribosomes, proteins and mRNAs to provide for the oocyte. These nutrients are transported to the oocyte through the ring canals.

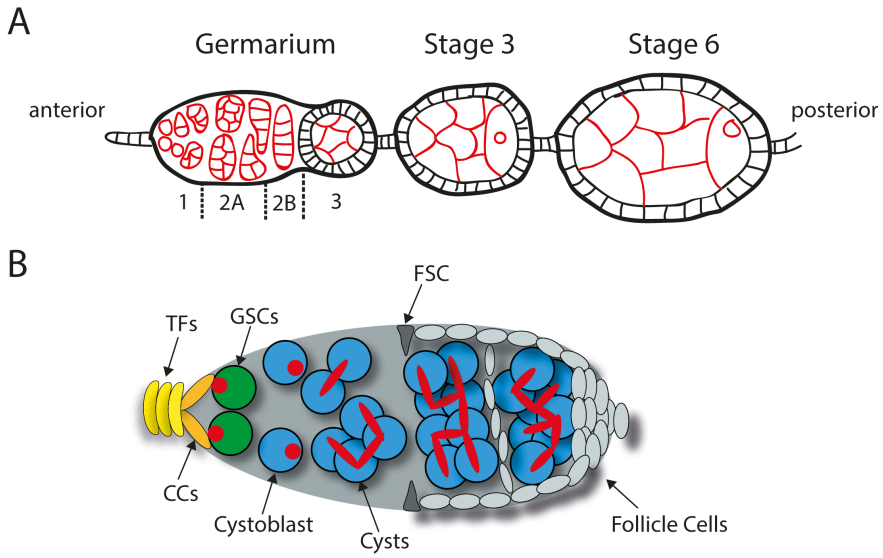

Figure 1: Schematic diagram of the germline of *D. melanogaster*.
(A) Each ovariole is composed of progressively more mature egg chambers towards the posterior end. An egg chamber contains 16 germline cells surrounded by a monolayer of follicle cells. The egg chambers are generated at the anterior part of the ovariole, the germarium. The germarium is sub-divided into four morphological regions along the anterior-posterior axis. (B) The germline stem cells (GSCs) are located at the most anterior part of the germarium in region 1 (left, green cells). The niche of the GSCs is composed of cap cells (CCs, orange cells) and terminal filament cells (TFs, yellow cells). GSCs divide and give rise to a cystoblast and a remaining GSC. The cystoblast divides four times to produce a 16 cell cyst in which the cells are connected by ring canals. At the border of region 2A/2B the follicle stem cells (FSCs) are located. They divide and their progeny start to surround the germline cells.

So called escort cells reside adjacent to the cap cells and line the anterior portion of the germarium. These cells act to accompany the germ cells during the earliest stages of their differentiation, after which developing germline cysts are enveloped by somatic follicle cells (Kirilly & Xie, 2007). At the junction between region 2A and region 2B cysts are forced into a single row as they encounter the two follicle stem cells (FSCs) and begin to acquire a follicular layer. Follicle cells that are derived from both FSCs in the germarium then encapsulate the cysts of germline cells (Nystul & Spradling, 2010). Under the influence of the continued somatic cell growth the cysts

round up, enter region 3 and bud from the germarium as a new egg chamber that remains connected to other egg chambers by short cellular stalks.

One central aspect for the function of the germline is the maintenance and self-renewal of the GSCs. For continuous egg production it is necessary that the GSCs proliferate and continuously generate cystoblasts. The ability of GSCs to keep an undifferentiated identity and to produce differentiating daughter cells is influenced by many extrinsic and intrinsic factors. The cells of the niche produce diffusible factors, which are necessary for the maintenance of the GSCs. One example is the BMP pathway which is one of the best studied pathways for controlling GSC function which is both necessary and sufficient for GSC self-renewal and proliferation (Song et al., 2004; Xie & Spradling, 1998). GSCs themselves express different classes of intrinsic factors including transcription factors, chromatin remodeling factors, translation regulators and miRNAs, which control self-renewal by strengthening interactions with the niche and repressing various differentiation pathways (Fuller & Spradling, 2007). The germarium is an excellent experimental system as the direct proximity of different cell types in this tissue makes it easy to investigate the composition and interplay of epigenetic regulators and histone modifications. In this work the female germline was used as a model system to characterize histone modifications, their role in the regulation of cellular differentiation and the interplay between histone modifications and epigenetic regulators.

2 Material

2.1 Chemicals and reagents

Acetic acid (≥ 99.9%)	Sigma-Aldrich, St. Louis, MO, USA
Agarose Biozym LE	Biozym Scientific GmbH, Hessisch Oldendorf, Germany
Ammonium acetate (≥ 98%)	Sigma-Aldrich, St. Louis, MO, USA
Antarctic Phosphatase [5 U/µl]	New England Biolabs Inc., Ipswich, USA
AMPure XP beads	Beckman Coulter GmbH, Krefeld, Germany
β-mercaptoethanol	Sigma-Aldrich, St. Louis, MO, USA
Bromphenol Blue	Sigma-Aldrich, St. Louis, MO, USA
dNTP Mix	Thermo Fisher Scientific Inc., Waltham, USA
DAPI	Sigma-Aldrich, St. Louis, MO, USA
Dynabeads Protein G	Thermo Fisher Scientific Inc., Waltham, USA
EDTA [0.5M], pH 8	Thermo Fisher Scientific Inc., Waltham, USA
Ethanol p.a.	Merck, Darmstadt, Germany
Ethidium bromide [10 mg/ml]	Sigma-Aldrich, St. Louis, MO, USA
Fast SYBR green master mix	Thermo Fisher Scientific Inc., Waltham, USA
Fetal bovine serum	Thermo Fisher Scientific Inc., Waltham, USA
Formaldehyde solution (37% w/w)	Sigma-Aldrich, St. Louis, MO, USA
Glycogen RNA grade	Thermo Fisher Scientific Inc., Waltham, USA
Glycerol (≥ 99.5%)	Roth, Karlsruhe, Germany
Glycin	Sigma-Aldrich, St. Louis, MO, USA
HCl (25%)	Roth, Karlsruhe, Germany
HyperLadder™ 100bp	Bioline, London, GB
HyperLadder™ 200bp	Bioline, London, GB
Isopropanol	Sigma-Aldrich, St. Louis, MO, USA
$MgSO_4$	Sigma-Aldrich, St. Louis, MO, USA
NaCl	Fluka Analytical (Sigma-Aldrich), St. Louis, MO, USA
$NaHCO_3$	Sigma-Aldrich, St. Louis, MO, USA
NaOH (≥ 98%, pellets)	Sigma-Aldrich, St. Louis, MO, USA

NEBNext® ChIP-Seq Library Prep Master Mix Set for Illumina®	New England Biolabs Inc., Ipswich, MA, USA
6x Orange DNA Loading Dye	Thermo Fisher Scientific Inc., Waltham, USA
One Shot TOP10 Electrocomp *E. coli*	Invitrogen, Karlsruhe, Germany
Paraformaldehyde	Sigma-Aldrich, St. Louis, USA
Phenol/Chloroform/Isoamyl alcohol	Roth, Karlsruhe, Germany
Phenylmethanesulfonyl fluoride	Sigma-Aldrich, St. Louis, MO, USA
Phosphatase inhibitor tablets	Roche Diagnostics, Basel, Switzerland
Phusion HF DNA Polymerase	New England Biolabs Inc., Ipswich, USA
ProLong Gold Antifade Mountant	Thermo Fisher Scientific Inc., Waltham, U.S
Propionic acid	Roth, Karlsruhe, Germany
Protease inhibitor tablets Complete	Roche Diagnostics, Basel, Switzerland
Proteinase K [20 mg/ml]	Thermo Fisher Scientific Inc., Waltham, USA
Precision Plus Protein Standard	BioRad Laboratories, Munich
Restriction endonucleases	New England Biolabs Inc., Ipswich, USA
RNase A	Sigma-Aldrich, St. Louis, USA
DNase- and protease-free	Thermo Fisher Scientific Inc., Waltham, USA
SDS	Sigma-Aldrich, St. Louis, MO, USA
Drosophila Schneider's media	Invitrogen, Karlsruhe, Germany
Shrimp Alkaline Phosphatase	New England Biolabs Inc., Ipswich, MA, USA
Smart ladder (100-1000 bp)	Eurogentec, Liège, Belgium
SOC medium	Life Technologies, Darmstadt, Germany
Sodium acetate [3M], pH 5.2	Thermo Fisher Scientific Inc., Waltham, MA, USA
Sodium deoxycholate (≥ 97%)	Sigma-Aldrich, St. Louis, MO, USA
Sucrose (≥ 99.5%)	Sigma-Aldrich, St. Louis, MO, USA
Taq DNA Polymerase	New England Biolabs Inc., Ipswich, MA, USA
T4 DNA-Ligase	New England Biolabs Inc., Ipswich, MA, USA
Trizma® base (Tris base)	Sigma-Aldrich, St. Louis, MO, USA

2.2 Solutions and buffers

For all listed buffers and solutions water was derived from a Milli-Q® integral water purification system (EMD Millipore Corp., Billerica, MA, USA) and autoclaved at 121°C for sterilization.

LB	0,5% (w/v) NaCl 0.5% (w/v) yeast extract 0.1% (w/v) Glucose pH7
Lysis buffer	20 mM Tris-HCl pH7.5 200 mM NaCl 20 mM EDTA 2% (w/v) SDS
TAE buffer (50x)	0.2 M Tris base 5.7% (v/v) acetic acid 10 mM EDTA, pH 7.4
TE buffer (10x)	100 mM Tris base 10 mM EDTA pH 8.0 (for DNA)
PBS (10x)	137 mM Sodium chloride 2.7 mM Potassium chloride 10 mM Disodium hydrogen phosphate 1.8 mM Potassium dihydrogen phosphate

SDS-PAGE

6x SDS sample buffer:	375 mM Tris base, pH 6.8 6% (w/v) SDS 48% (v/v) glycerol 9% (v/v) β-mercaptoethanol 0.03% (w/v) bromphenol blue
10x SDS running buffer:	250 mM Tris base, pH 8.3 – 8.4 1.92 M glycin 1% (w/v) SDS

Western Blot

Blocking buffer:	10% nonfat dried milk in 1xPBS TBS-Tween (0.5%)
1x Blotting buffer:	48 mM Tris 39 mM glycine 20% methanol
1X TBST :	50 mM Tris.HCl, pH 7.4 150 mM NaCl 0.1% Tween 20.
Harsh stripping buffer:	2 % SDS 62.5mM Tris HCl pH 6.8 100mM ß-mercaptoethanol

Chromatin Immunoprecipitation

ChIP SDS buffer:	100 mM NaCl
	50 mM Tris-HCl, pH 8
	5 mM EDTA pH 8
	0.2% NaN_3
	1% SDS
	3% Triton X-100
ChIP Dilution buffer:	50 mM Tris-HCl, pH 8
	100 mM NaCl
	5 mM EDTA pH 8
	0.2% NaN_3
IP dilution buffer:	160 mM NaCl
	1% Triton X-100
	0.3% Sodium Deoxychelate
RIPA buffer:	140 mM NaCl
	1 mM EDTA
	1% (vol/vol) Triton X-100
	0.1% (wt/vol) SDS
	0.1% (wt/vol) sodium deoxycholate
	10 mM Tris-HCl (pH 8.0)
	Filtered, stored at 4°C
RIPA500:	500 mM NaCl
	1 mM EDTA
	1% (vol/vol) Triton X-100
	0.1% (wt/vol) SDS
	0.1% (wt/vol) sodium deoxycholate
	10 mM Tris-HCl (pH 8.0)
	Filtered, stored at 4°C

LiCl buffer:	250 mM LiCl
	1 mM EDTA
	0.5% (vol/vol) IGEPAL CA-630
	0.5% (wt/vol) sodium deoxycholate
	10 mM Tris-HCl (pH 8.0)
	Filtered, stored at 4°C

2.3 Media and food

Freezing medium for S2R+ cells:	Schneider's Drosophila medium
	20% FCS
	10% DMSO
	sterilize by filtration
	storage at 4°C

Fly food:	25 l
Agar-Agar	125 g
Brewer's yeast	360 g
Grafschafter Goldsaft	440 g
Maize flour	1600 g
Nipagin	100 ml
Propionic acid	125 ml
Soy fluor	200 g
Malt extract	1600 g

2.4 Antibodies

Antigen	Species	IF	WB	Cat.-No.	Reference
Abd-A	Mouse	1:250		FP6.87	DSHB*
alpha-Tubulin	Rabbit		1:1000	ab52866	Abcam
Antp	Mouse	1:250		4C3	DSHB*
bam	Mouse	1:400			DSHB*
Cleaved Caspase-3	Rabbit	1:250		Asp175	Cell Signalling Technology
DE-Cadherin	Rat	1:250		DCAD2	DSHB*
Fasciclin III	Mouse	1:500		7G10	DSHB*
hts	Mouse	1:20		1B1	DSHB*
H3K4me3	Rabbit	1:500		39915	Active motif
H3K9Ac	Rabbit	1:500		39137	Active motif
H3K9me3	Rabbit	1:500		ab8898	Abcam
H3S10Ph	Rabbit	1:500		04-817	Millipore
H3T11ph	Rabbit	1:500	1:1000	ab5168	Abcam
Vasa	Rabbit	1:500			Dr. Alf Herzig**
H3K14Ac	Rabbit	1:500		ab52946	Abcam
H3K18Ac	Rabbit	1:500		ab1191	Abcam
H3K23Ac	Rabbit	1:500		07-355	Millipore
H3K27me3	Mouse	1:500	1:1000	39535	Active motif
H3K27ac	Rabbit	1:500		39135	Active motif
H3S28Ph	Rabbit	1:500		07-145	Millipore
H3K36me3	Rabbit	1:500		ab9050	Abcam
H3K36Ac	Rabbit	1:500		39379	Active motif
H3K79me	Rabbit	1:500		ab2886	Abcam
H3K79me3	Rabbit	1:500		ab2621	Abcam
H4K5Ac	Rabbit	1:500		07-327	Millipore
H4K8Ac	Rabbit	1:500		ab15823	Abcam
H4K12Ac	Rabbit	1:500		39165	Active motif
H4K16Ac	Rabbit	1:500		07-329	Millipore
H4K20me	Rabbit	1:500		ab9051	Abcam
H4K20me3	Rabbit	1:500		ab78517	Abcam

Table 1: Overview of primary antibodies.

IF: Immunofluorescence, WB: Western Blotting

* Developmental Studies Hybridoma Bank, University of Iowa, Iowa, USA (http://dshb.biology.uiowa.edu)

** Max-Planck Institute for Infection Biology, Department of Cellular Microbiology, Charitèplatz 1. 10117 Berlin

Antigen	Host	Dilution	Reference
anti-mouse IgG Alexa Fluor 488	goat	1:500	Invitrogen
anti-mouse IgG Alexa Fluor 568	goat	1:500	Invitrogen
anti-mouse IgG Alexa Fluor 633	goat	1:500	Invitrogen
anti-rabbit IgG Alexa Fluor 488	goat	1:500	Invitrogen
anti-rabbit IgG Alexa Fluor 568	goat	1:500	Invitrogen
anti-rabbit IgG Alexa Fluor 633	goat	1:500	Invitrogen
anti-rat IgG Alexa Fluor 488	goat	1:500	Invitrogen
anti-mouse IgG HRP conjugate	goat	1:10000	Pierce
anti-rabbit IgG HRP conjugate	goat	1:10000	Pierce

Table 2: Overview of secondary antibodies.

2.5 Oligonucleotides

Name	Sequence 5'- 3'	Purpose
E(z)_fw	TAATACGACTCACTATAGGGTCTCCAGCGGTTCTTCAGTT	RNAi
E(z)_rev	TAATACGACTCACTATAGGGGTCCTCGATAAGGATGGCAA	RNAi
Su(z)12_fw	TAATACGACTCACTATAGGGGCGAGTCTGTGAGTGTGGAG	RNAi
Su(z)12_rev	TAATACGACTCACTATAGGGAGCTGCTCATTGGATAGCGT	RNAi
Gapdh1_2_fw	ACCGAACTCGTTGTCGTACC	ChIP-seq
Gapdh1_2_rA	CTTCTTCAGCGACACCCATT	ChIP-seq
abd-A_2_fw	CGAATAAGGCCGTGACATTT	ChIP-seq
abd-A_2_rev	AAACAGGAGCTGGGGTTTTT	ChIP-seq
Ubx_2_fA	GCGGCGGCTAGTTCTTCTAC	ChIP-seq
Ubx_2_rev	GCGCAAAAGCATAGGAAAAG	ChIP-seq
Opa-fw	ACCACTCAGCAATCGCAATA	ChIP-seq
Opa_rev	GAGAAAATCTCACAGCGTTGC	ChIP-seq
Gapdh1_fw	ACCGAACTCGTTGTCGTACC	ChIP-seq
Gapdh1_rev	TCAAGGCTAAGGTCGAGGAG	ChIP-seq

Table 3: Overview of Oligonucleotides.

2.6 Plasmids

Name	Purpose	Reference
pENTR221-HisGU	generation of T11A transgenic flies	Ufuk Günesdogan*
pENTRL4R1-HisGU	generation of T11A transgenic flies	Ufuk Günesdogan*
pENTRR2L3-HisGU	generation of T11A transgenic flies	Ufuk Günesdogan*
pDESTphiC31attB-1xGU	generation of T11A transgenic flies	Ufuk Günesdogan*
pDEST-HisGU-H3-T11A	generation of T11A transgenic flies	this work
pENTR221-HisGU-H3-T11A	generation of T11A transgenic flies	this work
pENTRL4R1-HisGU-H3-T11A	generation of T11A transgenic flies	this work
pENTRR2L3-HisGU-H3-T11A	generation of T11A transgenic flies	this work

Table 4: Overview of plasmids.

* Wellcome Trust/Cancer Research UK Gurdon Institute, University of Cambridge, Cambridge, United Kingdom

2.7 *Drosophila melanogaster* stocks

Genotype	Purpose	Reference
w^{1118}	reference stock (wildtype)	Bloomington Stock Center*
w^{1118};P{w^{+mC}=UbiGFP.nls}2LP{$ry^{+t7.2}$=neoFRT}40A/ CyO	His^{C} clones, GFP marker on chr. 2	Bloomington Stock Center*
w*; E(z)731 P{1xFRT.G}2A/TM6C, Sb^{1} Tb^{1}	E(z) null mutation on a FRT2A chromosome (Chr. 3)	(Muller *et al.*, 2002)
w*; b[1] P{$ry^{+t7.2}$=neoFRT}40A	FRT40A site on chromosome 2	Dr. Alf Herzig**
y^{1} w^{1118} P{$ry^{+t7.2}$=70FLP}3F/Dp(1;Y)y^{+}; sna^{Sco}/SM6a	stock carrying an inducible Flipase (FLP) upon heat-shock	Bloomington Stock Center*
w^{1118};P{w^{+mC}=UbiGFP.nls}2LP{$ry^{+t7.2}$=neoFRT}2A	Polycomb clones, GFP marker on chr.3	Bloomington Stock Center*
w*;Su(z)12^{2}P{$w^{+mW.hs}$=FRT(w^{hs})}2A/TM6C, Sb^{1} Tb^{1}	Su(z)12 null mutation on a FRT2A chromosome (Chr.3)	(Birve *et al.*, 2001)
P{$ry^{+t7.2}$=neoFRT}2A	FRT2A site on chromosome 3	Bloomington Stock Center*
P{$ry^{+t7.2}$=hsFLP}1, y^{1} w^{1118}; D^{3}/TM3, Sb^{1}	stock carrying an inducible Flipase (FLP)	Bloomington Stock Center*
w^{1118};Df(2L)His^{C}/CyO;M{3xHisGU.wt}Zh-86Fb, M{3xHisGU.wt}Zh-VK33	complete deletion of the histone locus with 6 His-GUs	Dr. Alf Herzig**
w^{1118};Df(2L)His^{C}/CyO;M{3xHisGU.wt}Zh-86Fb, M{3xHisGU.wt}Zh-68E	complete deletion of the histone locus with 6 His-GUs	Dr. Alf Herzig**
w^{1118};Df(2L)His^{C}/CyO;M{3xHisGU.K27R}Zh-86Fb, M{3xHisGU.K27R}Zh-VK33	complete deletion of the histone locus with 6 His-GUs carrying the K27R mutation	Dr. Alf Herzig**
w^{1118};Df(2L)His^{C}/CyO;M{3xHisGU.T11A}Zh-86Fb, M{3xHisGU.T11A}Zh-VK33	complete deletion of the histone locus with 6 His-GUs carrying the T11A mutation	this work
$His3.3B^{-}$hsp70-flp/$His3.3B^{-}$hsp70-flp;$His3.3A^{-}$ Df(2L)His^{C} FRT40A/SM6a	H3.3 deletion and His^{C} deletion on a FRT40A chromosome	Dr. Alf Herzig**
w^{1118};+/+;M{3xHisGU.T11A}Zh-86Fb, M{3xHisGU.T11A}Zh-VK33	6 His-GUs carrying the T11A mutation	this work
w^{1118};+/+;M{3xHisGU.K27R}Zh-86Fb, M{3xHisGU.K27R}Zh-VK33	6 His-GUs carrying the K27R mutation	Dr. Alf Herzig**
w^{1118};+/+;M{3xHisGU.K27R}Zh-86Fb, M{3xHisGU.K27R}Zh-VK33	6 His-GUs	Dr. Alf Herzig**
$His3.3B^{-}$hsp70-flp/$His3.3B^{-}$hsp70-flp;$His3.3A^{-}$ FRT40A/SM6a	stock with the H3.3 deletion carrying an inducible Flipase	Dr. Alf Herzig**

Table 5: Overview of fly stock.
*Bloomington Stock Center, Department of Biology, Indiana University, Bloomington, USA, (http://flystocks.bio.indiana.edu/)
** MPI for Infection Biology, Department of Cellular Microbiology, Charitèplatz 1. 10117 Berlin

2.8 Instruments

Alpha Imager	Protein Simple, San Jose, USA
Bioanalyzer	Agilent Technologies, Santa Clara, USA
BioruptorPlus Sonication System	Diagenode, Seraing, Belgium
CASY cell counter	Roche Diagnostics, Basel, Switzerland
Criterion™ Blotter Biorad	Bio-Rad Laboratories, Hercules, USA
Criterion™ electrophoresis chamber	Bio-Rad Laboratories, Hercules, USA
Dounce tissue grinder 40ml	Sigma-Aldrich, St. Louis, MO, USA
ECL Western Blotting System	GE Healthcare, Glattbrugg, CH
Qubit 2.0 Fluorometer	Thermo Fischer Scientific Inc; Waltham, USA
Microscopes	
Stemi 2000	Zeiss, Jena, Germany
Stereo Discovery.V8	Zeiss, Jena, Germany
TCS SP2 Confocal	Leica, Wetzlar, Germany
TCS SP5 Confocal	Leica, Wetzlar, Germany
TCS SP8 Confocal	Leica, Wetzlar, Germany

2.9 Consumables

Criterion™ TGX™ Precast Gels	BioRad Laboratories, Munich
Hyperfilm ECL	GE Healthcare, Glattbrugg, CH
Hybond-P PVDF Membrane	GE Healthcare, Glattbrugg, CH
µ-Slide 8 Well	iBidi GmbH. Munich
Qubit assay tubes	Life Technologies, Darmstadt

2.10 Kits

Agencourt AMPure XP	Beckman Coulter, Krefeld, Germany
MEGAscript RNAi Kit	Thermo Fischer Scientific Inc; Waltham, USA
MODified Histone Peptide Array	Active Motif, Belgium
MultiSite Gateway Pro	Thermo Fischer Scientific Inc; Waltham, USA
Chip DNA Clean and Concentrator Kit	Zymogen Research Germany
DNA Library Prep Kit for Illumina®	New England Biolabs Inc., Ipswich, USA
High Sensitivity DNA Analysis Kit	Agilent Technologies Inc

QIAprep Spin Miniprep Kit	Qiagen, Hilden, Germany
QIAGEN Plasmid Midi Kit	Qiagen, Hilden, Germany
QIAquick Gel Extraction Kit	Qiagen, Hilden, Germany
Qiaquick PCR purification Kit	Qiagen, Hilden, Germany

2.11 Software

Adobe Illustrator CS6	Adobe Systems, Inc., San Jose, USA
Adobe Photoshop CS6	Adobe Systems, Inc., San Jose, USA
DNASTAR Lasergene	DNASTAR Inc., Madison, USA
2100 Expert Software	Agilent Technologies inc., Santa Clara, USA
Filemaker Pro V11.0	FileMaker Inc., Santa Clara, USA
GraphPad Prism 5	GraphPad Software Inc., La Jolla, USA
ImageJ V1.49m	National Institutes of Health, Bethesda, USA
Leica Application Suite X	Leica Microsystems GmbH, Wetzlar, Ger
NanoDrop 2000/2000c V1.19	Thermo Fischer Scientific Inc; Waltham, USA
SDS V2.4	Thermo Fisher Scientific Inc., Waltham, USA
StepOnePlus Real-Time	Thermo Fisher Scientific Inc., Waltham, USA
ZEN lite 2012	Carl Zeiss Microscopy, Jena

3 Methods

3.1 Molecular cloning

3.1.1 Quantification of nucleic acids

3.1.1.1 NanoDrop Spectrophotometer

The NanoDrop2000 uses the UV-absorbance method based on the natural absorption of light of DNA and RNA molecules at 260 nm and proteins at 280 nm. The higher the DNA or RNA concentrations, the more light is absorbed. It allows a low volume measurement in the concentration range of 2 ng/µl to 15,000 ng/µl for double-stranded DNA. The NanoDrop2000 was calibrated on the control liquid, 1 µl of sample was pipetted on the designated platform, the absorption was measured at 260nm and 280 nm, and the concentration was displayed in ng/µl. The ratio of absorption at 260 nm and 280 nm stated the purity of the tested sample.

3.1.1.2 Qubit Fluorometer

The Qubit Fluorometer can be used to quantify the concentration of DNA, RNA and proteins. The concentration of the target molecule in the sample is reported by a fluorescent dye that emits a signal only when bound to the target. The Qubit dsDNA HS Assay Kit detects concentration ranges from 10 pg/µl to 100 ng/µl. The Qubit working solution was prepared containing HS reagent diluted 1:200 in HS buffer. The two DNA standards (Components A and B) were mixed 1:20 and the samples were mixed 1:100 to a final volume of 200 µl in the working solution, and incubated for 2 min at room temperature. The concentration of the sample was then measured using the Qubit fluorometer.

3.1.2 Restriction enzyme cleavage

Restriction enzymes recognize palindromic sequences in DNA molecules and produce blunt ends or sticky ends (overhang) by cutting the DNA at specific sites. They are used to generate matching sites in vectors and inserts for cloning experiments as well as the examination of positive cloning results. Restriction enzymes were used according to the manufacturer's directions (New England Biolabs).

3.1.3 Dephosphorylation of DNA

The 5'-phospho ends of vectors were cut off using Shrimp Alkaline Phosphatase (SAP) to prevent re-ligation of linearized vectors. After a restriction enzyme cleavage 1 U SAP was added and incubated for 30 min at 37°. The phosphatase was inactivated at 65°C for 20 min.

3.1.4 Ligation of restricted DNA fragments

Ligation reactions are used for the connection of linearized DNA fragments (inserts) with linearized vector molecules. The desired insert and vector were mixed in a molar ratio of 1:5. Usually, 25 ng of the vector were used as a starting point. The corresponding amount of insert was calculated according to the following formula:

$$\frac{Vector\ [ng] \times Insert[kb]}{Vector[kb]} \times molar\ ratio\ of\ \frac{Insert}{Vector} = Insert\ [ng]$$

For the ligation reaction, the amount of insert and vector were added to 2 µl of 10x ligation buffer and 1 µl of T4 DNA ligase in a total volume of 20 µl. The reaction was performed over night at 18°C.

3.1.5 Transformation of electrocompetent *E.coli* cells

Electrocompetent Top10 cells were generated based on standard protocols (Sambrook and Russel, 2001). For the transformation 50 µl of E.coli Top10 cells were mixed with 1-2 µl of plasmid DNA and gently mixed with the pipette tip. The cells were transferred to chilled electroporation cuvettes on ice. The cells were then electroporated using a MicroPulser Electroporator at 2.3 kV, 25 µF and 200 Ohm (Sambrook and Russel, 2001). SOC medium was quickly added to the cells and gently mixed. The solution was incubated at 37°C for 1 h to allow expression of the antibiotic resistance gene. 100 µl of this solution were spread on a prewarmed LB plate and incubated overnight at 37°C.

3.1.6 Plasmid DNA preparation

Plasmid DNA was purified using Qiagen Mini, Midi or Maxi Kits according to the manufacturer's directions.

3.1.7 Polymerase chain reaction (PCR)

The polymerase chain reaction is an *in vitro* method to amplify DNA fragments of interest using specific forward and reverse primers (Mullis et al., 1986). Genomic or plasmid DNA serves as a template and is replicated during cycling steps consisting of denaturation of the template, annealing of the primers and elongation of the newly synthesized strand. The reaction conditions were determined for each application depending on the used primers (the length and content of guanine (G) and cytosine (C) bases) as well as the fragment size. The Taq DNA polymerase, without proof reading capability, was applied for general testing such as cloning verification (colony PCR) while the Phusion DNA polymerase, including proof reading ability, was used for cloning experiments. The reaction conditions and pipetting schemes for the different polymerases are the following:

	Phusion Polymerase	**Taq Polymerase**
reaction buffer	10 µl	2.0 µl
dNTPs (2mM)	1.5 µl	0.4 µl
forward primer (25 pmol/ µl)	0.75 µl	0.5 µl
reverse primer (25 pmol/ µl)	0.75 µl	0.5 µl
Polymerase	0.5 µl	2.0 µl
template	10-100 ng	colony
H_2O	add to 50 µl	add to 20 µl

The primers for cloning experiments were designed with annealing temperatures varying from 52°C to 60°C, a guanine/cytosine (GC) content of 40-60% and a length between 18 and 24 nucleotides, matching the start and end point of the desired region. The elongation time depended on the fragment size and the pace of the employed DNA polymerase.

The cycling instructions for different PCR reactions are listed as follows.

step	Phusion	Taq	
1. Denaturation	98°C → 30 sec	95°C → 2 min	
2. Denaturation	98°C → 10 sec	95°C → 30 s	34x
3. Annealing	52-58°C → 30 sec	60°C → 30 s	
4. Elongation	72°C → 30s/kb	72°C → 60 s/kb	
5. Elongation	72°C → 5 min	72°C → 10 min	

3.1.8 Agarose gel electrophoresis

Negatively charged DNA or RNA molecules can be separated according to their size in agarose gels using an electric current at which smaller fragments can pass through the gel faster than larger ones (Sambrook and Russel, 2001). The amount of agarose for fragment separation was dissolved in 1x TAE (chosen according to the fragment size of interest) and ethidium bromide was added to an end concentration of 0.5 µg/ml. The electrophoresis was done in gel electrophoresis chambers filled with 1x TAE buffer at a voltage of 70 V. The nucleic acids were observed using UV light (254 nm).

3.1.9 Agarose gel extraction

Using the QIAquick gel extraction kit from Qiagen DNA molecules were purified from agarose gels. The purification was performed following the manufacturer's instructions.

3.1.10 DNA purification from PCR reactions

PCR products were purified using the Qiaquick PCR purification kit from Qiagen according to the manufacturer's instructions.

3.1.11 Phenol/Chloroform extraction

For purification of genomic DNA one volume of Phenol:Chloroform:Isoamylalcohol (25:24:1) was added to the fly lysate (chapter 3.1.13). This was then mixed and centrifuged for 5 min at 13000 rpm. The upper phase was transferred into a new tube. One volume Chloroform was added, mixed and centrifuged for 5 min at 13000 rpm. The upper phase was transferred into a new tube.

3.1.12 Ethanol precipitation of nucleic acids

DNA and RNA was precipitated by adding 1/10 volume 3 M sodium acetate (pH 5.5) and 2-3 volumes of 100 % Ethanol. The solution was mixed and incubated overnight at -20°C. The next day the solution was spun at 13000 rpm for 15 min at 4°C. The supernatant was discarded and the pellet was washed with 70 % Ethanol. The sample was centrifuged for 5 min at 13000 rpm, the supernatant was discarded and the pellet was dried at the air. The pellet was resuspended in 1x TE buffer.

3.1.13 Isolation of genomic DNA from adult flies

The protocol of (Schulz, Cherbas, & Cherbas, 1986) for isolation and purification of genomic DNA from adult flies was used. 10 flies were homogenized in 500 µl lysis buffer using a Dounce homogenizer. The lysate was incubated with RNase A (ad 50 µg/ml) for 20 min at 50°C. Afterwards Proteinase K (ad 2.5 µg/µl) was added and incubated for 60 min at 37°C. The purification of the DNA was done using the Phenol/Chloroform extraction method (chapter 3.1.11) followed by an ethanol precipitation (chapter 3.1.12).

3.1.14 MultiSite Gateway-System (Invitrogen)

For generation of plasmids carrying multiple histone gene units (His-GUs) with an alteration of threonine 11 of histone H3 to an alanine (H3T11A) the MultiSite Gateway system was used. The MultiSite Gateway System is a cloning method based upon the site specific recombination of lambda bacteriophage which catalyzes the recombination between two attachment sites (the bacteriophage attachment site attP and the bacterial attachment site attB) (Landy 1989 und Hartley et al 2000). The exact procedure of the MultiSite Gateway Recombination can be seen in the manufacturer's instructions. Three pENTR vectors were generated to conduct a multiple re-

combination reaction. The cloning strategy of pENTR vectors is described in chapter 3.1.15. The LR reaction was done to integrate three DNA fragments of pENTR vectors into a destination vector (pDEST). For the LR reaction 10 fmol of each pENTR vector, 20 fmol of a pDEST vector, 2 µl of the Clonase II Plus enzyme mix and TE buffer were mixed to a final volume of 10 µl. This reaction was incubated at 25°C over night. The next day 1 µl Proteinase K was added and incubated for 10 min at 37°C. 1 µl of the sample was transformed into electro competent Top10 cells (chapter 3.1.5). The resulting vector was then used for generation of transgenic flies (chapter 3.4.5).

3.1.15 Generation of transgenic constructs containing histone gene units

The recently published vectors pENTR221-HisGU, pENTR L4R1-HisGU and pENTR R2L3-HisGU were used to generate entry clones for the LR reaction (Gunesdogan et al., 2014). pENTR221-HisGU.H3T11A was generated by replacing an Acc65I/AgeI fragment of pENTR221-HisGU with a synthetic fragment (Mr Gene, Regensburg, Germany) containing an ACG into GCG codon exchange leading to the H3T11A mutation. The other entry clones were generated accordingly. The Multisite Gateway reaction (see chapter 3.1.14) using pENTR221-HisGU.H3T11A (Figure 2 A), pENTR L4R1-HisGU.H3T11A (Figure 2 B), pENTR R2L3-HisGU.H3T11A (Figure 2 C) and pDEST R4R3-phiC31 attB (Figure 2 D) generated the transgenic construct phiC31 attB- 3xHis-GU.T11A (Figure 2 E). The phiC31 attB- 3xHis-GU.T11A plasmid was then used to generate transgenic flies as described in chapter 3.4.5.

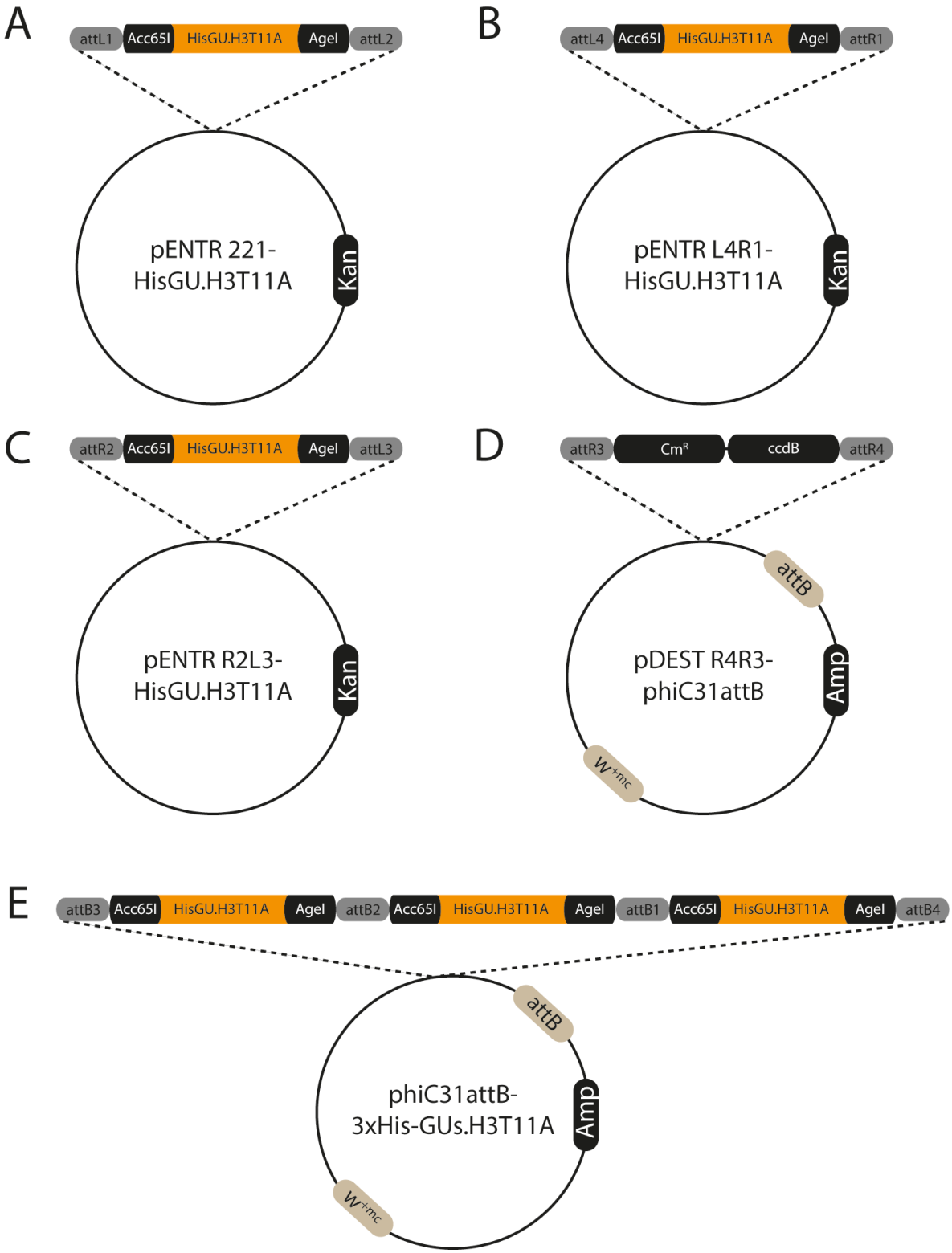

Figure 2: Generation of transgenes carrying His-GUs.H3T11A

The Multisite Gateway recombination of pENTR221-HisGU.H3T11A (A), pENTR L4R1-HisGU.H3T11A (B) and pENTR R2L3-HisGU.H3T11A (C) in pDEST R4R3-phiC31 attB (D) generated the final transgenic vector phiC31 attB- 3xHis-GU.T11A (E).

3.2 Chromatin-Immunoprecipitation

Chromatin-immunoprecipitation is a method for selective enrichment of protein-bound DNA. The addition of formaldehyde covalently links protein-protein as well as protein-DNA interactions (cross-linking) (Jackson, 1978). The second step after cross-linking consists in fragmentation by ultrasound. This results in a set of fragments with a defined length that still contains bound as well as unbound fragments. In order to separate these two classes from each other, the bound fraction is captured by protein-specific antibodies that are attached to magnetic beads. The cross-linking can be reversed and captured DNA can be detected by qPCR or by high-throughput sequencing. The following protocol for the Chromatin Immunoprecipitation was adapted from (Bonn, Zinzen, Perez-Gonzalez, et al., 2012).

3.2.1 Preparation of crosslinked S2R+ cells

Drosophila S2R+ cells were grown in Schneiders Insect Cell Medium supplemented with 10% FBS and 1% Penicillin/Streptomycin and were kept at 25°C. S2R+ cells were grown in a cell culture flask until they were confluent. Cells were centrifuged at 1300 rpm for 5 min at RT and resuspended in 1x PBS. From this cell suspension 10 µl were used to measure the cell concentration using the CASY cell counter. For fixation of the cells 37 % formaldyhyde was added to the cell suspension to an end concentration of 1.8 % and incubated for 5 min at RT. The fixation reaction was quenched with 125 mM Glycine and within the next 5 min incubated on ice. The fixed cells were then centrifuged at 3000 g at 4°C for 5 min. The supernatant was discarded and the cells were washed 2 times with 1x PBS. The cell pellets were either frozen in liquid nitrogen and stored at -80°C or immediately used for ChIP. For each ChIP an aliquot of chromatin derived from approximately $8x10^6$ cells was used.

3.2.2 Preparation of chromatin

A pellet of $8x10^6$ cells was incubated with 100 µl RIPA buffer (supplemented with PMSF and protease inhibitor tablets) for 30 min at RT. For shearing 100 µl chromatin were aliquoted in 1.5 ml TPX tubes and placed in a Diagenode Bioruptor Plus. The parameters on the machine were set to obtain DNA fragments at a range of 150 to 300 bp (35 cycles: 30 seconds ON, 30 seconds OFF, high mode). The sonicated chromatin was centrifuged for 10 min at maximum speed at 4°C. The supernatant

was then transferred to a new DNA low binding 1.5 ml tube. For quality control of the shearing efficiency 20 µl of the chromatin were aliquoted.

3.2.3 Determination of chromatin size and concentration

The quality control (QC) sample was adjusted to 100 µl with 1x TE buffer and RNase was added to a final concentration of 50 µg/ml and incubated at 37°C for 30 min. The QC samples were incubated with 0.5 % (wt/vol) SDS and 0.5 mg/ml Proteinase K at 37 °C overnight. The next morning the QC samples were incubated at 65°C for 6 h to reverse the formaldehyde cross-links. The ChIP-ed DNA was then purified using the "Chip DNA Clean and concentrator" kit from Zymogen. The DNA was eluted in 20 µl and the DNA concentration was measured using a Qubit 2.0 Fluorometer (see chapter 3.1.1.2). Afterwards approximately 100 ng from the QA sample was loaded on a 1.5 % agarose gel. The average fragment size was around 200 bp.

3.2.4 Chromatin Immunoprecipitation

For immunoprecipitation (IP) the chromatin was adjusted to 500 µl with RIPA buffer per IP. 10 % of the chromatin was aliquoted and stored at 4 °C for input control. Antibodies were added to the chromatin accordingly and incubated on a rotating wheel at 4 °C over night (ON). For each IP 10 µl of a Protein G magnetic bead suspension were washed twice with 1 ml ice cold RIPA buffer on a rotating wheel at 4°C. The beads were pelleted with a dynamic stand, the supernatant was discarded and the beads were resuspended in 100 µl RIPA buffer. 100 µl bead suspension was added to each chromatin sample and incubated at 4 °C on a rotating wheel for 3 hours. To purify the antigen-antibody-complexes the beads were pelleted with a magnetic stand, the supernatant was discarded and the beads were rinsed once with 1 ml of ice cold RIPA buffer. The washing conditions of the beads varied for each antibody and can be seen in table 6.

antibody	amount antibody	chromatin	washes
H3K27me3 (Active Motif , 39535)	1 µl	5 µg	1xRIPA, 4xRIPA500, 1xLiCl, 2xTE buffer (10 min each)
H3T11Ph (Abcam, ab5168)	1 µg	5 µg	1xRIPA, 4xRIPA500, 1xLiCl, 2xTE buffer (5 min each)

Table 6: Conditions for the IPs.

After washing the beads were transferred into a new 1.5 ml tube and washed again for 5 min in 1 ml 1x TE buffer. The beads were resuspended in 100 µl 1x TE buffer. From this point on the 10 % input sample was also included. 1x TE buffer was added to the 10 % input sample to yield a final volume of 100 µl before RNase addition. RNase was added to a final volume of 50 µg/ml and incubated at 37 °C for 1h. The samples were adjusted to a final concentration of 0.5 % (wt/vol) SDS and 0.5 mg/ml Proteinase K and incubated at 37 °C overnight. The next morning the samples were incubated at 65 °C for 6 h to reverse the formaldehyde cross-links.

3.2.5 DNA Purification

The ChIP-ed DNA was purified using the Chip DNA Clean and concentrator kit from Zymogen. The DNA was eluted in 20 µl and the DNA concentration was measured using a Qubit 2.0 Fluorometer (chapter 3.1.1.2). The samples were further analysed by qPCR to evaluate the specificity of the ChIP samples.

3.2.6 ChIP confirmation

Oligonucleotide primers were designed closely to known sites on the genome where the investigated histone mark is enriched (“positive controls”), as well as within sequences depleted for the histone mark of interest (“negative control”). For each ChIP experiment typically a whole set of different oligonucleotide primers were used. The oligonucleotide primers were designed using Primer 3 (Rozen & Skaletsky, 2000). The recipe for one qPCR reaction is listed below.

Recipe for one reaction:

SYBR Green mix	5 µl
target primer mix (5 µM)	1.5 µl
H_2O	1.5 µl
Template DNA	2 µl
total	10 µl

Firstly 8 µl of reaction mix were added to each PCR reaction well and then 2 µl of template DNA (diluted 1:50 respectively) was added.

For amplification the following PCR protocol was used:

1. Denaturation	95°C	3 min	
2. Denaturation	95°C	30 sec	40x
3. Annealing	65°C	30 sec	
4. Elongation	72°C	30 sec	
5. Elongation	95°C	3 min	

First the cycle threshold for each reaction was determined across the plate within the linear range of the amplification curve. Then the average cycle threshold for each triplicate reaction of each sample was calculated. The relative DNA amount was then calculated for any given primer set as $2^{\Delta Ct(IP)-Ct(input)}$, where Ct is the average value of each triplicate qPCR reaction. With this quantification it was possible to calculate the enrichment of the ChIP samples over input for the given primer regions (% of input). The specificity was then calculated by comparing relative enrichment for the positive and the negative controls. This was accomplished by dividing the relative mean % of input-value of each sample for a target primer set by the corresponding value for a negative control primer set. The resulting quotient represents the efficiency of the ChIP experiment. This value varied depending on the histone marks as well as the location of the chosen target primer set.

3.2.7 Preparation of the Sequencing Library

After validation of a specific enrichment of positive control regions and a high value for the efficiency of the ChIP experiments the libraries for the sequencing were prepared using the NEB Ultra DNA Library Prep Kit for Illumina. Libraries were prepared from the ChIP sample as well as matching input DNA. Library samples were purified using the Agencourt AMPure beads system following manufacturer's instructions. This size selection of the sample ensures removal of unused adapters and selection of a proper fragment size for sequencing.

3.2.8 Library Quantification

The constructed libraries were assessed on a Bioanalyzer using the DNA High Sensitivity chip. The High Sensitivity DNA chip allows sizing and quantification of DNA samples in the single-digit pg/µl concentration range. The Bioanalyzer also allows visualization of possible adapter contamination. Adapter dimers are visible as a sharp peak at approximately 120 bp. Libraries having large adapter dimer peaks should not be sequenced, but they can be removed by an additional size selection step using the Agencourt AMPure beads system. The Bioanalyzer analysis also allows the calculation of the molarity of the libraries. The libraries were unified to a sequencing pool containing 2 nM of each library. To verify the correct molarity of the pool, qPCR was performed on the pool using primer pairs for the adapted indices of the libraries respectively. A reference pool served as a control to compare it to the results of the generated pool. A master reaction mix was prepared for each library with triplicate reactions per primer set.

Recipe for one reaction:

SYBR Green mix	2 µl
dNTPs	2 µl
$MgCl_2$	2 µl
qPCR Primer (P5)	0.8 µl
qPCR Primer (P7)	0.8 µl
Immolase (5U/ µl)	0.1 µl
H_2O	11.3 µl
DNA	1 µl
total	20 µl

For amplification the following PCR protocol was used:

1. Denaturation	95°C	10 min	
2. Denaturation	95°C	15 sec	40x
3. Annealing	65°C	30 sec	
4. Elongation	72°C	30 sec	
5. Elongation	95°C	3 min	

3.2.9 Library Sequencing

When the molarity of the pool was acceptable the samples were delivered to the sequencing core facility at the Max-Planck Institute for Molecular Genetics in Berlin, Dahlem. For sequencing the NextSeq 500 Illumina platform was used.

3.2.10 Data Analysis

The bioinformatic analysis was done in collaboration with Dr. Alisa Fuchs from the research group „Computational Epigenomics“ from the MPI for Molecular Genetics in Berlin. All bioinformatics analysis was run on a server at the MPI for Molecular Genetics and operated by using a locally installed version of the GALAXY platform (Blankenberg et al., 2010; Giardine et al., 2005; Goecks, Nekrutenko, Taylor, & Galaxy, 2010). The reads were mapped to the Drosophila genome Dm 2006 R5/dm3 which was provided by the Berkeley Drosophila Genome Project (BDGP) using the short read aligner Bowtie (Langmead, Trapnell, Pop, & Salzberg, 2009). After mapping a peak calling analysis using the peak calling algorithm MACS (Model-based Analysis of ChIP-Seq) was done to predict the regions of the genome where the ChIPed protein is bound by finding regions with significant numbers of mapped reads (peaks) (Bailey et al., 2013).

3.2.11 Validation of antibodies

The antibodies that were used for chromatin immunoprecipitation were subjected to a MODified™ Histone Peptide Array from Active Motif to validate the cross-reactivity with other PTMs following manufacturer’s instructions. The MODified Histone Peptide Arrays screen 59 acetylation, methylation, phosphorylation, and citrullination modifi-

cations on the N-terminal tails of histones H2A, H2B, H3 and H4. Each peptide array contains 384 unique histone modification combinations in duplicate.

3.3 *Drosophila* Schneider (S2R+) cell culture

3.3.1 Maintenance of S2R+ cells

Drosophila Schneider cells were received from the *Drosophila* Genomics Resource Center (DGRC) in Bloomington. S2R+ cells were cultured in cell culture flasks at 25°C using *Drosophila* Schneider's media supplemented with 10% fetal bovine serum (FBS) and 1% Penicillin/Streptomycin. After 2-3 days cells reached a density about 90% and were splitted in a ratio of 1:4 using fresh media and fresh flasks. All cell culture operations were performed under sterile conditions in a sterile hood.

3.3.2 Thawing and freezing of S2R+ cells

Well growing, confluent, healthy cultures of S2R+ cells were grown to the mid-exponential growth phase (approximately $5x10^6$ cells/ml) and collected by centrifugation for 3 min at 1300 rpm. The supernatant was discarded and the cells were resuspended in freezing medium to give a final concentration of approximately $2x10^7$ cells/ml. The cell suspension was dispensed into cryovials (0.5 ml per vial). The cryotubes were placed into a freezing box and stored at -80°C for some days to allow the ampoules to slowly cool to the temperature of the freezer. For long-term storage the frozen ampoules were transferred to liquid nitrogen.

For thawing of an ampoule of S2R+ cells 5 ml of Schneider's medium + 10% FBS + 1% Pen/Strep was placed in a 25 cm^2 cell culture flask. The ampoule was removed from the liquid nitrogen storage place and a few drops of medium were added to the cell suspension. Using a Pasteur pipet the cell suspension was pipetted up and down to thaw and mix the cells. The cell suspension was then transferred to the cell culture flask. The flask was placed into an incubator for 1 h. After 1 h most of the cells were adhering loosely to the flask and the supernatant was gently removed and replaced with 5 ml of fresh medium. The flask was left in the incubator overnight, and the medium was changed again the next day.

3.3.3 Polyacrylamide gel electrophoresis (SDS-PAGE)

The Polyacrylamide gel electrophoresis was done according to a standard protocol (Ausubel, 1990). Protein samples were prepared in 6x SDS sample buffer and boiled at 99°C for 10 min. The samples were separated on 8-16 % Criterion Precast Gels. Gels were placed into the gel chamber. The chamber was filled with 1x SDS running buffer and the proteins were separated at 120 V for 1 h. Proteins were denatured in the presence of SDS and 2-mercaptoethanol as thiol reducing agent and acquired a uniform charge-to-mass ratio proportional to their molecular weights. The protein sizes were determined by comparing the migration of the protein band to a molecular mass standard (Precision Plus Protein™ Kaleidoscope™).

3.3.4 Western-Blotting

Proteins were transferred from the SDS gel onto a PVDF membrane for 60 min at 350 mA using a Criterion Blotter Apparatus in 1x blotting buffer. After bathing in blocking buffer for 1 h at RT to reduce unspecific binding, the membrane was incubated with a primary antibody, diluted in blocking buffer overnight. Next, the membrane was washed three times with TBS-Tween (0.5%) for 10 min and then incubated with appropriate secondary antibodies coupled to horseradish peroxidase (HRP) diluted in blocking buffer for 1 h at RT. The membrane was washed six times with TBS-Tween (0.5%) for 10 min. The protein bands were detected using the chemiluminescent substrate from Amersham biosciences and visualized on Amersham ECL films after automatic development in a Curix 60 film processor.

3.3.5 Western Blot membrane stripping

Western blot membranes were stripped to remove primary and secondary antibodies to make a proper loading control of the Western blot. As a loading control an alpha-Tubulin antibody was chosen as alpha-Tubulin exhibits a high-level and constitutive expression in S2R+ cells. For stripping the membrane was added to a small plastic bag and covered with harsh stripping buffer. The membrane was then incubated at 50°C for 45 min with some agitation. The buffer was discarded and the membrane was rinsed under running water for approximately 10 min. The membrane was incubated in blocking buffer and further processed as described in chapter 3.3.4.

3.3.6 RNAi in S2R+ cells

3.3.6.1 Template design

The primers were designed using the online tool Primer 3 (Rozen & Skaletsky, 2000). The dsRNAs corresponded to exon sequences and had a length of 334 bp for the knockdown of E(z) and 585 bp for the knockdown of Su(z)12. After choosing the primer sequence, the T7 promoter sequence (TAATACGACTCACTATAGGG) was added to the 5' end of both primers.

3.3.6.2 Amplification of templates

Templates were generated by PCR on genomic DNA from S2R+ cells. In a 0.5 ml tube 20 µl 5x Phusion HF, 2 µl of 10 m*M* dNTP-mix, 0.2 µ*M* each primer, 1 µg of genomic DNA, and water to a final volume of 100 µl were mixed. The template was amplified in a thermal cycler for 30 cycles: 94°C for 30 s, 55°C for 30 s and 72°C for 30 s. The PCR product was purified using a QIAquick PCR Purification Kit and eluted in 50 µl RNase-free water. The concentration of the PCR product was measured using a NanoDrop and analyzed by agarose gel electrophoresis.

3.3.6.3 Production of dsRNA

DsRNA was generated using an Ambion MEGAscript Kit according to the manufacturer's directions. The RNA concentration was measured by using a NanoDrop. To be in a linear range the samples were diluted 1:100. The yield was calculated as followed:

A_{260} * dilution factor * 40= µg/ml dsRNA

The integrity of the dsRNA was analyzed by agarose gel electrophoresis. The dsRNA was stored at -20 °C until it was further needed.

3.3.6.4 RNAi treatment of cells

S2R+ cells were cultured in 25-mm dishes to a density of $1x10^6$ cells/ml. The cells were resuspended, transferred to a 15 ml falcon and centrifuged for 3 min at 1300 rpm. The cells were resuspended in 10 ml Schneiders medium and centrifuged for 3 min at 1300 rpm. 1 ml of the cells was added into each well of a six-well plate. 15 µg/ml of the corresponding dsRNA was added to the cell suspension together with

2ml Schneiders medium. The cells and the dsRNA were incubated for 1 h at room temperature. S2R+ cells were treated 5 days with dsRNA against Su(z)12 and E(z). The old medium was replaced by fresh medium containing dsRNA (15 µg/ml) every day.

3.3.6.5 Preparation of RNAi-treated S2R+ cells for Western Blot

S2R+ cells were removed after 5 days of treatment with dsRNA, placed in a 1.5 ml tube and centrifuged. The supernatant was discarded and suspended in 100 µl PBS + Protease inhibitors. Then 100 µl 1x SDS-Page loading dye was added. The samples were sonicated in a Biorupter Plus for 2 cycles (30 s ON, 30 s OFF, high mode) and afterwards heated to 99°C for 10 min. The samples were stored at -20°C and were ready to be used for Western Blotting as described in chapter 3.3.4.

3.3.6.5 Immunofluorescence of RNAi-treated S2R+ cells

For immunofluorescence 80.000 S2R+ cells were seeded in an iBidi 8-well plate and treated with the corresponding dsRNA at a concentration of 15 µg/ml. The old medium was exchanged every day and replaced with fresh medium containing dsRNA. The cells were treated with dsRNA for 5 days. After 5 days the cells were washed three times with PBS and fixed in 4% PFA for 15 min. The cells were washed three times with PBS. For blocking the cells were incubated with PBS (supplemented with 10% GS) for 30 min. Primary antibodies were diluted in PBS (supplemented with 10% GS) and incubated over night at 4°C. The next day the cells were washed three times with PBS for 5 min each. Secondary antibodies were diluted in PBS (supplemented with 10% GS), added to the cells and incubated for 1 h. The cells were then washed three times with PBS. For DNA-staining the cells were incubated with PBS containing DAPI (1:1000 dilution) and incubated for 5 min. Then the cells were washed once with PBS and once with water. The cells were mounted with Prolong Gold directly in iBidi dishes and analyzed using a confocal microscope.

3.4 *Drosophila melanogaster* techniques

3.4.1 Fly husbandry

Flies were maintained under standard conditions (Ashburner, 1989).

3.4.2 Immunostaining of *D. melanogaster* ovaries

The ovaries of female flies were dissected in Schneider's cell culture medium at room temperature and the ovarioles were fixed in 4% Paraformaldehyde (PFA) for 10 min. The fixed tissue was rinsed at RT in PBTx and then extracted with 10% Triton X-100 for 30 min. After that the samples were blocked with 10% goat serum in PBTx for at least 30 min. Staining with primary antibodies was done in blocking solution at 4°C overnight. After three washes for 20 min in PBTx accordingly, the tissues were incubated with secondary antibodies in 10% goat serum for 2 h at RT. After two washes for 20 min in PBTx, the tissue was treated with 1 mg/ml RNaseA in PBTx for 30 min followed by staining with DAPI (1:1000) in PBTx for 10 min in order to visualize the DNA. The tissue was then washed in PBTx and mounted using Prolong Gold antifade reagent. Images were acquired using a Leica TCS SP8 confocal microscope.

3.4.3 Immunostaining of *D. melanogaster* wing discs

For dissection of wing imaginal discs 3rd instar larvae were dissected in Schneider's cell culture medium at room temperature. The larvae were ripped open at the posterior part and then inverted by pushing the forceps into the anterior part of the larvae. The wing discs were still attached to the body wall and removed using a forceps. The wing discs were fixed in 4% PFA for 10 min. The fixed tissue was rinsed at RT in PBTx and extracted with 10% Triton X-100 for 30 min and blocked with 10% GS in PBTx for at least 30 min. Staining with primary antibodies was done in blocking solution at 4°C overnight. After three washes for 20 min each in PBTx, the tissue was incubated with secondary antibodies in 10% GS for 2 hours at RT. After two washes for 20 min in PBTx, the tissue was treated with 1 mg/ml RNase A in PBTx, for 30 min followed by staining with DAPI (1:1000) in PBTx for 10 min in order to visualize the DNA. The tissue was then washed finally in PBTx and mounted in Prolong Gold antifade reagent. Images were acquired using a Leica TCS SP8 confocal microscope.

3.4.4 Clonal analysis in *D. melanogaster*

The genotypes of flies that were used for the generation of genetic mosaics via heat shock induced expression of a recombinase were as follows:

Analysis of PcG mutations

$y^1 w^{1118}$ hsflp122/+; +/+; $E(z)^{731}$, FRT2A/ y^+ hs-nGFP, FRT2A
$y^1 w^{1118}$ hsflp122/+; +/+; $Su(z)12^4$, FRT2A/ y^+ hs-nGFP, FRT2A
$y^1 w^{1118}$ hsflp122/+; +/+; FRT2A/ y^+ hs-nGFP, FRT2A

Analysis of histone transgenes in the *His^C* background

ΔH3.3, hsflp/ ΔH3.3; ΔH3.3, His^C, FRT40A/ Ubi-GFP, FRT40A; 6xHis-GUs.T11A/+
ΔH3.3, hsflp/ ΔH3.3; ΔH3.3, His^C, FRT40A/ Ubi-GFP, FRT40A; 6xHis-GUs.K27R/+
ΔH3.3, hsflp/ ΔH3.3; ΔH3.3, His^C, FRT40A/ Ubi-GFP, FRT40A; 6xHis-GUs/+
ΔH3.3, hsflp/ ΔH3.3; ΔH3.3, His^C, FRT40A/ Ubi-GFP, FRT40A; +/+
ΔH3.3, hsflp/ ΔH3.3; ΔH3.3, FRT40A/ Ubi-GFP, FRT40A; +/+
hsflp/ +; His^C, FRT40A/ Ubi-GFP, FRT40A; 6xHis-GUs.T11A/+
hsflp/ +; His^C, FRT40A/ Ubi-GFP, FRT40A; 6xHis-GUs.K27R/+
hsflp/ +; His^C, FRT40A/ Ubi-GFP, FRT40A; 6xHis-GUs/+
hsflp/ +; His^C, FRT40A/ Ubi-GFP, FRT40A; +/+
hsflp/ +; His^C, FRT40A/ Ubi-GFP, FRT40A; 6xHis-GUs.T11A/6xHis-GUs.T11A
hsflp/ +; His^C, FRT40A/ Ubi-GFP, FRT40A; 6xHis-GUs.K27R/6xHis-GUs.K27R
hsflp/ +; His^C, FRT40A/ Ubi-GFP, FRT40A; 6xHis-GUs/6xHis-Gus

For induction of mutant clones female flies of the desired genotypes were aged for 2 days. Subsequently, three heat shocks each at 37.5°C were applied at intervals of approximately 12 h. The heat shocks were performed for 1 h each. During the heat shocks, the flies were placed in big empty vials closed with moist foam stoppers in a water bath at 37.5°C. In between the heat shocks the flies were kept on yeast at 25°C for recovery. Following heat shock treatments flies were mated to wild type male flies and kept well fed at 25°C. 2 days post the last heat shock, the tissues were dissected and stained for the desired protein according to chapter 3.4.2.

Using GFP fluorescence, the mutant and twin clones were analyzed using a Leica TCS SP8 confocal microscope. For induction of mutant clones in wing imaginal discs larvae were heat shocked 72 h after egg-laying at 37.5°C for 1 h. The dissection and staining of the wing imaginal discs were done as described in chapter 3.4.3. Using GFP fluorescence, the mutant and twin clones were analyzed using a Leica TCS SP8 confocal microscope.

3.4.5 Transgenesis of modified histones

Plasmids carrying modified histone gene units were cloned (described in chapter 3.1.15) and then recombined using the Multisite Gateway System as described in chapter 3.1.14. The transgenic flies were generated by Rainbow Transgenic Inc. using the phiC31 integration system. phiC31 integration system is a site-specific integration approach which applies bacteriophage phiC31 integrase to mediate the sequence-specific recombination between two largely different attachment sites (attB and attP). By selection of attP sites in the genome (landing platforms) and an expression vector containing the complementary attB site (phiC31 attB- 3xHis-GU.T11A, shown in figure 2 E), a transgene can be integrated on the pre-selected site on the genome (Bischof, Maeda, Hediger, Karch, & Basler, 2007). The genotypes of the injected flies were:

y^1 M{vas-int.Dm}ZH-2A w^*; PBac{y^+-attP-3B}VK00033
y^1 M{vas-int.Dm}ZH-2A w^*; M{3xP3-RFP.attP'}ZH-86Fb

To generate flies carrying 6xHis-GUs.T11A the transgenic flies 3xHis-GUs.T11A.VK33 and 3xHis-GUs.T11A.86Fb were crossed to induce recombination. The crosses were done as follows.

♀ *+/+;3xHisGU.86Fb/3xHisGU.86Fb* x *+/+; 3xHisGU.VK33/3xHisGU.VK33*

→ ♀ *+/+; 3xHisGU.86Fb/3xHisGU.VK33* x D^3*/TM3Sb*

→ single ♂ *3xHisGU.86Fb, 3xHisGU.VK33/TM3Sb* x D^3*/TM3Sb*

→ *3xHisGU.86Fb, 3xHisGU.VK33/TM3Sb* ♀x♂

→ stable stock *3xHisGU.86Fb, 3xHisGU.VK33/3xHisGU.86Fb, 3xHisGU.VK33*

The crosses for getting the transgenes into the His^c-background and *ΔH3.3;*His^C-background were performed by Alf Herzig.

3.4.6 Quantification of fluorescence intensity in follicle stem cells

For quantification of the H3T11ph signal in follicle cells, flies with the according genotype were collected and clones were induced as described in chapter 3.5.6. The ovaries were dissected 5 d after the third heat shock. The immunostaining was done as described in chapter 3.4.2. For each genotype 3 independent rounds of setting up the crosses, dissecting the ovaries and analyzing the ovaries using the confocal microscope were done. In each round pictures of 5 egg chamber in stage 5/6 were acquired. The egg chambers were chosen when approximately 5-10 GFP negative cells were lying in the same confocal plane as the same amount of GFP positive cells directly next to each other. The pictures were acquired without saturating the pixels. The quantification was done using the software ImageJ. The threshold for the H3T11ph signal was chosen so that the neighbouring cells were still separated from each other. In each picture the background signal was also measured. For the analysis the values for the Integrated Density, Area and Mean Gray Value were measured. The Mean Gray Value is the sum of the gray values of all the pixels in the selection divided by the number of pixels. Integrated Density is the product of Area and Mean Gray Value.

From these values the Corrected Total Cell Fluorescence (CTCF) was calculated:

CTCF= Integrated Density – (Area of selected cell x Background Mean Gray Value)

The data was normalized to the signal of H3T11ph of GFP positive cells, the average value considered as 100 % of signal. Data analysis was done using the software GraphPad Prism 6. The statistical analysis was done using an unpaired t test.

4 Results

4.1 Characterization of post-translational histone modifications in the female germline of *Drosophila melanogaster*

4.1.1 Distribution of histone modifications in the female germline

To get an impression of how the distribution pattern of different histone modifications looks in the germline of *Drosophila melanogaster* (*D. melanogaster*), an antibody screen was performed. 21 antibodies against various histone modifications were used for immunostaining of the different morphological parts of the germline of wild-type females. The antibodies were used at different dilutions to find the optimal staining conditions for the occurence of the specific modification. The fixed and stained ovaries were analyzed using a confocal microscope and representative pictures of different regions of the ovaries were taken. The intensity of the signal for each mark was classified into one of the four categories high: +++, medium: ++, low: +, absent: - (Table 7). The aim was to identify histone modifications that could be potential regulators of the maintenance of GSCs and to study the overall distribution of histone modifications in different cell types of the ovary. The two most promising candidates were H3K27me3 and H3T11ph as both showed a very strong signal in GSCs and notably weaker staining in differentiated germline cells (Table 7). Both histone modifications were also present in follicle cells of all stages.

	germ line cells						follicle cells			
	region 1	region 2A	region 2b	region 3	nurse cells	karyosome	region 3	stage 2-8	stage 8-10	mitotic cell
H3K4me	++	+	+	++	+	+++	++	++	-	-
H3K4me2	++	++	++	+	++	++	++	++	-	-
H3K4me3	++	+	+	+	++	-	++	++	-	+
H3K9Ac	++	+++	++	+	++	+	++	++	-	+
H3K9me3	+++	+++	+++	+++	+++	+++	+++	+	-	+
H3S10Ph	+	+	+	+	++	+++	+	+	-	+++
H3T11Ph	+++	++	++	++	++	++	++	++	+	+
H3K14Ac	++	+++	+	-	+	+++	++	++	+	+
H3K18Ac	+	+	+	+	-	++	++	++	-	-
H3K23Ac	+	-	-	-	-	-	++	++	++	-
H3K27Ac	++	++	++	++	++	+++	+++	++	++	-
H3K27me3	+++	+	+	+	+	+++	+	+	+	-
H3S28Ph	+	+	+	+	-	+	+	-	-	+++
H3K36Ac	+	+	+	+	+	-	++	++	-	-
H3K36me	++	+	+	+	+	++	+++	++	++	++
H3K36me3	+	+	+	+	+	++	+++	++	+	+
H4K5Ac	++	+	+	+	-	-	+++	++	+	-
H4K8Ac	++	+	+	+	-	++	++	++	+	-
H4K12Ac	+	+	+	+	-	-	++	++	+	-
H4K16Ac	++	++	++	+	++	+++	++	++	+	-
H4K20me	+	++	+	++	++	++	++	++	++	+

Table 7: Results of the antibody screen.

The signal intensities for each specific modification in particular parts of the ovary were classified into one of the following four categories high: +++, medium: ++, low: +, absent: -. The investigated regions of the germarium were subdivided into region 1, 2A, 2B and 3, nurse cells in stage 3 egg chambers and the enrichment on the chromatin of the future oocyte (karyosome). Furthermore, the enrichment of the PTMs was analyzed in follicle cells of region 3 egg chambers, stage 2-8 and stage 8-10 egg chambers respectively. Mitotic cells in egg chambers in early stages were validated as well.

4.1.2 Distribution of H3K27me3 in ovaries of *D. melanogaster*

The occurence of H3K27me3 in ovarioles of *D. melanogaster* was analyzed by immunostaining using modification specific antibodies (Figure 3). Two GSCs at the most anterior part of the germarium were reliably identified by their location (located at the posterior side of the cap cells) and size (the biggest cells at the tip of the germarium). The immunostaining pattern revealed that H3K27me3 is present in high amounts in the germline stem cells present in region 1 of the germaria (Figure 3 A, B, dashed lines). The signal of H3K27me3 progressively decreases with differentiation of the cells. H3K27me3 could either be actively removed upon differentiation or diluted by replication and subsequent cell division. In differentiated cysts and nurse cells the signal for H3K27me3 is restricted to heterochromatic regions which can be identified by a stronger DNA staining as heterochromatin results in a denser compaction of DNA (Figure 3 D-F, marked by white arrowheads).

In the karyosome the signal is highly abundant all over the chromatin (Figure 3 D, E, marked by an asterisks). In follicle cells the signal for H3K27me3 is weak and located at heterochromatic regions (Figure 3 G-I, marked by white arrowheads).

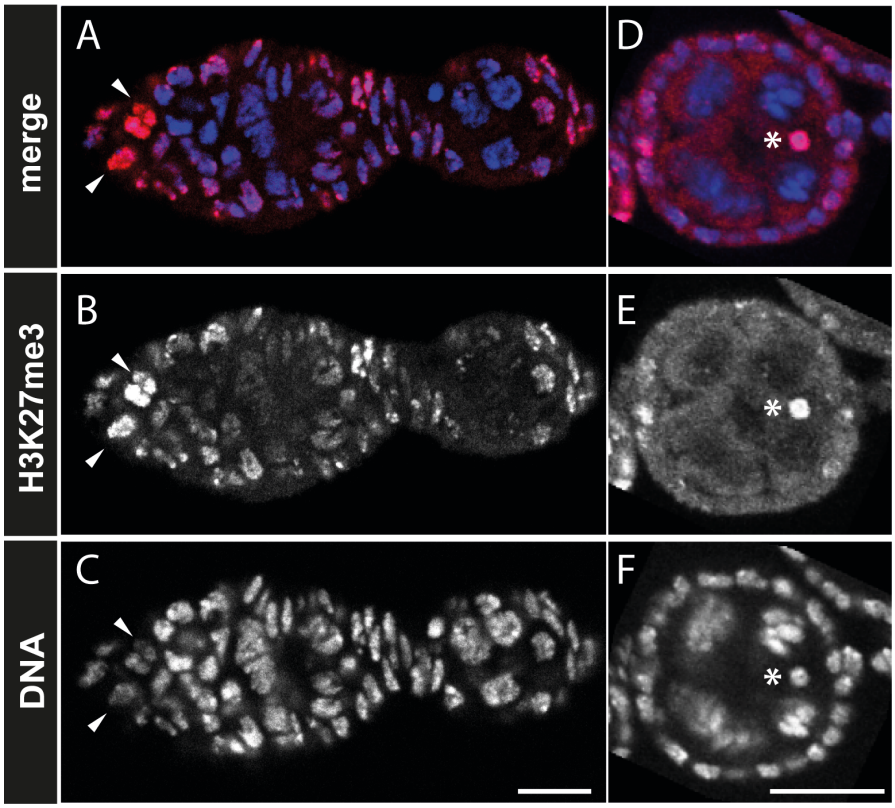

Figure 3: Distribution of H3K27me3 in ovaries of *D. melanogaster.*

Wildtype female flies were dissected and the ovaries were fixed and stained. DAPI staining was performed to visualize the DNA. All images represent confocal sections. The germaria anterior to posterior orientation is left to right in the panel. (A-C) H3K27me3 signal is abundant in GSCs (marked by dashed lines). GSCs were identified by their location close to the niche cells. The signal intensity for H3K27me3 declines in differentiating germline cells. (D-F) H3K27me3 is enriched on the karyosome which is marked by asterisks. In nurse cells the signal is enriched on heterochromatin which is marked by white arrowheads. (G-I) In follicle cells of stage 8 egg chambers the signal of H3K27me3 is restricted to heterochromatic region as marked by white arrowheads. Scale bar in A-I represents 10 µm.

4.1.3 Change in co-localization of H3K27me3 and H3K27ac upon differentiation

It is known that H3K27 can also be acetylated (H3K27ac), a mark that is highly enriched at promotor regions of transcriptionally active genes in a variety of different organisms (Garcia et al., 2007; Suka, Suka, Carmen, Wu, & Grunstein, 2001). Thereby H3K27ac seems to act as a complementary mark to H3K27me3 (Tie et al., 2009). Since H3K27me3 decorates the entire nucleus of GSCs, stainings were performed against H3K27ac to address whether this mark is absent in GSCs (Figure 4 A-D). However, it appears that both marks are widely distributed in these cells at the tip of the germarium and are not confined to a specific territory within the nucleus. H3K27me3 seems to be more enriched in these undifferentiated cells (Figure 4 B) although H3K27ac is also present (Figure 4 C). In differentiated cells of the germline in later staged egg chambers (Figure 4 E-H) the signal for H3K27me3 and H3K27ac seems to be mutually exclusive. Thus, it appears that H3K27me3 is broadly distributed in undifferentiated cells, but restricted to distinct regions of the chromatin in differentiated cells, while H3K27ac appears not to change its distribution significantly. Furthermore, the staining shows that H3K27me3 is enriched on denser heterochromatic regions and H3K27ac is broadly distributed across euchromatic regions. The distribution of H3K27me3 and H3K27ac was also investigated in early follicle cells in region 3 of the germarium (Figure 4 I-L) and late follicle cells (Figure 4 M-P). The stainings revealed an overlap between H3K27me3 and H3K27ac in early follicle cells (Figure 4 L). In later follicle cells, H3K27me3 seems to be restricted to a particular territory within the chromatin while H3K27ac is more widespread, but absent from territories where H3K27me3 is present (Figure 4 P).

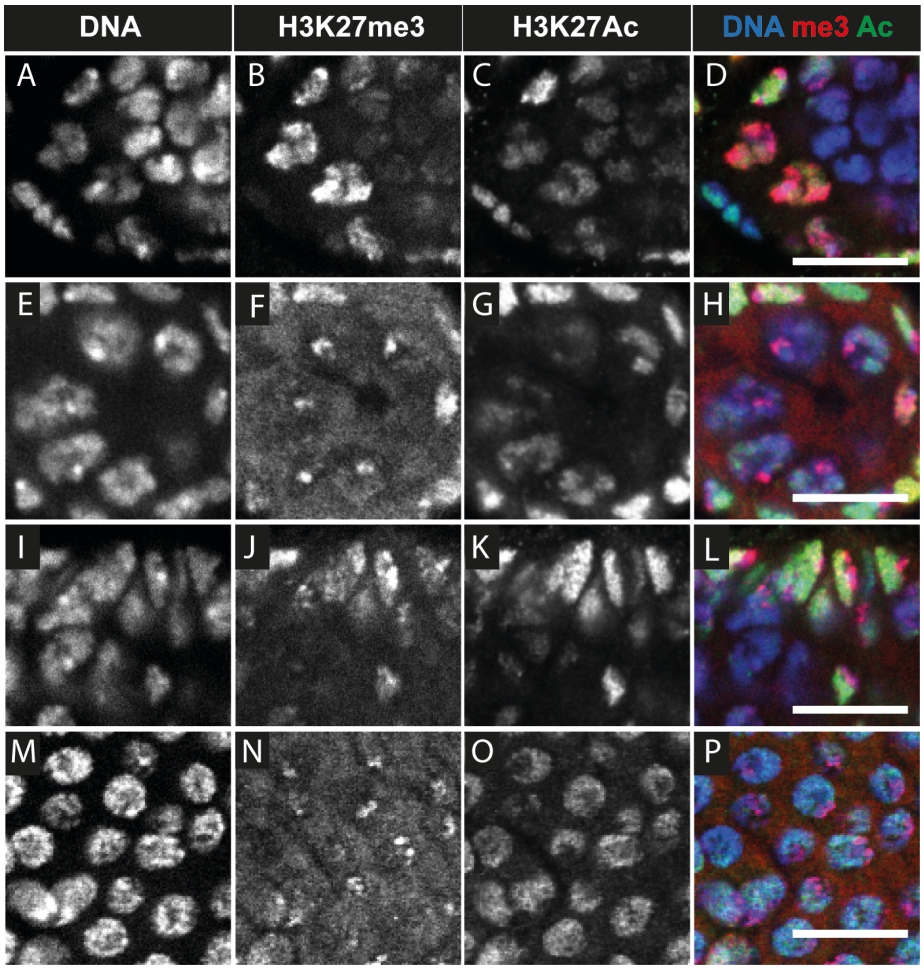

Figure 4: The distribution of H3K27me3 and H3K27ac changes upon differentiation in germline and somatic cells.

Representative images of ovaries dissected from wildtype flies double-stained for H3K27me3 and H3K27ac are shown. The DAPI staining was performed to reveal the nuclei. All images represent confocal sections. (A-D) H3K27me3 is abundant and widespread in GSCs. The signal for H3K27ac is also widespread in the GSCs but not enriched. (E-H) The nuclei of nurse cells in early egg chambers have mutually exclusive territories for H3K27me3 and H3K27ac. The widespread H3K27ac signal covers the entire nucleus except a small territory where H3K27me3 is restricted. (I-L) In nuclei of early follicle cells of the germarium the signal for H3K27me3 and H3K27ac is partially overlapping and in other regions mutually exclusive. (M-P) Differentiated follicle cells of later stage egg chambers have H3K27me3 confined to a small territory which is mutually exclusive from the H3K27ac signal which covers the rest of the nucleus. Scale bars represent 10 µm.

4.1.4 Distribution of H3T11ph in ovaries of *D. melanogaster*

The occurence of H3T11ph in ovarioles of *D. melanogaster* was also analyzed in detail by immunostaining using modification-specific antibodies (Figure 5). The stainings revealed that H3T11ph is abundant in GSCs (Figure 5 A-C, white arrowheads). The GSCs were identified by their location next to the CCs, their size and additionally by the anterior localization of the spectrosome, a round structure in the GSCs assessed by a Hu-li Tai Shao (HTS) staining (Lin et al., 1994). In GSCs this spectrosome is always orientated towards the niche cells whereas in CBs the orientation of the spectrosome occurs randomly (de Cuevas, Lilly, & Spradling, 1997). During differentiation of the CBs to 16-cell cysts the spectrosome is transformed into the fusome which connects the cells with each other (Lin et al., 1994). The signal of H3T11ph decreases in differentiating germline cells, but not as dramatically as the signal for H3K27me3 (Figure 3 A, B and Figure 5 A, B). The signal for H3T11ph is enriched on the karyosome (Figure 5 B, D, white asterisks).

In follicle cells H3T11ph is enriched in all developmental stages of the egg chambers and is broadly distributed across the chromatin.

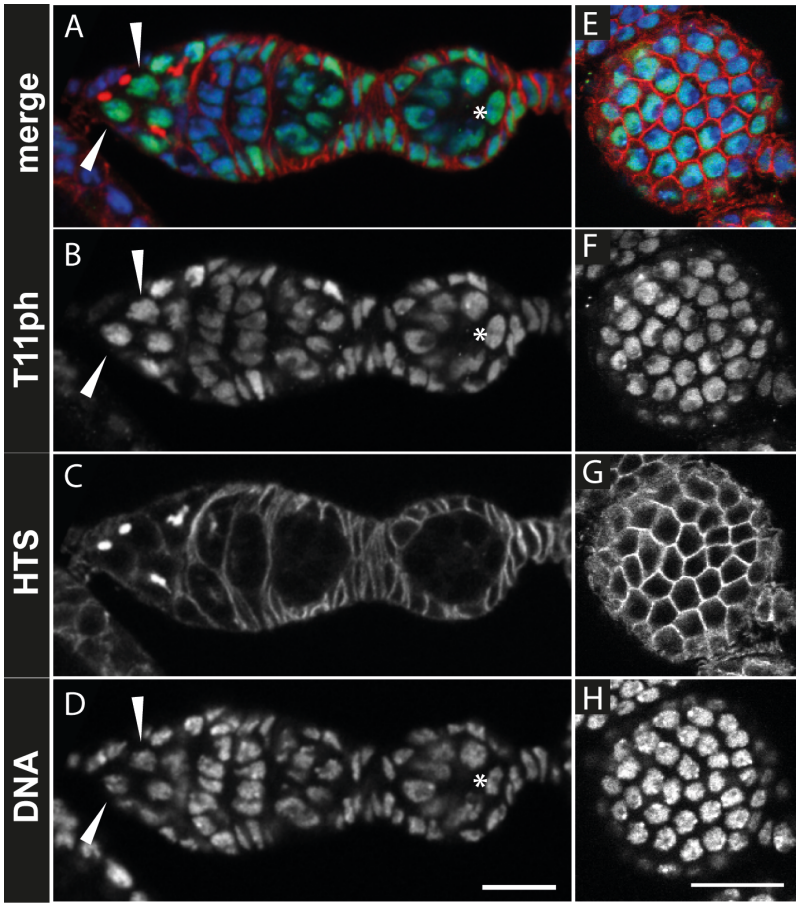

Figure 5: Occurrence of H3T11ph in the female germline of *D. melanogaster*.
Representative images of ovaries dissected from wildtype flies stained for HTS (C, G) to reveal the cell boundaries and for H3T11ph (B, F). The DAPI staining was performed to reveal the nuclei (D, H). All images represent confocal sections. (A-D) The signal for H3T11ph is enriched in GSCs (marked by white arrowheads) and moderately enriched in differentiated germline cells. On the karyosome the signal for H3T11ph is enriched as marked by an asterisk. (E-H) H3T11ph is enriched in nuclei of follicle cells of early staged egg chambers. Scale bars in D and H represent 10 µm.

4.2 Characterization of the role of the Polycomb system in the germline

A typical feature of stem cells is their ability to stay undifferenciated and to proliferate over a long period of time. At the same time, stem cells produce cells that terminally differentiate after dividing a few times. In the female germline, GSCs ensure continuous egg production and tissue homeostasis. Until recently, the analysis of stem cells and their lineages has largely focused on transcriptional regulation. Emerging evidence, however, suggests that the genome undergoes major epigenetic alterations during development and stem cells differentiation (Reik, 2007; Rugg-Gunn, Cox, Ralston, & Rossant, 2010). Among the chromatin modifiers, Polycomb group (PcG) proteins function as gene repressors and are involved in the regulation of stem cell characteristics (J. A. Simon & Kingston, 2009). Previous studies have shown the importance of Polycomb factors for stem cell maintenance using various PcG-knockout mice. Specifically, knockout mice embryos for the PRC2 components Suz12, Ezh2 and Eed die during early postimplantation stages (Faust, Schumacher, Holdener, & Magnuson, 1995; O'Carroll et al., 2001; Pasini et al., 2004). *In vitro* studies using ES cells (embryonic stem cells) demonstrated that cells lacking Eed or Suz12 could not maintain their pluripotency and were prone to differentiation (Faust et al., 1995; Pasini et al., 2004). Although many aspects of PcG gene structure and functions are conserved from flies to mammals, little is known about the roles of PcG genes in adult stem cell lineages in *D. melanogaster*. In chapter 4.1.3 it was shown that the histone modification H3K27me3 is highly enriched in GSCs in the ovary of *D. melanogaster*. This together with the results of recent published data from mammals suggests that PcG genes might be involved in the maintenance of stem cells in the ovary of *D. melanogaster* and was further investigated.

4.2.1 Generation of GFP marked cell clones using the FLP/FRT technique

To investigate the role of PcG components in germline and somatic cells of the ovary of *D. melanogaster* the FLP-FRT technique was used to generate mutant homozygous cells in heterozygous tissue (Chou & Perrimon, 1992). The FLP/FRT system is a site-directed recombination technology based on the targeting of a recombination

enzyme (flipase - FLP) to specific DNA regions designated as flipase recognition target (FRT) sites. Initially identified in *S.cerevisiae*, the yeast FLP-enzyme and its FRT recombination targets were successfully transferred into each major chromosome arm in *D. melanogaster* (Golic & Lindquist, 1989). This offers the ability to mediate mitotic recombination *in vivo* during development in a controlled manner (Theodosiou & Xu, 1998). The controlled induction of the mitotic recombination events was performed by expressing the FLP under the control of a heat-shock promoter. A schematical overview of the FRT/FLP-system to generate genetic mosaics is illustrated in figure 6. Flies were generated with a FRT-carrying chromosome harboring an ubiquitously expressed GFP transgene *in trans* to a FRT-chromosome carrying a PcG mutation. FLP can induce mitotic recombination between FRT sites on homologous chromosome arms. After cell division a homozygous mutant cell is generated marked by the absence of GFP. At the same time a wildtype cell is generated which is called twin clone cell. This twin clone cell carries the wildtype form of the gene of interest and two copies of GFP and shows stronger GFP expression compared to heterozygous cells.

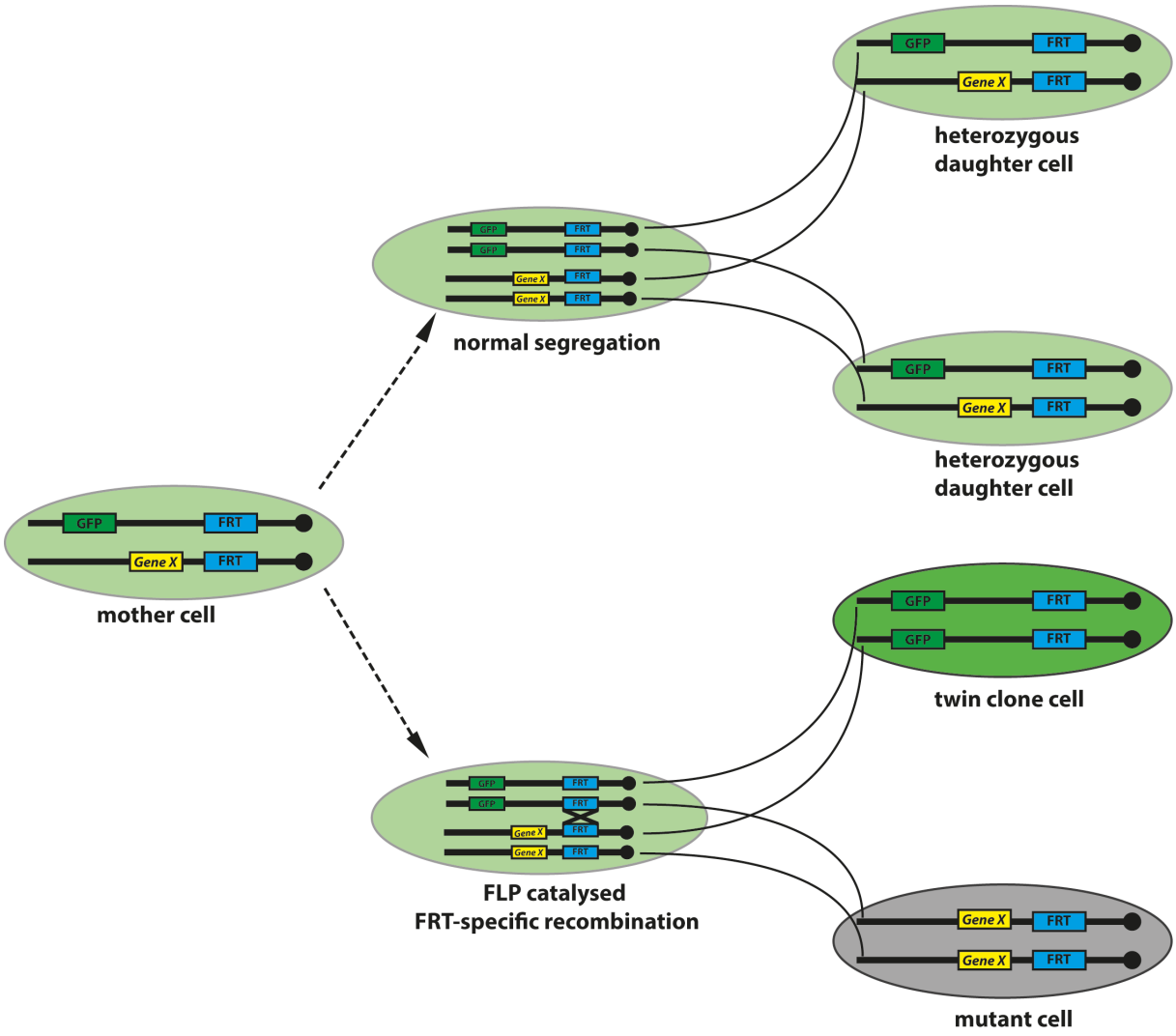

Figure 6: Generating and labeling mutant cell clones using the FLP/FRT system.

In a heterozygous parental cell, FLP induces mitotic recombination between FRT sites (FRT, blue) on homologous chromosome arms. The FRT sites are located on identical integration sites on homologous chromosomes. Distal from the FRT sites one of the chromosomes carries the GFP sequence (green), the other one a mutation in a gene of interest (*gene X*, yellow). Heterozygous cells carry one copy of the cell marker GFP and show a moderate GFP expression (light green cell). Segregation of recombinant chromosomes at mitosis produces two daughter cells: A mutant cell bearing two copies of the mutant allele and a wild-type cell containing only the wild-type form of the gene. The cell marker GFP co-segregates with the wild-type gene (dark green cell) and the mutant clones are labeled by the absence of GFP expression (grey cell).

4.2.2 Generation of E(z) mutant cell clones in ovaries of *D. melanogaster*

The FRT/FLP system was used to generate clones that are mutant for the histone methyltransferase Enhancer of zeste (E(z)). E(z) can catalyze three successive methyl transfer reactions via its SET domain to specifically methylate lysine 27 of histone H3 (Jones & Gelbart, 1993; Muller et al., 2002). A recently characterized loss-of-function allele *E(z)*^{731} on a FRT chromosome was used to generate genetic mosaics in the ovary of female flies (Muller et al., 2002). This mutant allele carries a point mutation at position 638 where a tryptophan codon (TGG) is changed to a stop codon (TGA). The clones were induced as described in chapter 3.4.4 and dissected 2 d after the last heat shock.

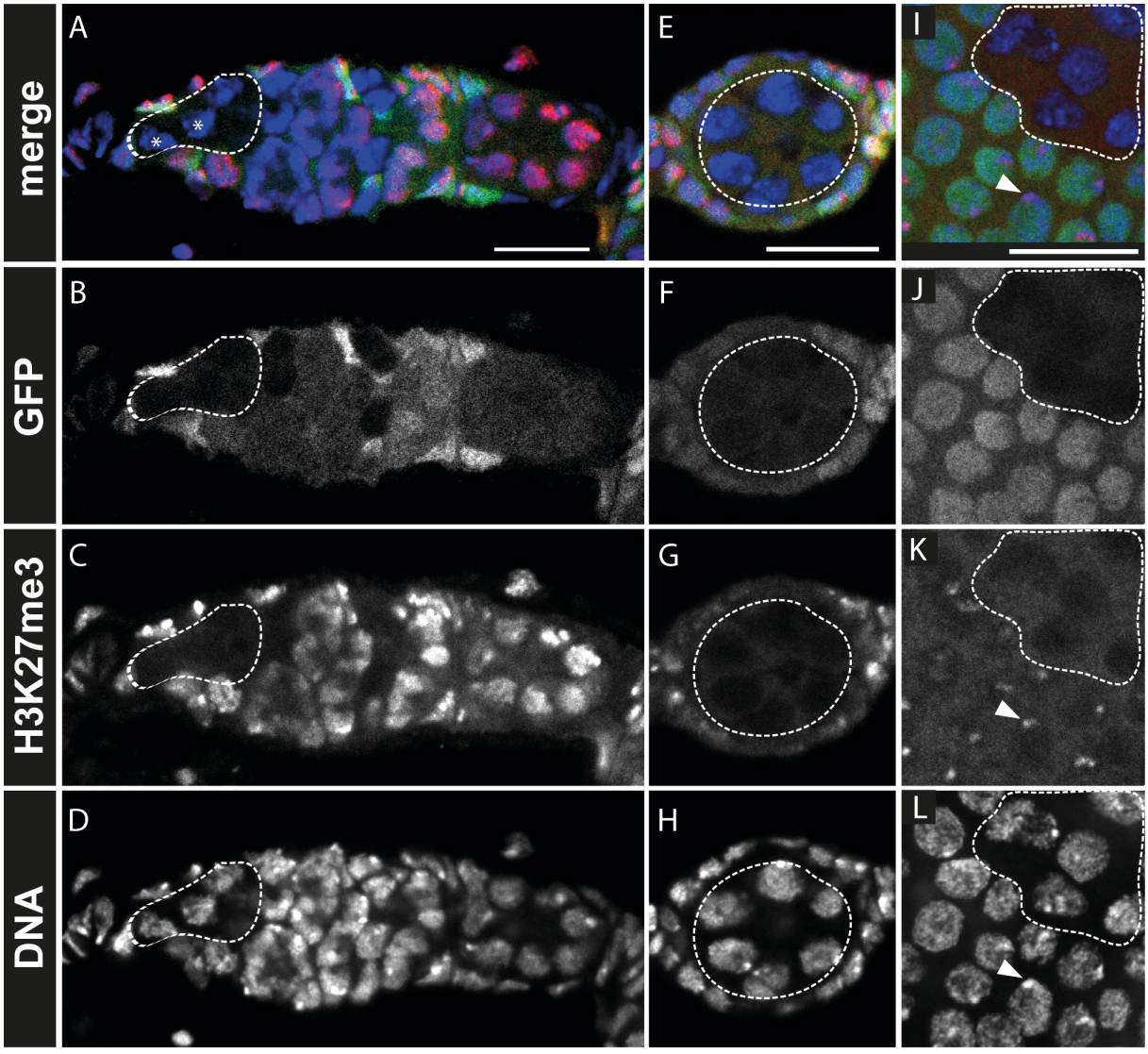

Figure 7: H3K27me3 is downregulated in E(z) mutant germline and somatic cell clones.
The germaria were dissected 2 d after the last heatshock. *E(z)*^{731} mutant cells (dashed lines) were identified by the absence of GFP fluorescence. The tissues were stained for H3K27me3 and DNA. (A-D) In *E(z)*^{731} mutant GSCs (marked by asterisks) no signal for H3K27me3 was detectable. (E-H) In mutant *E(z)*^{731} nurse cells the signal for H3K27me3 was completely abolished. (I-L) In *E(z)*^{731} mutant follicle cells the signal for H3K27me3 was completely absent. In heterozygous cells carrying a wildtype allele of E(z) the signal for H3K27me3 is co-localized with more tightly packed areas of the DNA (marked by arrows). Scale bars represent 10 µm.

E(z) mutant cells were identified by the absence of GFP expression. The loss of E(z) activity correlates with the loss of H3K27me3 staining in the mutant clones. This is true both for GSCs (marked by asterisks in figure 7 A) and for egg chambers with mutant nurse cells (Figure 7 C, G). The H3K27me3 signal is also completely absent in mutant follicle cell clones for E(z) (Figure 7 I, K). Beside being trimethylated H3K27 can be acetylated and the question was whether the loss of the antagonizing mark H3K27me3 has any influence on the distribution of H3K27ac. *In vitro* studies showed that a reduction in H3K27me3 via E(z) RNAi knockdowns in S2 cells results in an increase of H3K27ac (Tie et al., 2009). Thus double stainings were performed to analyze the effect of the E(z) null mutation on the distribution of H3K27ac in the ovary (Figure 8).

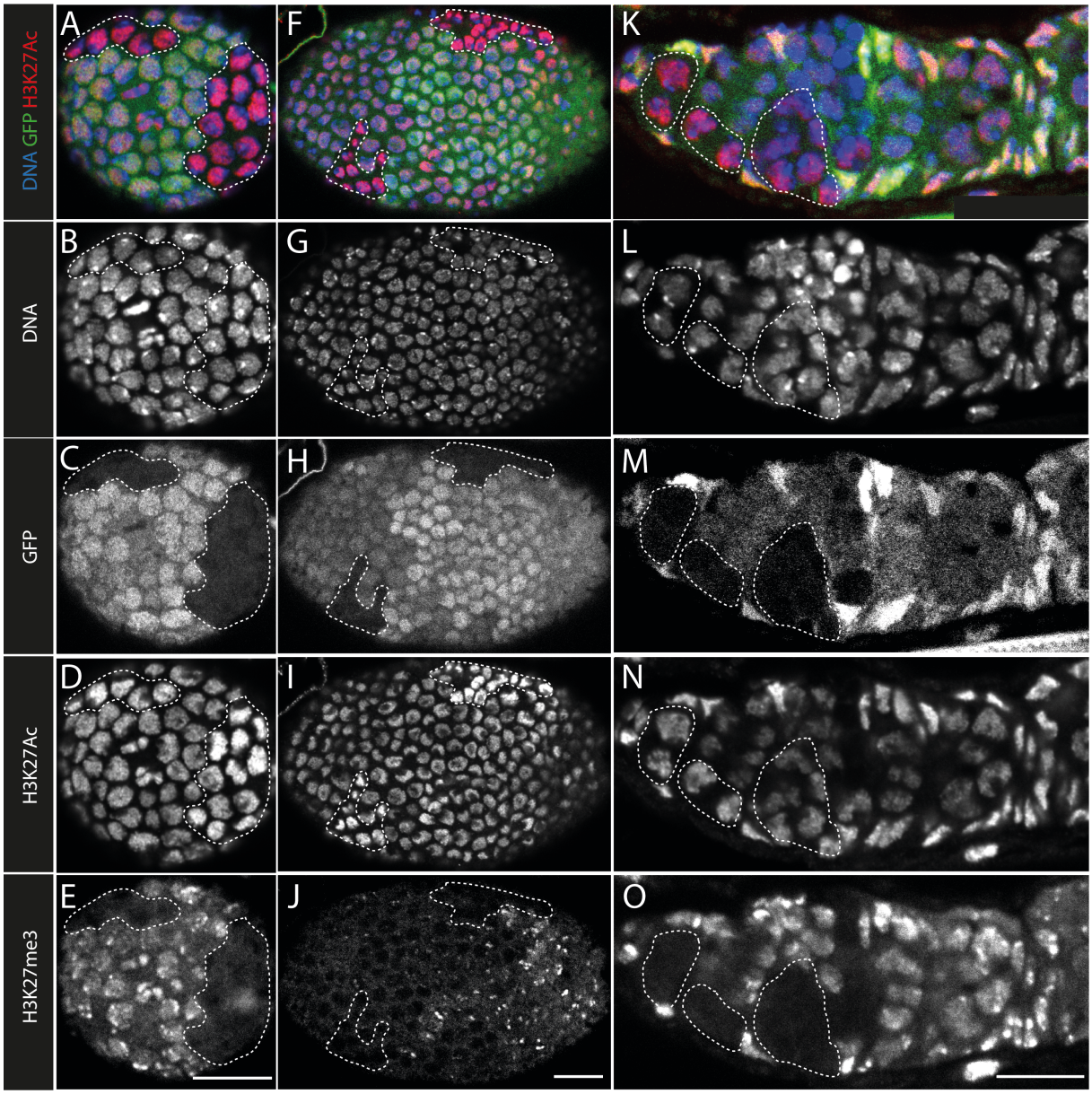

Figure 8: H3K27ac is upregulated in E(z) mutant follicle cell clones.

The ovaries were dissected 2 d after the last heatshock. *E(z)*^{731} mutant cells (dashed lines) were identified by the absence of GFP fluorescence (C, H, M). The tissues were stained for H3K27me3 (E, J, O), H3K27ac (D, I, N) and DNA (B, G, L). (A-E) In *E(z)*^{731} mutant follicle cells of early staged egg chambers the signal for H3K27me3 was completely absent and the signal for H3K27ac is upregulated in most of the cells compared to non-mutant cells. (F-J) In *E(z)*^{731} mutant follicle cells of late staged egg chambers the signal for H3K27me3 is completely absent and the signal for H3K27ac is upregulated compared to non-mutant cells. (K-O) In *E(z)*^{731} mutant germline cells of early staged egg chambers the signal for H3K27me3 is completely absent and the signal for H3K27ac appears to be slightly upregulated. Scale bars represents 10 µm.

In follicle cells of early staged egg chambers the signal of H3K27ac appears to be upregulated in E(z) mutant cells (Figure 8 D). In follicle cells of late staged egg

chambers the signal for H3K27ac appears to be upregulated as well (Figure 8 I). In germline cells in the germarium the signal for H3K27ac seems slightly enriched (Figure 8 N) but the effect was clearly less obvious than in the somatic lineage. Thus, the staining for H3K27ac indeed revealed that H3K27ac is upregulated in E(z) mutant follicle cells compared to neighbouring non-mutant cells. Nevertheless H3K27ac does not appear to spread in heterochromatin as it is still enriched in euchromatin and depleted in heterochromatin which can be distinguished by the overlay of DNA and H3K27ac staining (Figure 8 A, F, K).

4.2.3 Function of E(z) for the maintenance of germline stem cells in the germarium of *D. melanogaster*

The ability for self-renewal and generation of differentiating daughter cells is characteristic of the proliferation of GSCs. To clarify the necessity of E(z) for the maintenance of GSCs, the prevalence of $E(z)^{731}$ mutant GSCs was investigated 2d, 5d and 10d after they were generated (Figure 9). As described before, GSCs were identified by their localization right next to the stem cell niche in the anterior part of the germarium and by HTS staining labeling of the spectrosome. Homozygous $E(z)^{731}$ mutant GSCs were induced in adult female flies through heatshocks, dissected and stained as described in chapter 3.4.4. Homozygous $E(z)^{731}$ mutant GSCs were identified as mutant through the absence of GFP (Figure 9 A, B). The number of GFP negative GSCs was counted for each genotype derived from 3 independent experiments 2d, 5d and 10d after the last heatshock, respectively. The prevalence of mutant GSCs, calculated as the ratio of GFP negative GSCs per germarium, was then compared to non mutant control GSCs that were generated identically but omitting the E(z) mutation (Figure 9 E).

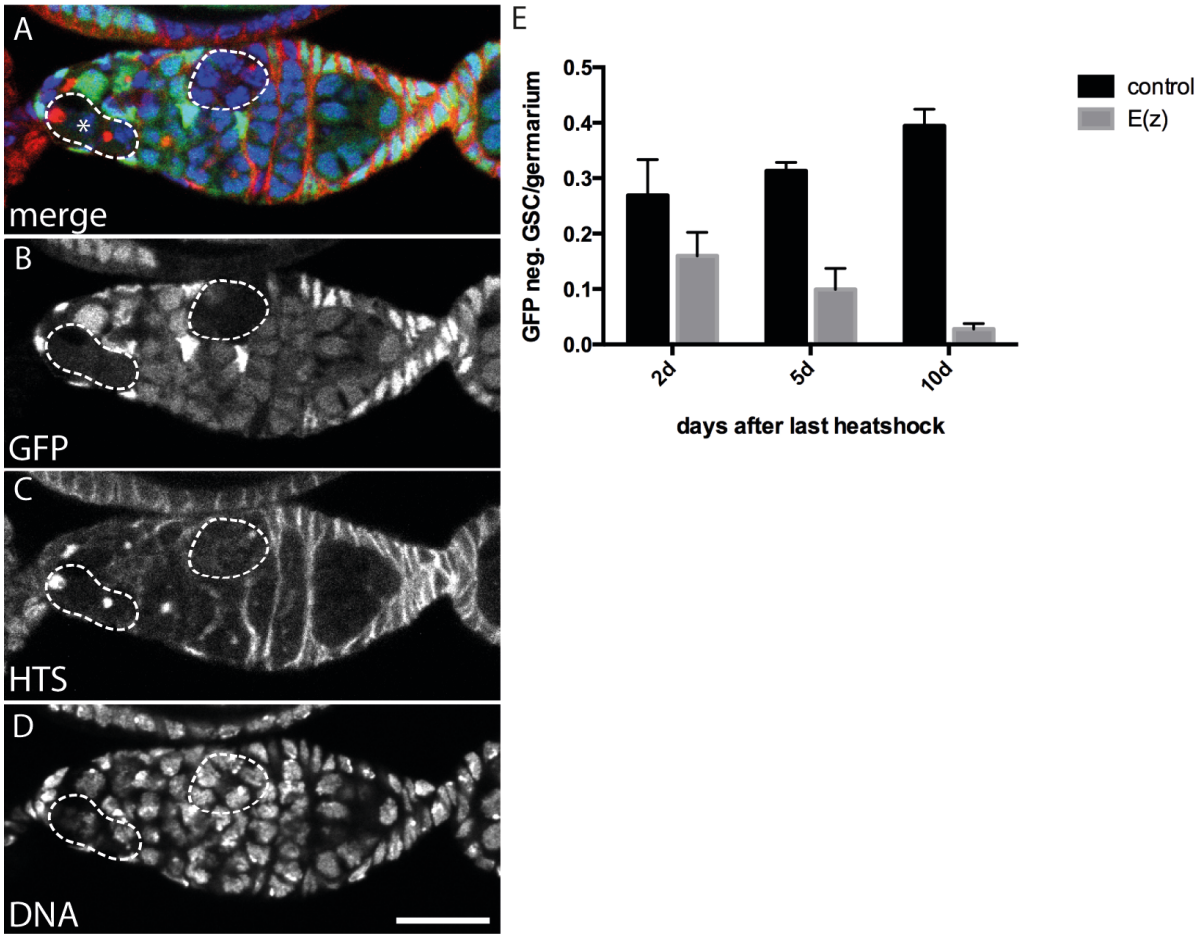

Figure 9: The enzymatical activity of E(z) is necessary for the maintenance of GSCs.
(A-D) Representative confocal image of a germarium of adult female flies 2d after the last heatshock stained for HTS (C) and DNA (D). The identification of *E(z)*^{731} mutant GSCs was performed by the absence of GFP fluorescence (B). A mutant GSCs and a corresponding mutant cyst was marked by dashed lines. The *E(z)*^{731} mutant GSC is marked by an asterisk (A). (E) In stainings 2d, 5d and 10d after the last heatshock the number of homozygous *E(z)*^{731} mutant GSCs was captured as well as the number of control GFP negative GSCs. While the frequency of homozygous *E(z)*^{731} mutant GSCs is decreasing the number of control GSCs remains constant over time. The total number of evaluated germaria carrying the inducible E(z) null mutation was n= 166 (2d after last heatshock), n= 165 (5d) and n= 141 (10d). The numbers of control germaria was n= 160 (2d), n= 163 (5d) and n= 152 (10d). Scale bar in A-D represents 10 µm.

Two days after the last heatshock the number of homozygous *E(z)*^{731} mutant GSCs per germarium is 0.16 ± 0.04 (n=166 germaria). *E(z)*^{731} mutant GSCs per germarium further decline 5d after the last heatshock to 0.09± 0.03 (n=165 germaria). 10d after the last heatshock almost no homozygous *E(z)*^{731} mutant GSCs per germarium are found with 0.02± 0.01 (n=141 germaria). In comparison, the number of GFP negative control GSCs remains stable over time (Figure 9 E). Two days after the last heats-

hock their prevalence is 0.26 ± 0.06 (n=160 germaria), which slightly increases to 0.31 ± 0.01 (n=163 germaria) and 0.39 ± 0.02 (n=152 germaria), by five and ten days after the last heat shock, respectively. This result clearly shows that E(z) is required for the maintenance of GSCs. It is important to mention that the *E(z)*^{731} mutant GSCs do not remain in the stem cell niche but are eliminated from the niche. This might be due to differentiation of the GSCs or to apoptosis of the cells. While investigating the role of E(z) for the function of stem cell maintenance stainings for cleaved Caspase-3 were also performed. Cleaved Caspase-3 is the activated form of Caspase-3 and is a molecular marker for apoptotic cells. In none of the stainings were apoptotic mutant GSCs found (data not shown). Therefore, apoptosis can be excluded as an explanation for the loss of homozygous *E(z)*^{731} mutant GSCs. Although it can not completely ruled out that E(z) mutant cells die in an apoptosis independent way, the results suggest that they are lost from the stem cell niche due to differentiation, which indicates that the activity of E(z) is required for the GSCs to retain their stem cell identity.

4.2.4 Function of E(z) for the maintenance of follicle stem cells in the germarium of *D. melanogaster*

Apart from GSCs there is another stem cell system in the ovaries of the fly. Responsible for the formation of somatic follicle cells in the germarium are follicle stem cells (FSCs) (Lin & Spradling, 1993). FSCs divide and give rise to follicle cells which terminally differentiate after a couple of divisions. The FCs encapsulate the 16-cell cysts in region 2 of the germarium and generate the follicle epithelium which covers the egg chambers. FCs finish their proliferation in stage 5 of oogenesis and become polyploid (Lin & Spradling, 1993). It was shown recently that there are exactly two FSCs at opposite sides at the border of region 2A and 2B in the germarium (Nystul & Spradling, 2010). FSCs have a triangular or oval shaped nucleus that can be distinguished from nuclei of escort cells, which are somatic cells that are coating germline cysts in the germarium. The FSCs and their niche remain fixed at specific positions in the germarium, despite the highly dynamic activities within this region including the constant passage and inward movement of cysts and the alternate migration of FSC daughters from the two niches. There are several ways that FSCs may maintain their positions in this dynamic environment. First, FSCs may be anchored in place through cell adhesion to adjacent escort cells. ß-Catenin and E-Cadherin, two principle com-

ponents of epithelial cell adherens junctions, have previously been shown to be important for FSC maintenance (Song et al., 2004). Secondly, the FSCs may gain stability through transient cell-cell contacts with their own daughter cells (Nystul & Spradling, 2007). It was also shown recently that long-range signals from the CCs and TFs are necessary for the maintenance of FSCs (Yamashita, 2010). Analogous to the experiments in the germline homozygous $E(z)^{731}$ mutant cells were generated and the influence of the mutation was investigated for its role in the maintenance of FSCs (Figure 10). For this purpose recombination was induced and the ovaries were dissected 5d, 10d, 15d and 20d after the last heat shock and the fixed samples were stained for Vasa (Figure 10 C) and Fas-3 (Figure 10 D). Vasa is a protein that specifically marks germline cells (Liu, Han, & Lasko, 2009). Fasciclin-3 (Fas-3) is a transmembrane protein of the cell membrane of FCs and acts as a cell adhesion molecule (Snow, Bieber, & Goodman, 1989), however it is absent from FSCs. FSCs can be identified by these two stainings as these are the cells that do not show any staining of Vasa and Fas-3. In addition to this, their unique triangular shape and their cellular location at the border of region 2A and 2B in the germarium allow them to be clearly identified. A $E(z)^{731}$ mutant follicle stem cell is shown in figure 10 A-E as marked by an arrowhead. The FSC is negative for Vasa staining (Figure 10 C) as well as negative for Fas-3 staining (Figure 10 D) and has a triangular shape.

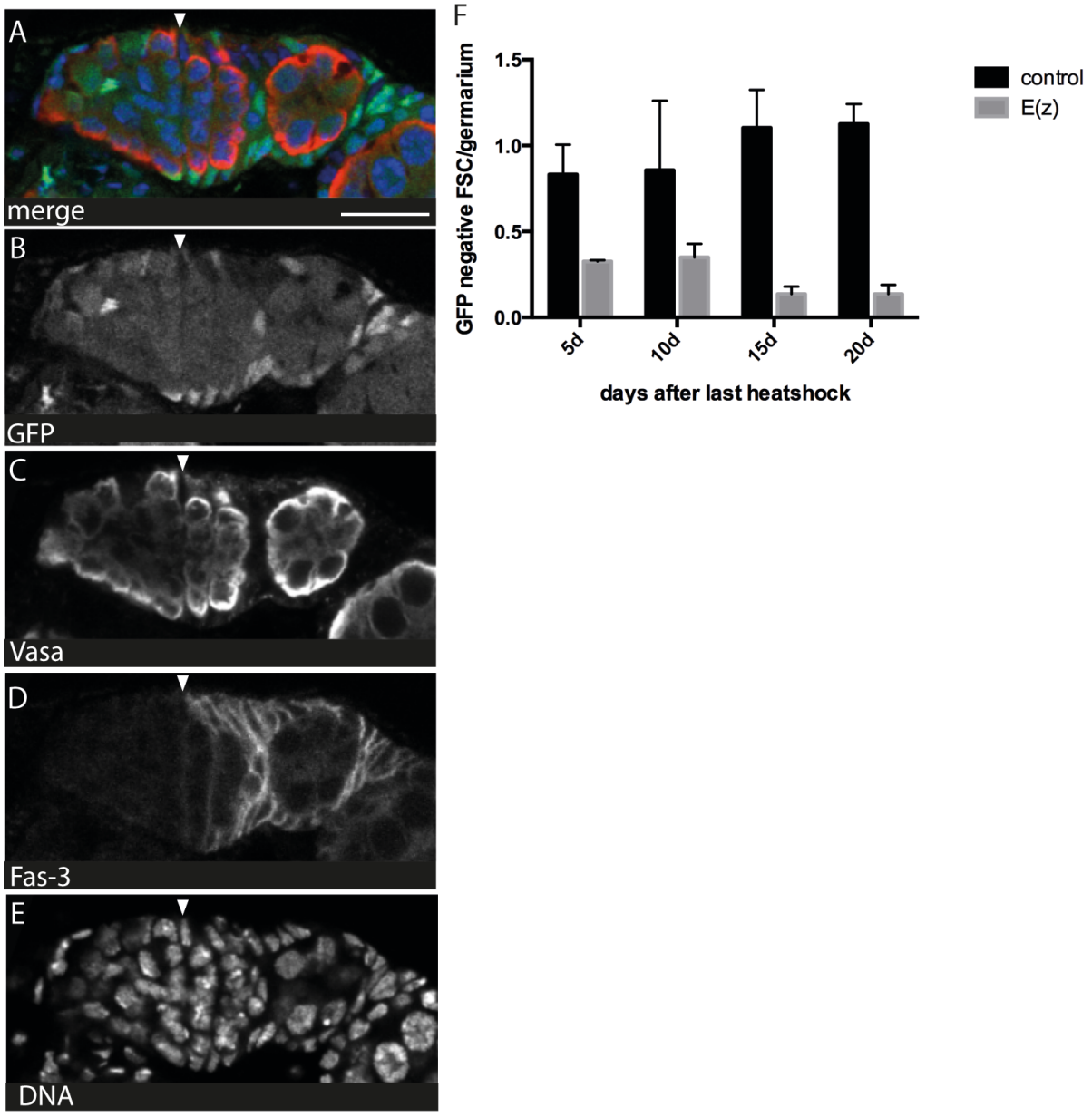

Figure 10: Enzymatical activity of E(z) is necessary for the maintenance of FSCs

(A-E) Representative confocal images of a germarium of an adult female fly 5 d after the last heatshock stained for Vasa (C), Fas-3 (D) and DNA (E) are shown. *E(z)*^{731} mutant FSCs were identified by the absence of the GFP fluorescence (B). A mutant FSCs is marked by an arrowhead. (F) In stainings 5d, 10d, 15d and 20d after the induction the number of homozygous *E(z)*^{731} mutant FSCs was captured as well as the number of control GFP negative FSCs. While the frequency of homozygous *E(z)*^{731} mutant FSCs decreases, the number of control GSCs remains constant over time. Total number of evaluated E(z) germaria was n= 135 (5d after last heatshock), n= 129 (10d), n= 125 (15d) and n= 137 (20d). The total number of control germaria was n= 151 (5d), n= 138 (10d), n= 139 (15d) and n= 136 (20d). Scale bar represents 10 µm.

Similar to previous experiments, the numer of mutant stem cells per germarium was investigated (Figure 10 F). Five days after the last heatshock the number of homozygous *E(z)*^{731} mutant FSCs per germarium is 0.32 ± 0.007 (n= 135 germaria). Ten days after the last heatshocks this number stays more or less constant with 0.35 ± 0.08 (n= 129 germaria) homozygous *E(z)*^{731} mutant FSCs per germarium. *E(z)*^{731} mutant FSCs are reduced by half 15d after the last heatshock with 0.13 ± 0.04 (n= 125 germaria) homozygous *E(z)*^{731} mutant FSCs per germarium. At 20d after the last heatshock this number stays more or less the same with 0.13 ± 0.05 (n= 137 germaria) homozygous *E(z)*^{731} mutant FSCs per germarium. In comparison, the number of GFP negative control FSCs even slightly increases over time. Therefore, this result shows that the activity of E(z) is also necessary for the maintenance of somatic follicle stem cells. In conclusion, the activity of E(z) seems to be a general factor required for the maintenance of different stem cell types in the ovary of *D. melanogaster*.

4.2.5 Function of Su(z)12 for the maintenance of stem cells in the germarium of *D. melanogaster*

Analogous to the experiments investigating the role of E(z) for the maintenance of germline stem cells in *D. melanogaster*, the role of Su(z)12, another subunit of the PRC2 complex, was investigated. For these experiments the allele *Su(z)12*^{4}*,* caused by a base substitution changes the codon for Glycine at position 274 into a codon for Aspartic Acid, was used (Birve et al., 2001). Animals that are homozygous for *Su(z)12*^{4} die during the first or second larval instar. The most notable phenotypes of *Su(z)12* mutants are strong homeotic transformations caused by the widespread misexpression of several Hox genes in embryos and in larvae (Birve et al., 2001; S. Chen, Birve, & Rasmuson-Lestander, 2008). The FRT/FLP system was used to generate clones that are mutant for the PRC2 subunit Su(z)12. The clones were induced as described under chapter 3.4.4 and dissected 2 d after the last heat shock.

In Su(z)12 mutant cell clones the signal for H3K27me3 is completely abolished in GSCs, cysts and follicle cells (Figure 11).

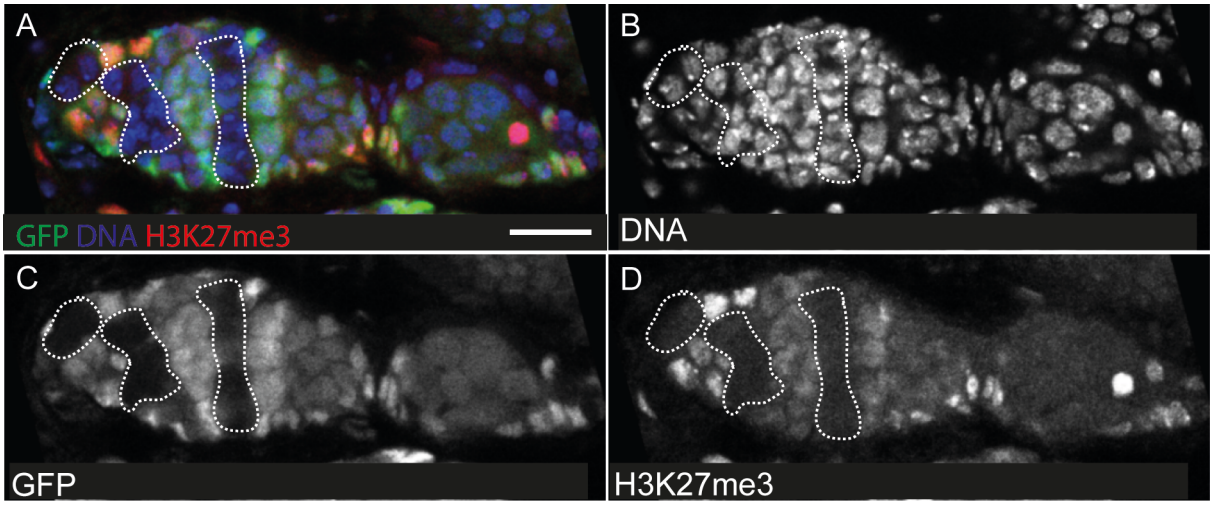

Figure 11: H3K27me3 is downregulated in Su(z)12 mutant germline and somatic cell clones.
The germaria were dissected 2 d after the last heatshock. *Su(z)12*^{4} mutant cells (dashed lines) were identified by the absence of GFP fluorescence. The tissues were stained for H3K27me3 and DNA. In *Su(z)12*^{4} mutant GSCs, cysts and follicle cells no signal for H3K27me3 was detectable. Scale bars represent 10 µm.

Next the function of Su(z)12 activity for the maintenance of GSCs was investigated. Recombination to generate mutant clones in adult female flies was induced through heatshocks and the ovaries were dissected 2d, 5d and 10 d after the last heatshock. Homozygous *Su(z)12*^{4} mutant GSCs were identified as mutant through the absence of GFP and the numbers of mutant GSCs per germarium was calculated. As a control flies carrying a FRT site without any mutations were used.

The control flies were treated the same as *Su(z)12*^{4} flies (Figure 12 A).

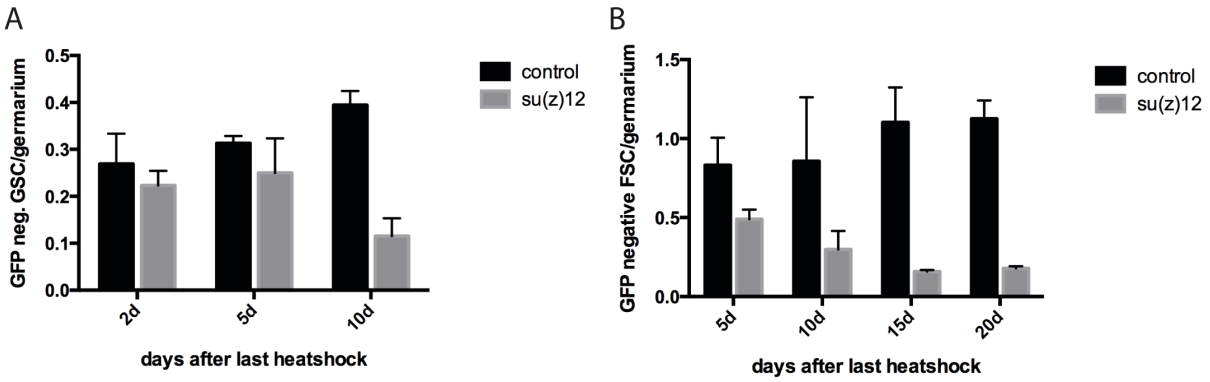

Figure 12: Activity of Su(z)12 is necessary for both the maintenance of GSCs and FSCs.
(A) In stainings 2d, 5d and 10d after the induction of recombination the number of homozygous *Su(z)12*^{4} mutant GSCs was captured as well as the number of control GFP negative GSCs. While the frequency of homozygous *Su(z)12*^{4} mutant GSCs decreases, the number of control GSCs remains constant over time. Total number of evaluated Su(z)12 germaria was n= 153 (2d after last heatshock), n= 135 (5d) and n= 141 (10d). The total number of control germaria was n= 160 (2d), n= 163 (5d) and n= 152 (10d). (B) In stainings 5d, 10d, 15d and 20d after the induction the number of homozygous *Su(z)12*^{4} mutant FSCs was captured as well as the number of control GFP negative FSCs. While the frequency of homozygous *Su(z)12*^{4} mutant FSCs decreases the number of control GSCs remains constant over time. Total number of evaluated Su(z)12 germaria was n= 144 (5d after last heatshock), n= 134 (10d), n= 151 (15d) and n= 145 (20d). The total number of control germaria was n= 151 (5d), n= 138 (10d), n= 139 (15d) and n= 136 (20d).

Two days after the last heatshock the prevalence of homozygous *Su(z)12*^{4} mutant GSCs per germarium is 0.21 ± 0.03 (n= 153 germaria). This number of *Su(z)12*^{4} mutant GSCs stays more or less the same 5d after the last heatshock with 0.25± 0.07 (n= 135 germaria). 10d after the last heatshock the number for *Su(z)12*^{4} mutant GSCs is reduced almost by half with 0.11± 0.01 (n= 141 germaria). In comparison to that the number of control GSCs remained stable over time (Figure 12 A). Two days after the last heatshock the number of control GSCs per germarium is 0.26 ± 0.06 (n= 160 germaria), 0.31 ± 0.01 (n= 163 germaria) by five days and 10 d after the last heatshock the value increased slightly to 0.39 ± 0.02 (n= 152 germaria). Stainings for cleaved Caspase-3 were performed to investigate if the reduced numbers of *Su(z)12*^{4} mutant GSCs was due to apoptosis. In none of the investigated *Su(z)12*^{4} mutant GSCs the staining for cleaved Caspase-3 was positive (data not shown). The re-

duced number of *Su(z)12*^{4} mutant GSCs is most likely not due to apoptosis but instead correlating with an enforced differentiation. Thus, Su(z)12 is also necessary for the maintenance of germline stem cells even though the phenotype is not as drastic as found for *E(z)*^{731} mutant GSCs.

Analogous to the experiments in the germline, I adressed the function of Su(z)12 in the somatic lineage and generated *Su(z)12*^{4} mutant FSCs (Figure 12 B). For this, recombination was induced and the ovaries were dissected 5d, 10d, 15d and 20d after the last heat shock and the fixed samples were stained for Vasa and Fas-3 for proper identification of the FSCs. Five days after the last heatshock the number of homozygous *Su(z)12*^{4} mutant FSCs per germarium is 0.49 ± 0.06 (n= 144 germaria). Ten days after the last heatshocks this numer decreases to 0.30 ± 0.10 (n= 134 germaria) homozygous *Su(z)12*^{4} mutant FSCs per germarium. *Su(z)12*^{4} mutant FSCs are reduced by half at 15d after the last heatshock with 0.15 ± 0.01 (n= 151 germaria) homozygous *Su(z)12*^{4} mutant FSCs per germarium. At 20d after the last heatshock this value stays more or less the same with 0.17 ± 0.01 (n= 145 germaria) homozygous *Su(z)12*^{4} mutant FSCs per germarium. In comparison, the number of control FSCs remains stable over time. Five days after the last heatshock the number of GFP negative control FSCs per germarium is 0.82 ± 0.17 (n= 151 germaria). Ten days after the last heatshock the number of control FSCs per germarium is 0.86 ± 0.4 (n= 138 germaria). 15 d after the last heatshock the value increases to 1.1 ± 0.22 (n= 139 germaria) homozygous GFP negative control GSCs per germarium. This value stays more or less the same at 20 d after the last heatshock with 1.08 ± 0.11 (n= 136 germaria) of homozygous GFP negative control FSCs per germarium. This result shows that the activity of Su(z)12 is necessary for the maintenance of FSCs in the ovary of *D. melanogaster*.

4.3 Characterization of the role of H3T11ph in the germline

The initial antibody based screen (chapter 4.1.2) revealed that the H3T11ph mark similarly to the H3K27me3 mark is highly enriched in GSCs. The only known methylation target of the PRC2 complex is H3K27, this complex is however indirectly required for ubiquitination of H2A via stimulation of the PRC1 complex (H. Wang et al., 2004). Therefore, although there was no evidence that PRC1 could be directly responsible for H3T11 phosphorylation it was conceivable to test whether PRC2 might be functionally required to introduce this phosphorylation on H3T11.

4.3.1 Distribution of H3T11ph in E(z) and Su(z)12 mutant cell clones

The distribution of H3T11ph in *E(z)*^{731} mutant cell clones (Figure 13) and in *Su(z)12*^{4} mutant cell clones (Figure 14) both in germline and somatic cells was investigated. The corresponding tissues were dissected 2 d after the last heatshock and stained for H3T11ph and DNA. In *E(z)*^{731} mutant cell cysts in the germarium (Figure 13 A-D) the signal for H3T11ph is reduced (Figure 13 C, dashed lines). The signal for H3T11ph is decreased in comparison to the staining of H3T11ph in a non-mutant egg chamber. In follicle cells the *E(z)*^{731} mutation also has an effect on H3T11ph as the signal decreases in these somatic cells (Figure 13 I-L). Thus, the null mutation of E(z) clearly has an effect on the phosphorylation level of H3T11 in all cell types of the ovary as the signal is decreased in all E(z) mutant cells.

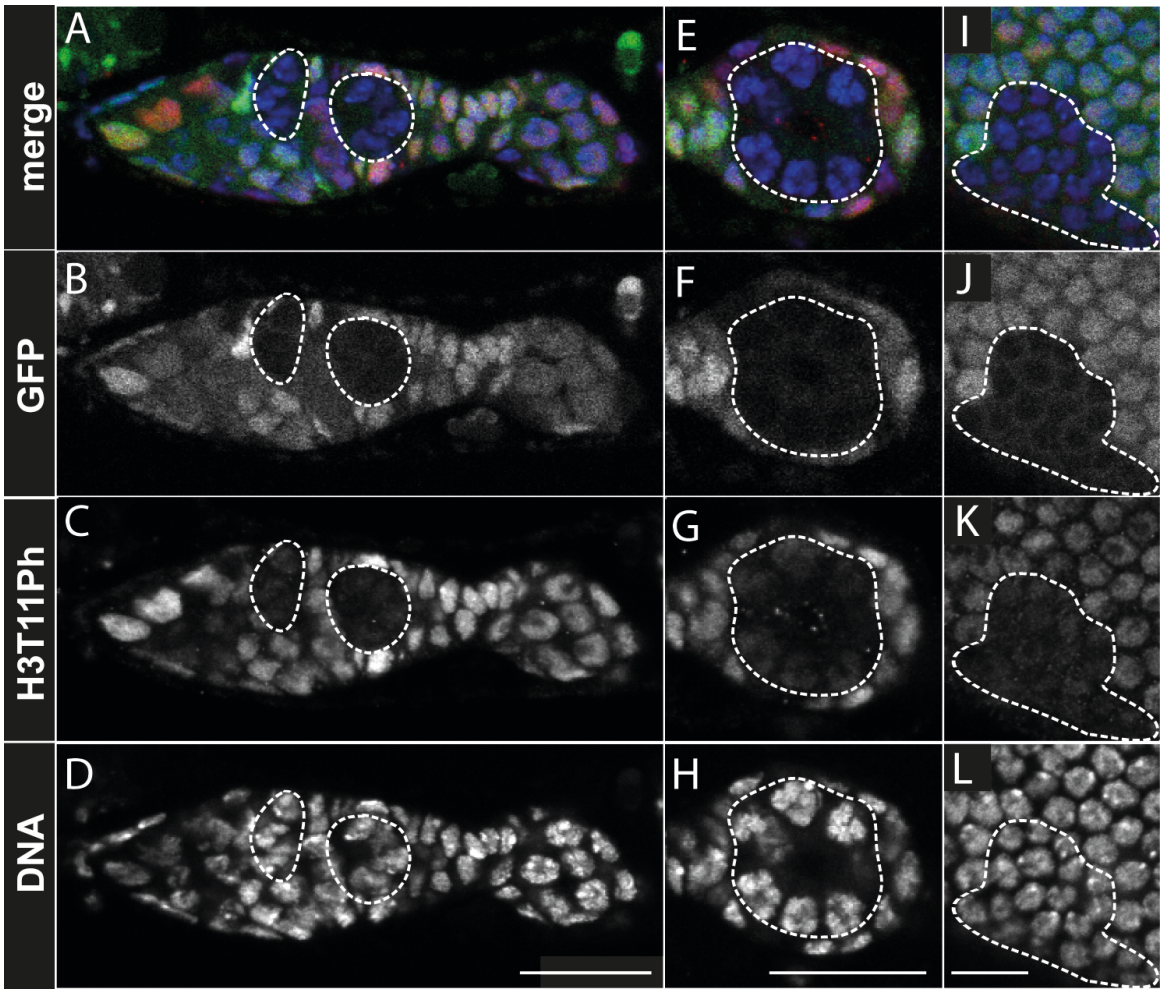

Figure 13: H3T11ph is downregulated in E(z) mutant cell clones.

The germaria were dissected 2 d after the last heatshock. *E(z)*^{731} mutant cell clones (dashed lines) were identified by the absence of GFP fluorescence. The tissues were stained for H3T11ph and DNA. (A-D) A germarium is shown carrying an *E(z)*^{731} mutant cell cyst (dashed lines). In this cell cyst the signal of H3T11ph is reduced in comparison to surrounding non-mutant cysts. (E-H) In the *E(z)*^{731} mutant egg chamber the signal for H3T11ph in nurse cells is reduced in comparison to the staining of H3T11ph in a non-mutant egg chamber shown in figure 10 C. (I-L) The signal for H3T11ph is reduced in follicle cells in comparison to the surrounding non-mutant follicle cells. Shown here are follicle cells that surround an egg chamber in stage 6. Scale bars represent 10 µm.

To investigate if this is an effect due to the inactivity of the PRC2 complex or a E(z)-specific phenotype, the distribution of H3T11ph in *Su(z)12*^{4} mutant cell clones in the ovary was also examined. In *Su(z)12*^{4} mutant cell cysts in the germarium (Figure 14 A-D, dashed lines) the signal for H3T11ph is not affected in comparison to the surrounding non-mutant cell cysts (Figure 14 C).

This is consistent with the signal of H3T11ph in *Su(z)12*^{4} mutant follicle cells (Figure 14 E-H) as in these cells the signal for H3T11ph remains unchanged compared to adjacent non-mutant follicle cells.

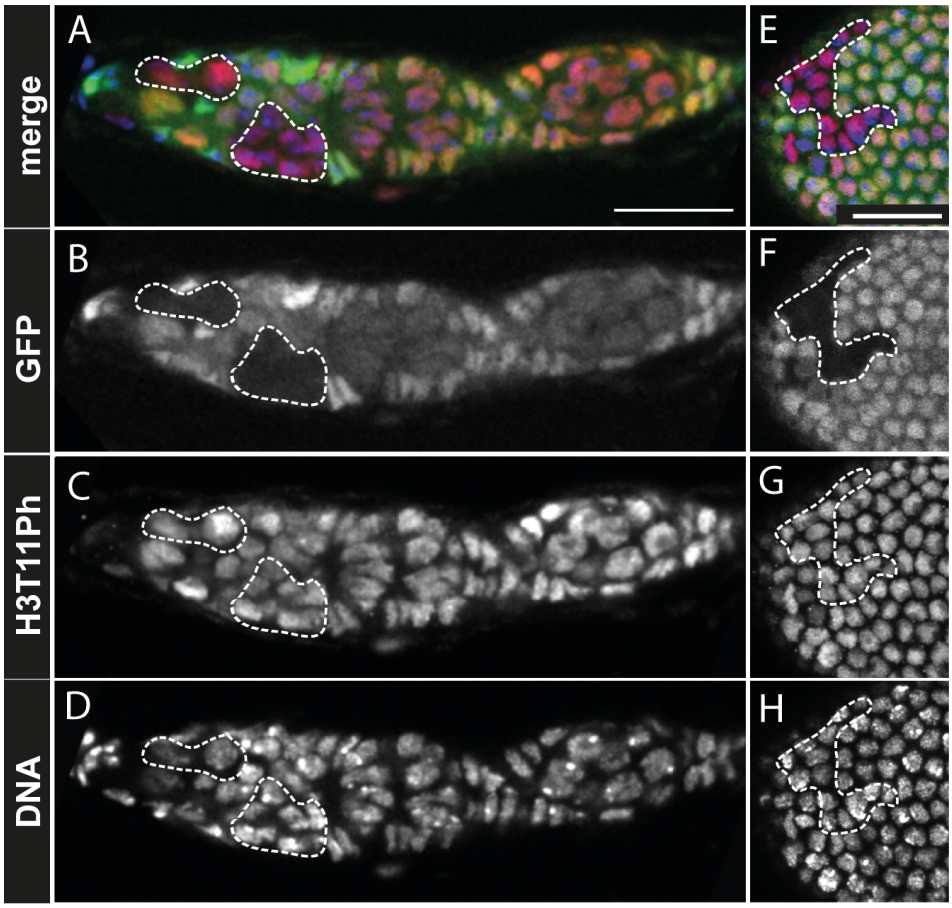

Figure 14: The signal of H3T11ph is not affected in Su(z)12 mutant cell clones.
The germaria were dissected 2 d after the last heatshock. *Su(z)12*^{4} mutant cell clones (dashed lines) were identified by the absence of GFP fluorescence. The tissues were stained for H3T11ph and DNA. (A-D) A germarium is shown carrying two *Su(z)12*^{4} mutant cell cysts (dashed lines). In both cell cysts the signal of H3T11ph is unchanged in comparison to surrounding non-mutant cysts. (E-H) The signal for H3T11ph remains unchanged in follicle cells in comparison to the surrounding non-mutant follicle cells. Shown here are follicle cells that surround an egg chamber in the developmental stage 6. Scale bars represent 10 µm.

4.3.2 Quantification of the signal for H3T11ph in mutant follicle cell clones

To quantify the effect of the mutations *E(z)*^{731} and *Su(z)12*^{4} with regard to the extent of H3T11ph in the ovary, the signal intensity of H3T11ph was quantified in follicle cells (described in detail in chapter 3.4.6). Briefly, mutant cells were identified by the

absence of GFP fluorescence (Figure 15 A-D, dashed outlines) and cells close to the clonal border were used for quantifying flourescence signal. Thereby it was ensured that nuclei from these cells (marked by white and black asterisks) were in the same focal plane. In total 130 *E(z)*^{731} mutant follicle cells and 130 non-mutant follicle cells were quantified resulting from 3 independent experiments each. Genetic mosaics are a perfect system for measuring the signal intensity as the non-mutant cells serve as an internal control. Thus, the detected value for the signal intensity of T11ph in mutant cells could be normalized to the signal of H3T11ph in GFP positive cells. In *E(z)*^{731} mutant follicle cells the signal intensity for H3T11ph is reduced to a value of 48.7 % ± 1.52 compared to non-mutant follicle cells. This result proved to be extremely significant with a p value of p<0.0001 (unpaired t test).

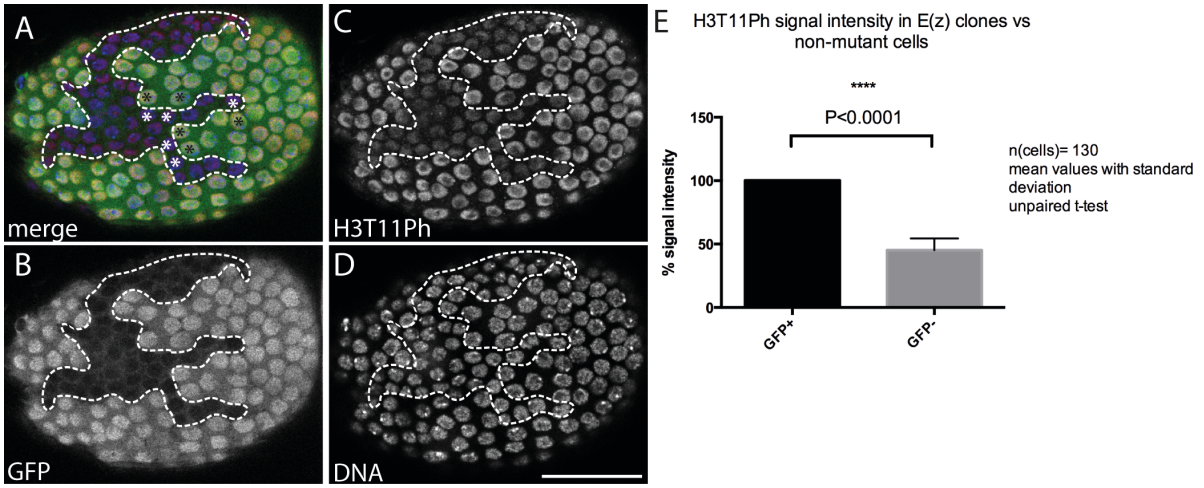

Figure 15: Analysis of the signal intensity of H3T11ph in E(z) mutant follicle cell clones.
(A-D) Representative images of a quantified egg chamber for the signal intensity of H3T11ph are shown. *E(z)*^{731} mutant follicle cells were identified by the absence of GFP fluorescence (B) and are marked by dashed lines. The tissues were stained for H3T11ph (C) and for DNA (D). Quantified *E(z)*^{731} mutant follicle cells are marked by white asterisks and the quantified neighbouring non-mutant follicle cells are marked by black asterisks (A). (E) The signal intensity of H3T11ph is reduced to a value of 48.7% ± 1.52 in *E(z)*^{731} mutant follicle cells compared to non-mutant follicle cells. In total 130 cells were analyzed in *E(z)*^{731} mutant follicle cells and non-mutant follicle cells each. The scale bar in (D) represents 10 µm.

Next the signal intensity of H3T11ph was quantified in *Su(z)12*^{4} mutant follicle cells (Figure 16). In total 132 *Su(z)12*^{4} mutant follicle cells and 132 non-mutant follicle cells were quantified resulting from 3 independent experiments each. In *Su(z)12*^{4} mutant follicle cells the signal intensity for H3T11ph does not change significantly and has a

value of 103.1 % ± 3.21 in comparison to non-mutant follicle cells. An unpaired t test was performed showing that there are no statistically significant differences in the signal intensity for H3T11ph comparing *Su(z)12*^{4} mutant follicle cells to non-mutant follicle cells with a p value of 0.34.

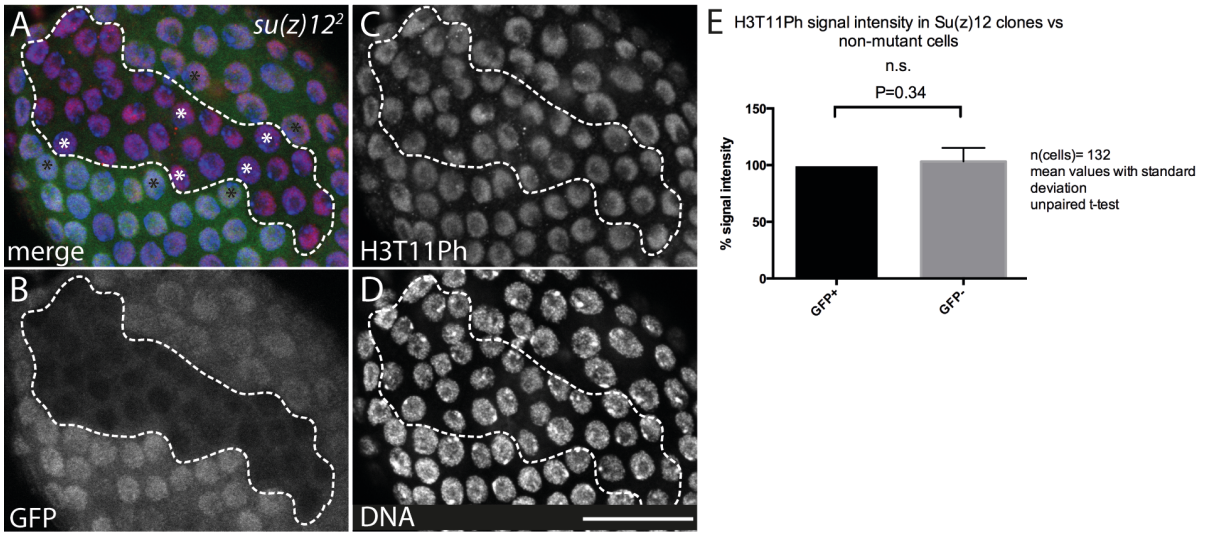

Figure 16: Analysis of the signal intensity of H3T11ph in Su(z)12 mutant follicle cell clones.
(A-D) Representative images of a quantified egg chamber used for the quantification of the signal intensity of H3T11ph are shown. *Su(z)12*^{4} mutant follicle cells were identified by the absence of GFP fluorescence (B) and marked by dashed lines. The tissues were stained for H3T11ph (C) and for DNA (D). Quantified *Su(z)12*^{4} mutant follicle cells are marked by white asterisks and the quantified neighbouring non-mutant follicle cells are marked by black asterisks (A). (E) In *Su(z)12*^{4} mutant follicle cells the signal intensity for H3T11ph does not change significantly and has a value of 103.1 % ± 3.21 in comparison to non-mutant follicle cells. In total 132 cells were analyzed in *Su(z)12*^{4} mutant follicle cells and non-mutant follicle cells respectively. The scale bar in (D) represents 10 µm.

Together these results indicate that E(z) but not Su(z)12 plays a role in the phosphorylation of H3T11, which argues for a novel, PRC2 independent function of E(z). It is noteworthy however that the lack of E(z) activity does not completely abolisch H3T11 phosphorylation, suggesting additional E(z) independent mechanisms involved in H3T11 phosphorylation.

4.4 Replacement of the histone gene complex in *D. melanogaster*

Complementary to mutating enzymes that are responsible for introducing histone modifications it is also possible to mutate modification sites on histones directly (Gunesdogan et al., 2010). In *D. melanogaster* all canonical histone genes are clustered in a single chromosomal locus on chromosome 2. The histone gene complex is composed of 23 histone gene repeat units, each carrying a gene array encoding the five canonical histones (His-GUs) (Gunesdogan et al., 2010). Gunesdogan, *et al.* deleted the entire endogenous histone gene locus and generated a molecularly defined histone null mutation (*His*^{c}). Homozygous His^{c} mutant embryos die during embryogenesis at cell cycle 15. This lethality can be rescued in a dose-dependent manner by introducing wildtype histone gene unit (His-GU) transgenes. Twelve transgenes resulted in a complete rescue as viable and fertile adults are able to develop (Gunesdogan et al., 2010). This experimental system can be used to specifically generate transgenic flies that carry histones with altered modification sites and to address the relevance of this site for the development of the organism. The histone replacement system was used to generate H3T11A and H3K27R transgenes and to investigate their role at the cellular level. Firstly, it was necessary to adapt the histone replacement system to the FLP/FRT system to generate homozygous mutant cell clones in adult flies.

4.4.1 Adapting the histone replacement system to the germline of *D. melanogaster*

The histone replacement system was used to analyze the proliferation of *His*^{C} deficient follicle cell clones carrying transgenes with different numbers of His-GUs and a recently established H3K27R mutation (Pengelly et al., 2013). In this H3K27R mutation the lysine on position 27 of histone H3 was replaced in all His-GUs by an arginine to prevent lysine methylation. To adapt the histone replacement system to the FRT/FLP system in the germline of *D. melanogaster* crosses were set up to obtain flies carrying the *His*^{C} deletion on a FRT chromosome and different numbers of His-GUs on the third chromosome. GFP was used as a marker to identify mutant cell clones. Induction of recombination between the two FRT sites on chromosome 2 of

the flies upon heatshock, led to the generation of mutant clones that lack GFP expression and twin clones which contain two copies of GFP in comparison to the heterozygous population. The clonal populations were analyzed in follicle cells two days after the last heat shock to investigate the complementation of *His*^{c} mutant cells lacking the endogenous histone complex with transgenes encoding histone gene units. It is important to note that a single His-GU contains one gene for each canonical histone expressed from their endogenous promotors, thereby mimicking the expression of endogenous histones. The flies were heatshocked and dissected as described in chapter 3.4.2 and 3.4.4. Histone deficient cells, carrying no His-Gus, were not able to form cell clones, reflecting the requirement of histone synthesis for cell proliferation (Figure 17 A-D). Mutant clones produced by recombination during the heatshock can not proliferate in the absence of histones and most likely die. Mitotic cells exhibit less GFP signal due to the fact that upon disintegration of the nuclear membrane, the nuclear GFP signal gets dispersed in the cytosol. Thus, cells that appear to be GFP negative in figure 17 A and B are mitotic cells which can be proved by the HTS staining showing the disintegration of the nuclear membrane as well as the typical shape of nuclei in anaphase revealed by DNA staining.

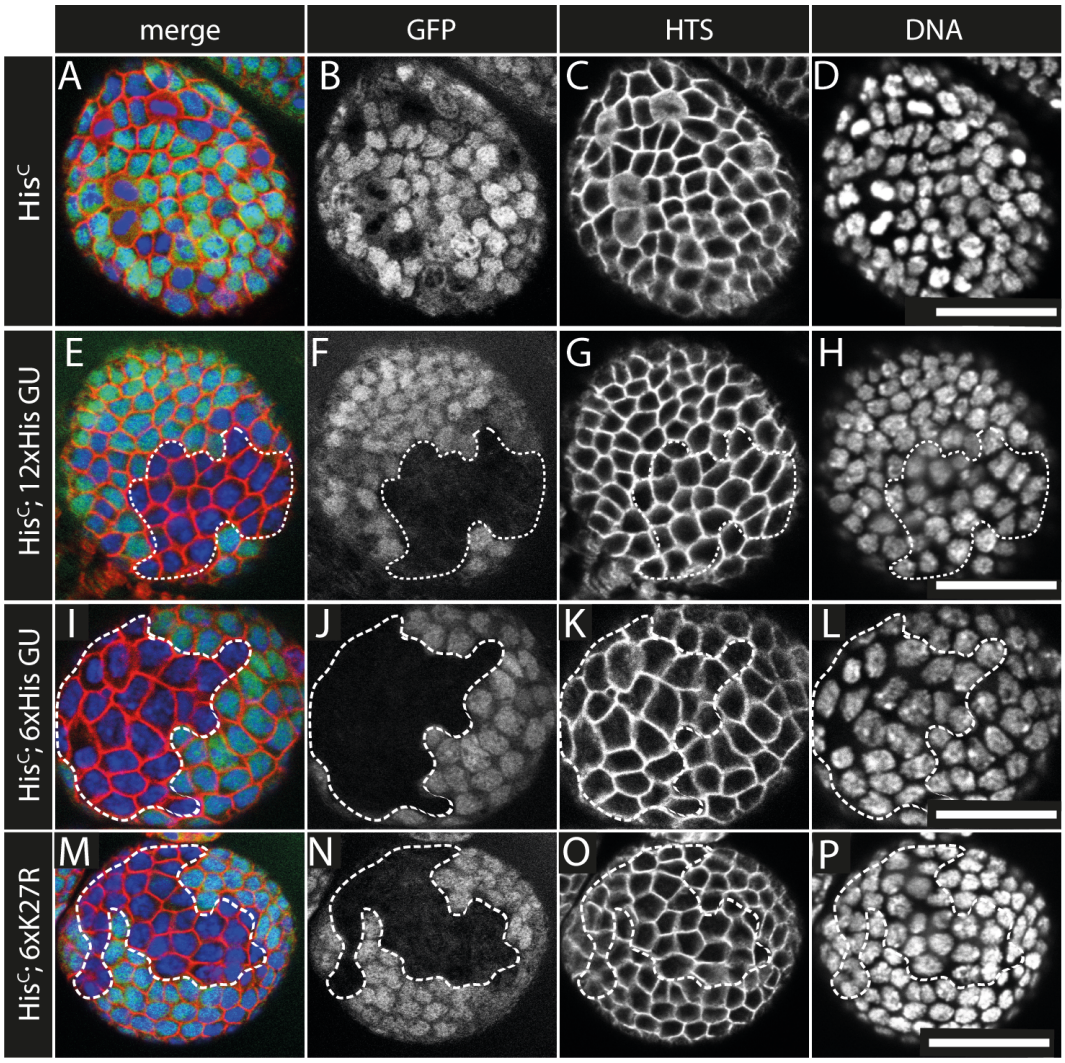

Figure 17: Generation of *His*^{C} mutant somatic cell clones.

Examples of *His*^{C} mutant cell clones induced by recombination using the FLP/FRT system in follicle cells of early staged egg chambers. Mutant clones were identified by the absence of the GFP signal (dashed outlines). The follicle cells were counterstained with HTS to reveal cell boundaries and DNA to reveal the nuclei. The egg chambers were dissected 2 days after the last heat shock. (A-D) Histone deficient mutant clones are not visible in egg chambers of flies that lack any His-GU. (E-H) Mutant clones that are deficient for endogenous histones but are complemented with 12 His-GUs survive and proliferate. (I-L) Mutant clones complemented with six His-GUs survive and proliferate. (M-P) Mutant clones complemented with six His-GUs bearing the H3K27R mutation respectively are visible. The scale bars represent 10 µm.

In histone deficient cells that are complemented with 12 His-GUs, the mutant cell populations are visible as large clones (Figure 17 E-H, dashed lines) as 12 transgenic His-GUs sufficiently complement the histone deficiency allowing them to survive and to proliferate. In histone replacement experiments published previously, twelve His-GUs have been shown to overcome the histone deficiency and produce viable, fertile adult flies with no morphological or developmental defects (Gunesdogan et al., 2010). To test whether fewer His-GUs can also suffice to overcome the histone deficiency in mutant follcile cell clones, mutant cells were analyzed that have only 6 His-GUs to complement the histone deficiency. The analysis of follicle cells in these flies revealed the presence of mutant cell clones (Figure 17 I-L, dashed lines) that are comparable to mutant cells bearing 12 His-GUs. This indicates that 6 His-GUs are sufficient for adult follicle cells to survive and proliferate. To study whether the H3K27R mutation plays a role in cellular proliferation, cells were analyzed that are complemented with 6 His-GUs carrying the H3K27R mutation respectively. These cells should express histones at a level high enough that adult cells can survive and proliferate, but the H3 synthesized in these cells carries the K27R mutation. This eliminates the deposition of any PTMs on this residue. The analysis in follicle cells reveals the presence of mutant clones in these flies as well (Figure 17 M-P, dashed lines) indicating that the PTMs on H3K27 are not essential for survival and proliferation of somatic follicle cells in the ovaries of *D. melanogaster*.

4.4.2 Complementation of the *His^{C}* deletion with 6xK27R histone transgenes

To check whether the replacement of the histone complex deficiency with 6 His-GUs bearing the K27R mutation really abolishes the PTMs on H3K27, stainings for H3K27me3 and the antagonizing histone mark H3K27ac were performed (Figure 18).

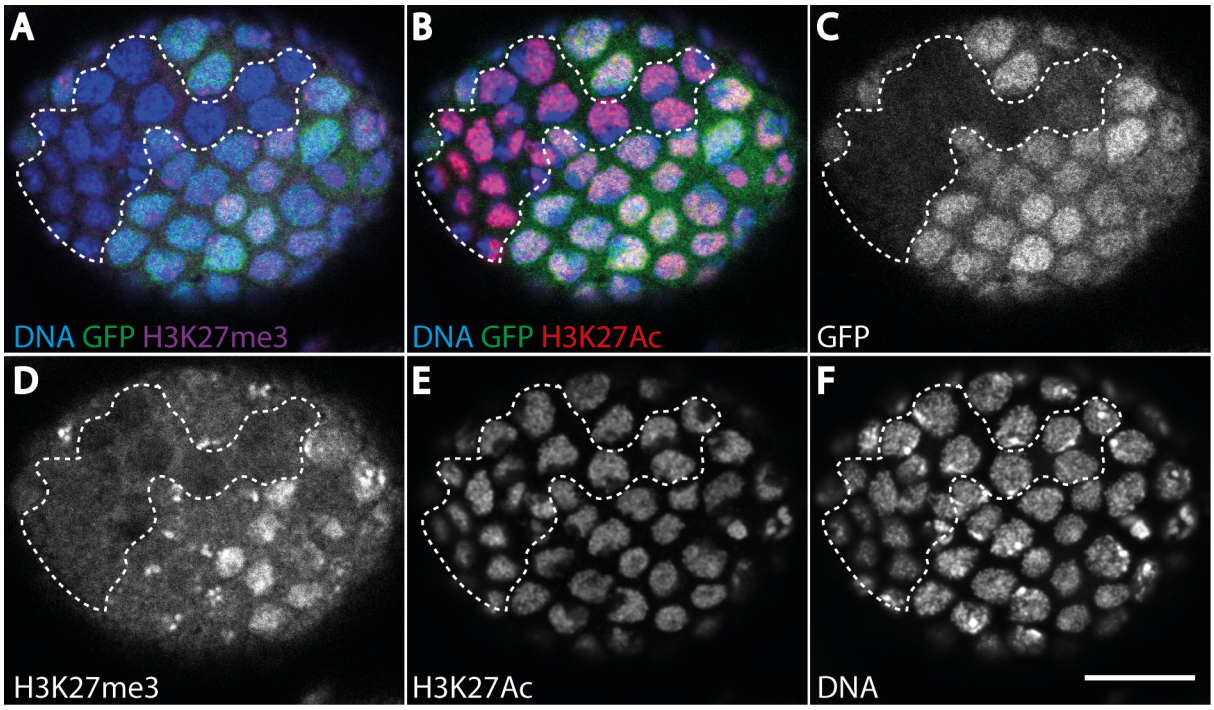

Figure 18: The signal for H3K27me3 is absent and the signal for H3K27ac is still present in *His^{C};6xK27R* mutant cell clones.

The egg chambers were dissected 2 d after the last heatshock. *His^{c}; 6xK27R* mutant cell clones (dashed lines) were identified by the absence of GFP fluorescence (C). The tissues were stained for H3K27me3 (D), H3K27ac (E) and DNA (F). (A) Shown is an overlay of H3K27me3, DNA and GFP. In *His^{c}; 6xK27R* mutant follicle cells of early egg chambers the signal for H3K27me3 is absent compared to the surrounding non-mutant cells. (B) Shown is an overlay of H3K27ac, DNA and GFP. In *His^{c}; 6xK27R* mutant follicle cells of early egg chambers the signal for H3K27ac is still present and shows the same signal intensity compared to neighbouring non-mutant cells. Scale bar in F represents 10 µm.

Recombination was induced in *His^{c}; 6xK27R* flies and the egg chambers were dissected and stained 2 d after the last heatshock. Mutant cell clones were identified due to the absence of GFP (Figure 18 C). The staining for H3K27me3 (Figure 18 A and D) revealed that the signal for H3K27me3 was indeed absent in *His^{c}; 6xK27R* clones.

However the staining for H3K27ac (Figure 18 B and E) showed that the signal for H3K27ac was still present in *His^{c}; 6xK27R* clones.

The histone replacement system, as outlined above, completey replaces the canonical, replication dependent histones by the respective transgene derived versions. However, in addition to the replication dependent histones flies express variant histones that are encoded by genes outside the histone gene complex. It is known that the deposition of the H3 variant protein, H3.3, takes place in nucleosomes of euchromatin at actively transcribed genes in the fly (Ahmad & Henikoff, 2002). Accordingly, the H3.3 variant carries predominantly histone marks that are associated with gene activation, such as acetylation marks and H3K4me3, whereas marks associated with gene silencing such as H3K27me3 and H3K9me3 are predominantly found on the replication dependent canonical histone H3 (Hake et al., 2006). Thus, the remaining presence of H3K27ac in *His^{c}; 6xK27R* clones might be due to the H3K27ac mark on the histone variant H3.3. In order to test this hypothesis I generated cell clones that additionally to the H3K27R mutation in H3, lacked expression of H3.3. These results are sumarized in chapter 4.5.2.

4.4.3 Quantification of the H3T11ph signal in *His^{C}; 6xK27R* mutant follicle cell clones

Even without additional deletion of the variant histone H3.3, my data as well as published data indicate, that H3K27R mutation in the canonical histone H3 alone is sufficient to abrogate modification of H3K27me3. Therefore, I adressed the signal intensity of H3T11ph in cell clones mutant for H3K27R. Histone deficient cells complemented with 6 His-GUs carrying the H3K27R mutation were stained with an H3T11ph antibody and analyzed as described in 3.4.6 (Figure 19). Quantified *His^{c},6xK27R* mutant follicle cells are marked by white asterisks and the quantified neighbouring non-mutant follicle cells are marked by black asterisks. In total the signal intensity of H3T11ph in 74 *His^{c},6xK27R* mutant follicle cells and 74 non-mutant follicle cells was quantified resulting from 3 independent experiments respectively. The detected value for the signal intensity of T11ph in mutant cells was normalized to the signal intensity of H3T11ph in GFP positive non mutant cells. In *His^{c}; 6xK27R* mutant follicle cells the signal intensity for H3T11ph does not change significantly and has a value of 100.2 % ± 5.7 in comparison to non-mutant follicle cells. In control experiments the signal

intensity of H3T11ph was assayed in *His^{c}; 6xHis-GUs* cells (Figure 19 F). Here the signal intensity of H3T11ph remained unchanged compared to non-mutant neighbouring cells with a value of 104.4 % ± 3.9.

In these experiments 94 *His^{c}, 6xHis-GUs* mutant follicle cells and 94 non-mutant follicle cells were quantified in regard to the H3T11ph signal intensity.

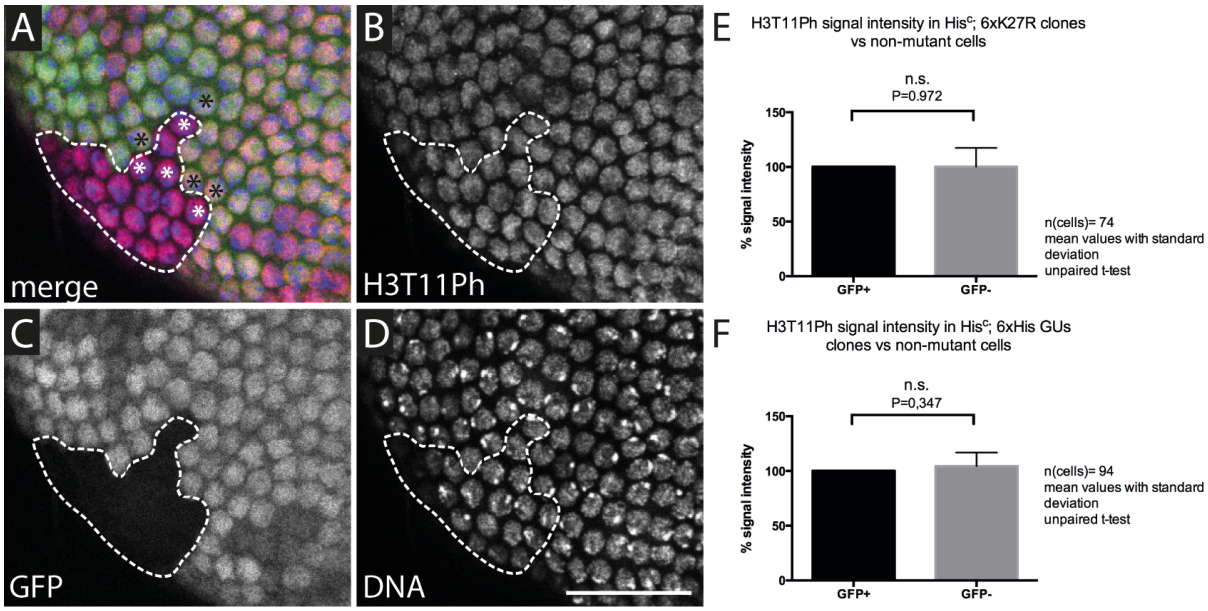

Figure 19: The signal of H3T11ph is not affected in *His^{C}; 6xK27R* and *His^{C}; 6xHis-GUs* mutant follicle cell clones.

(A-D) Representative images of an egg chamber for the quantification of the signal intensity of H3T11ph are shown. *His^{c}, 6xK27R* mutant follicle cells are identified by the absence of GFP fluorescence (C) and marked by dashed lines. The tissues were stained with an antibody against H3T11ph (B) and with DAPI for visualisation of DNA (D). Quantified *His^{c}; 6xK27R* mutant follicle cells are marked by white asterisks and the quantified neighbouring non-mutant follicle cells are marked by black asterisks (A). (E) In *His^{c}; 6xK27R* mutant follicle cells the signal intensity for H3T11ph does not change at all and has a value of 100.2 ± 5.7 in comparison to non-mutant follicle cells. 74 cells were analyzed in *His^{c},6xK27R* mutant follicle cells and in non-mutant follicle cells respectively. (F) In *His^{c}; 6xHis-GUs* mutant follicle cells the signal intensity for H3T11ph does not change at all and has a value of 104.4 % ± 3.9 in comparison to non-mutant follicle cells. 94 cells were analyzed in *His^{c}; 6xHis-GUs* mutant follicle cells and non-mutant follicle cells respectively.The scale bar represents 10 µm.

4.4.4 Generation and characterization of H3*T11A* transgenic fly lines

Next, transgenic fly lines were generated that carry His-GUs in which threonine at position 11 on histone H3 (H3T11) was altered to an alanine (H3T11A). Thus, in

animals carrying the histone complex deletion complemented with His-GUs carrying T11A, the signal for the phosphorylation of H3T11 should be abolished. The fly strains were generated using the Multisite Gateway System as described under 3.1.14. Flies were generated carrying 6 His-GUs with the H3T11A mutation as 6 His-GUs seem to be enough for adult follicle cells to survive and to proliferate (see chapter 4.4.1). Recombination was induced, the egg chambers were dissected 2 d after the last heatshock and stained for H3T11ph (Figure 20). Overall, *His^{c}; 6xT11A* mutant follicle cell clones were small and found rarely. Surprisingly, the signal for H3T11ph was still present in *His^{c}; 6xT11A* mutant follicle cell clones and showed no change in signal intensity compared to the surrounding non-mutant cells. This observation is reminiscent of what was found in case of H3K27ac modification and suggests that H3T11ph could be a mark that is deposited on H3.3. Therefore, for the investigation of the T11A mutation it was necessary to generate fly stocks that in addition to the *His^{c}* deletion carry deletions of both genes that encode H3.3.

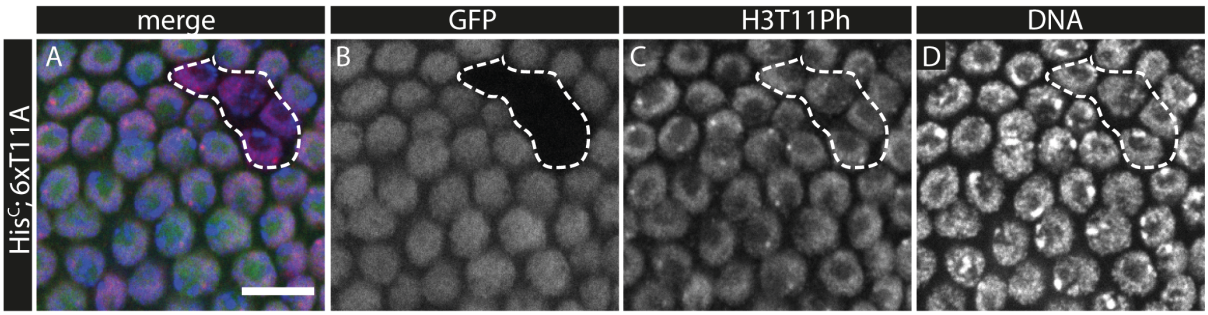

Figure 20: In *His^{c}; 6xT11A* mutant follicle cell clones the signal of H3T11ph is still present.
Egg chambers were dissected 2 d after the last heatshock. Mutant cell clones (dashed lines) were identified by the absence of GFP fluorescence (B). The tissues were stained for H3T11ph (C) and DNA (D). (A-D) In *His^{c}; 6xT11A* mutant follicle cells of egg chambers at stage 6 the signal for H3T1Ph is still present, and the signal intensity appears to be unchanged compared to surrounding non-mutant cells. *His^{c}; 6xT11A* mutant follicle cell clones are small and seem to have a proliferation deficit. Scale bar represents 10 µm.

4.5 Generation of *His^{C}* mutant cell clones in the absence of H3.3

The variant histone H3.3 is synthesized in a replication-independent manner and has been shown to replace canonical H3 at actively transcribed genes in *D. melanogaster* (Ahmad & Henikoff, 2002; McKittrick et al., 2004; B. E. Schwartz & Ahmad, 2005; Wirbelauer, Bell, & Schubeler, 2005). As described in chapter 4.4.2 and 4.4.4, in *His^{c}; 6xK27R* and *His^{c}; 6xT11A* mutant cell clones the signal for the histone mark H3K27ac and H3T11ph were still present respectively. For H3K27ac it was already known that this mark is enriched at actively transcribed genes (Garcia et al., 2007; Suka et al., 2001), and for H3T11ph there is also evidence that this mark is enriched at actively transcribed genes (Metzger et al., 2008). Therefore, the next step was to generate flies that carry the histone deletion in conjunction with the deletion of both genes that encode H3.3 (His3.3A on chromosome 2 at position 25C and H3.3B on the X chromosome at position 8C), and secondly to cross these flies to flies carrying six histone gene unit with the K27R mutation (6xHis-GUs.K27R) or with the T11A mutation (6xHis-GUs.T11A) respectively and subsequently check whether the corresponding histone mark is still present or absent.

4.5.1 Cell proliferation of *ΔH3.3; His^{C}; 6xGU* follicle cell clones

Firstly, the proliferation of mutant follicle cells bearing the deletion of both H3.3 genes, the *His^{C}* deletion and six His-GUs (*ΔH3.3; His^{C}; 6xGU*) was analysed to determine whether the additional deletion of H3.3 has any effect on the growth of this cell population (Figure 21).

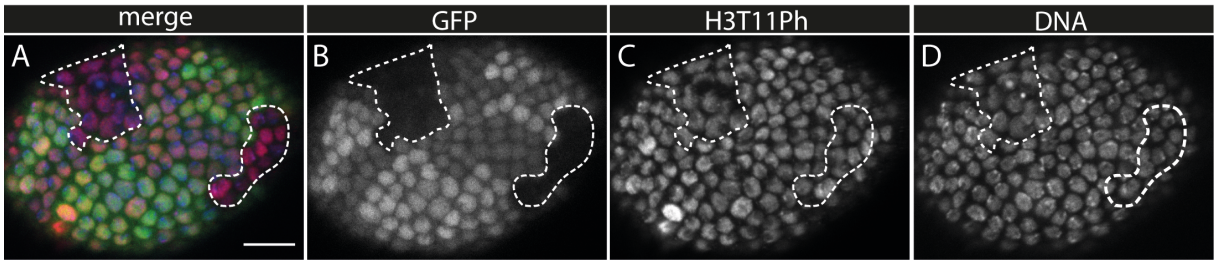

Figure 21: Proliferation of *ΔH3.3; His^{C};6xHis-GUs* follicle cell clones.
The egg chambers were dissected 2 d after the last heatshock. Mutant cell clones (dashed lines) were identified by the absence of GFP fluorescence (B). The tissues were stained for H3T11ph (C) and DNA (D). In *ΔH3.3;His^{c}; 6xGU* mutant follicle cells the signal for H3T11ph is not affected and the cell proliferation is just slightly affected compared to the surrounding twin clone cell clones. Scale bar represent 10 µm.

ΔH3.3; His^{C}; 6xGU mutant follicle cells still proliferate to form cell clones, however they might be slightly affected in their proliferation as the mutant cell clones seem to be smaller compared to their twin clones. Nevertheless, the deletion of H3.3 together with the *His^{C}* deletion can be rescued by 6 His-GU. The signal for H3T11ph appears not be affected in *ΔH3.3; His^{C}; 6xGU* mutant follicle cells clones.

4.5.2 Distribution of H3K27ac in *ΔH3.3; His^{C}; 6xK27R* follicle cell clones

In *His^{C}; 6xK27R* mutant follicle cell clones the signal for H3K27ac is still detectable and remained unchanged compared to surrounding non-mutant follicle cells (see chapter 4.4.2). Thus, clones were induced that additionally lack H3.3 in addition to carrying the H3K27R mtation (*ΔH3.3; His^{C}; 6xK27R*). The ovaries were dissected 2 d after the last heatshock and the presence of *ΔH3.3; His^{C}, 6xK27R* mutant follicle cell clones was investigated (Figure 22).

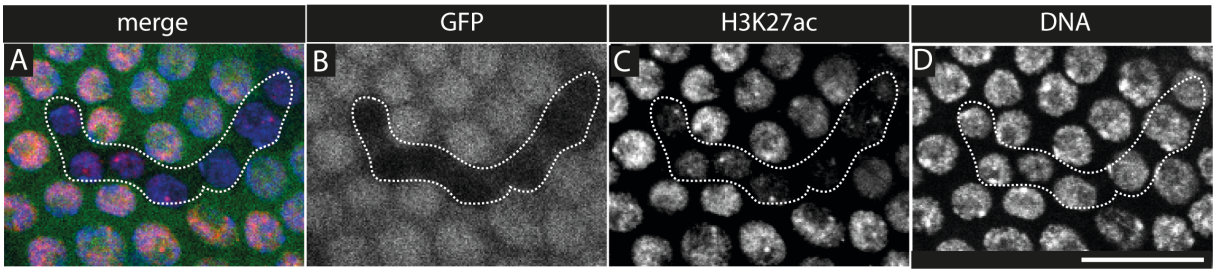

Figure 22: Localization of H3K27ac in *ΔH3.3; His^{C};6xK27R* follicle cell clones.
The egg chambers were dissected 2 d after the last heatshock. Mutant cell clones (dashed lines) were identified by the absence of GFP fluorescence (B). The tissues were stained for H3K27ac (C) and DNA (D). In *ΔH3.3;His^{c}; 6xK27R* mutant follicle cells of early egg chambers the signal for H3K27ac is downregulated and almost completely absent compared to non-mutant cells. Scale bar represents 10 µm.

The signal for H3K27ac (Figure 22 C) in *ΔH3.3; His, 6xK27R* mutant follicle cell clones is decreased and almost not detectable. Thus, indeed K27 on the histone variant H3.3 is able to compensate for the loss of K27 on the canonical histone H3.

4.5.3 Distribution of H3T11ph in *ΔH3.3; His^{C};6xK27R* follicle cell clones

Next, the results from chapter 4.4.3 were challenged by investigating the signal intensity of H3T11ph in *ΔH3.3; His^{C}; 6xK27R* mutant follicle cell clones of early egg chambers (Figure 23).

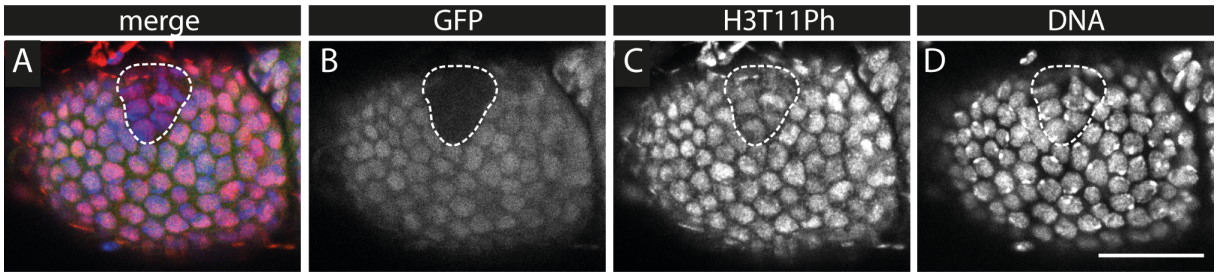

Figure 23: Localization of H3T11ph in *ΔH3.3; His^{C}; 6xK27R* follicle cell clones.
The egg chambers were dissected 2 d after the last heatshock. Mutant cell clones (dashed lines) were identified by the absence of GFP fluorescence (B). The tissues were stained for H3T11ph (C) and DNA (D). In *ΔH3.3; His^{c}; 6xK27R* mutant follicle cells of early egg chambers the signal for H3T11ph is still present and the signal intensity appears to be unchanged compared to non-mutant cells. Scale bar represents 10 µm.

4.5.4 Histone modifications in *ΔH3.3; His^{C}; 6xT11A* follicle cell clones

In *His^{C}; 6xT11A* mutant follicle cell clones the signal for H3T11ph was still detectable and remained unchanged compared to surrounding non-mutant follicle cells (see chapter 4.4.4). To answer the question if H3.3 is able to compensate for the loss of the canonical H3 in regard to the phosphorylation of threonine 11, flies were crossed accordingly. Cell clones were induced, the ovaries were dissected 2 d after the last heatshock and the presence of *ΔH3.3; His^{C}, 6xT11A* mutant follicle cell clones was investigated (Figure 24).

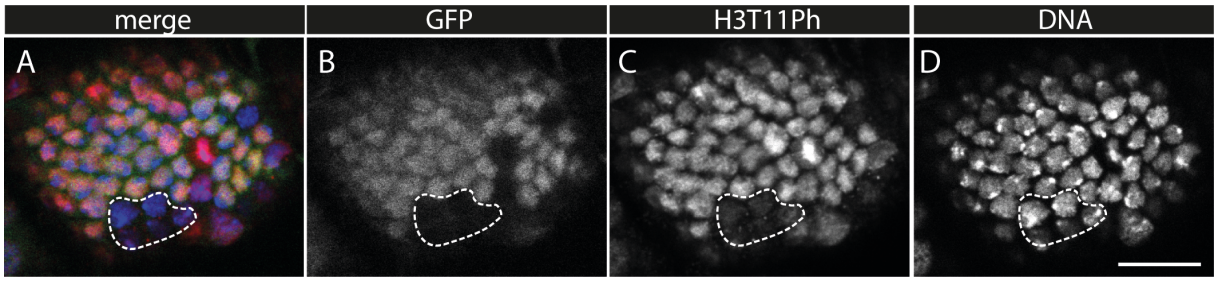

Figure 24: Distribution of H3T11ph in *ΔH3.3; His^{C}; 6xT11A* follicle cell clones.
The egg chambers were dissected 2 d after the last heatshock. Mutant cell clones (dashed lines) were identified by the absence of GFP fluorescence (B). The tissues were stained for H3T11ph (C) and DNA (D). (A-D) In *ΔH3.3; His^{c}; 6xT11A* mutant follicle cells of early egg chambers the signal for H3T11ph is almost completely absent. Scale bar represents 10 µm.

It is worth noting that *ΔH3.3; His,* 6xT11A mutant cell clones are rarely detectable and these clones are small. The signal for H3T11ph (Figure 24 C) in *ΔH3.3; His^{C}, 6xT11A* mutant follicle cell clones is dramatically decreased and hardly detectable. Thus, indeed T11 on the histone variant H3.3 is able to compensate the loss of T11 on the canonical histone H3.

Furthermore the distribution of H3K27me3 was examined in *ΔH3.3; His^{C}; 6xT11A* follicle cell clones. The signal for H3K27me3 is very low in follicle cell clones in late egg chambers around stage 8-10 of oogenesis. In *ΔH3.3; His^{C}; 6xT11A* follicle cell clones of stage 8 egg chambers the signal for H3K27me3 is highly increased (Figure 25). The DNA in these *ΔH3.3; His^{C}; 6xT11A* follicle cell clones is more condensed compared to surrounding non-mutant cells (Figure 25 D). In follicle cell clones of earlier egg chambers this effect was not detected (data not shown).

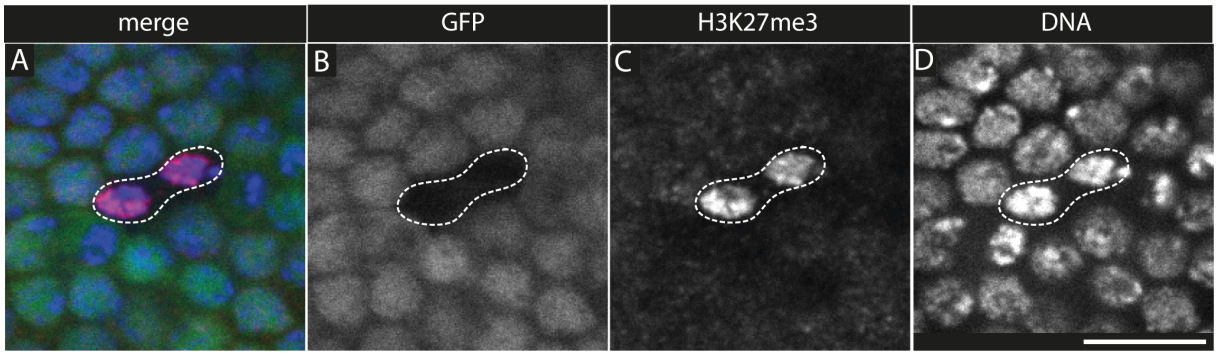

Figure 25: Distribution of H3K27me3 in *ΔH3.3; His^{C}; 6xT11A* follicle cell clones.

The egg chambers were dissected 2 d after the last heatshock. Mutant cell clones (dashed lines) were identified by the absence of GFP fluorescence (B). The tissues were stained for H3K27me3 (C) and DNA (D). In *ΔH3.3; His^{c}; 6xT11A* mutant follicle cells of late egg chambers the signal for H3K27me3 is highly enriched and the chromatin is more condensed compared to surrounding non-mutant follicle cells. The scale bar represents 10 µm.

4.6 Wing imaginal discs as a model system to study the effect of H3T11ph on known Polycomb target genes

After characterization of the T11A and K27R mutation in follicle cells I addressed the physiological function of H3T11ph. It was shown earlier (see chapter 4.3.2) that the presence of the histone mark H3T11ph is based on the enzymatic activity of the histone methyltransferase E(z). Using the histone replacement system it was shown that the presence of H3T11ph is not dependent on the presence of the histone mark H3K27me3, which is the modification directly introduced by the methyltransferase E(z). An effective system to study the functional role of histone modifications and modification writers are the wing imaginal discs of *D. melanogaster* larvae (Hodl & Basler, 2009, 2012; Pengelly et al., 2013; Yung et al., 2015). Pengelly et al., 2013 (and many others before) showed that the null mutation $E(z)^{731}$ causes a strong Polycomb phenotype in cell clones of wing imaginal discs resulting in a misexpression of Hox genes. In the same paper the authors showed that the H3K27R mutation also resulted in a misexpression of Hox genes in cell clones of wing imaginal discs, demonstrating that the H3K27me3 modification is instructive for the silencing of Hox genes. To check whether it is possible to reproduce these results in ovaries, antibody stainings for Hox proteins were performed in $E(z)^{731}$ follicle cell and germline cell clones (data not shown). Unfortunately none of the stainings (Ubx, Abd-B, Scr, Antp) in ovaries showed any enrichment of the proteins at all. Therefore, further experiments were performed using wing imaginal discs as a model system. The first step was to investigate whether the phenotypes found in the ovaries are transferable to wing imaginal discs. Firstly, it was investigated if the null mutation $E(z)^{731}$ also causes a reduction of H3T11ph in wing imaginal disc clones. Secondly, the histone mutants (H3K27R and H3T11A) were characterized and analyzed for a putative misexpression of Hox genes in wing imaginal disc clones.

4.6.1 Distribution of H3T11ph in E(z) mutant cells in wing imaginal discs

The wings of *D. melanogaster* develop from the larval precursor cells of imaginal discs. Imaginal discs are monocellular epithelial layers that consist of undifferentiated, proliferating cells. During the larval stage the cells in the growing disc are undifferentiated, but their developmental fate in the adult is already determined. The wing imaginal disc comprises ~20 cells when it is formed during embryonic development. These cells proliferate during the three larval stages to generate a disc of approximately 50.000 cells in the late third instar (Klein, 2001; Lawrence & Morata, 1977). Shortly after the beginning of pupariation, cell divisions cease and the differentiation of adult structures begins. For induction of $E(z)^{731}$ and $Su(z)12^{4}$ cell clones in the wing imaginal discs larvae were heatshocked 72 h after egg laying. The dissection and staining of the wing imaginal discs were accomplished as described in chapter 3.4.3. The discs were stained with antibodies for H3K27me3 (Figure 26).

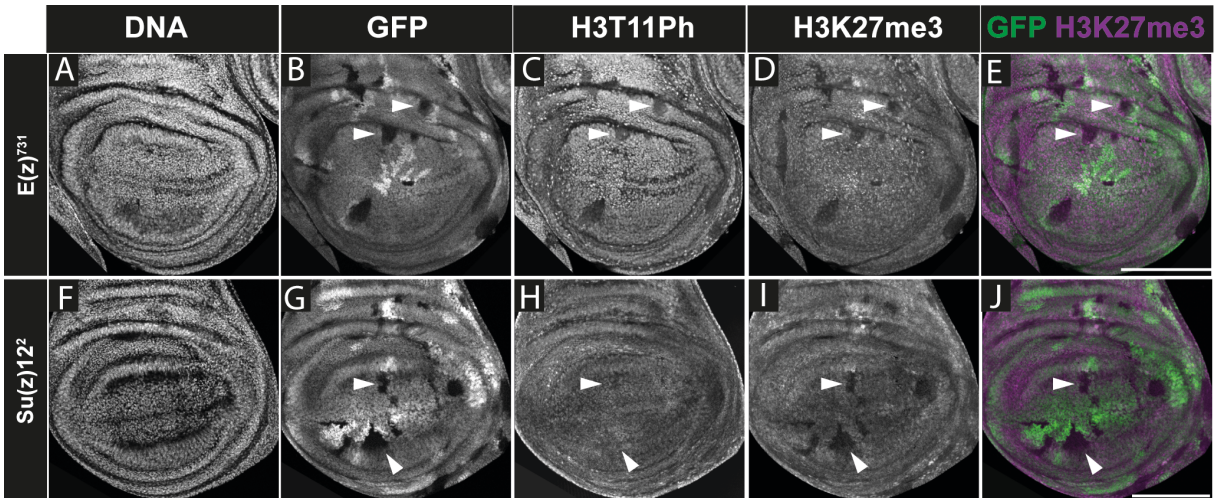

Figure 26: Distribution of H3K27me3 and H3T11ph in $E(z)^{731}$ and $Su(z)12^{4}$ mutant cell clones in wing imaginal discs.

The wing imaginal discs were dissected from late wandering 3rd instar larvae. Mutant cell clones were identified by the absence of GFP fluorescence (B, G). Two mutant clones were marked by white arrowheads. The discs were stained with an H3T11ph antibody (C, H), with DAPI for staining of the DNA (A,F) and with an H3K27me3 antibody (D,I). (A-E) In $E(z)^{731}$ mutant cell clones the signal for both H3T11ph and H3K27me3 is downregulated. (F-J) In $Su(z)12^{4}$ mutant cell clones the signal for H3K27me3 is absent and the signal for H3T11ph remains unchanged compared to the surrounding non-mutant cells. Scale bars represent 100 µm.

In *E(z)^{731}* mutant cell clones the signal for H3K27me3 is absent and the signal for H3T11ph is downregulated as well (Figure 26 A-E, white arrowheads). In *Su(z)12^{4}* mutant cell clones the signal for H3K27me3 is absent and the signal for H3T11ph is unchanged compared to the neighbouring non-mutant cells (Figure 26 F-J, white arrowheads). Thus, the earlier described phenotype in follicle cell clones regarding the downregulation of H3T11ph in *E(z)^{731}* mutant cell clones is reproducible in wing imaginal disc cells. Hence this system can be used to study the biological function of H3T11ph.

4.6.2 Adapting the histone replacement system to wing imaginal discs

For induction of cell clones in wing imaginal discs using the histone replacement system the first step was to investigate how many His-GUs are sufficient for survival and proliferation of the mutant cells (Figure 27). In flies carrying the *His^{c}* deletion without any His-GUs, there are no *His^{c}* mutant cell clones detectable in wing discs (Figure 27 A-D). However twin clones, which are homozygous for GFP, can be identified (Figure 27 B, black arrowhead) and survive as they have endogenous histones. The complementation of the *His^{c}* mutation with twelve His-GUs in wing imaginal disc clones generates many cell clones (Figure 27 E-H). To test whether fewer His-GUs can functionally compensate the histone deficiency in wing imaginal disc clones, cell clones were induced in flies which carry six His-GUs to complement the histone deficiency. Analysis of wing imaginal disc cell clones revealed the presence of many mutant clones carrying 6 His-GUs (Figure 27 I-L). Thus, in wing imaginal disc clones 6 His-GUs are sufficient to rescue the *His^{c}* phenotype and in all following experiments six His-GUs were used. As it was already shown in follicle cell clones that H3.3 can compensate for the loss of the canonical histone H3 with regard to the histone marks H3T11ph and H3K27ac (chapter 4.5.2 and 4.5.4 respectively), individuals were generated bearing the deletion of H3.3 in the genetic background. In wing imaginal disc cell clones bearing only the deletion of both H3.3 genes, mutant cell clones were found (Figure 27 M-P). Mutant cell clones carrying *ΔH3.3; His^{C}; 6xHis-GUs* are visible in wing imaginal disc (Figure 27 Q-T). The clones are smaller compared to *His^{C}; 6xHis-GUs* cell clones, but nevertheless many cell clones were found. All wing imaginal discs were stained for H3T11ph to investigate if the signal for this histone modi-

fication is altered by different numbers of wildtype His-GUs. The signal intensity of H3T11ph is not changed in any of the cell clones in figure 27 showing that the *His*^{C} and *ΔH3.3; His*^{C} deletion and replacement with wildtype His-GUs had no influence on the distribution of H3T11ph.

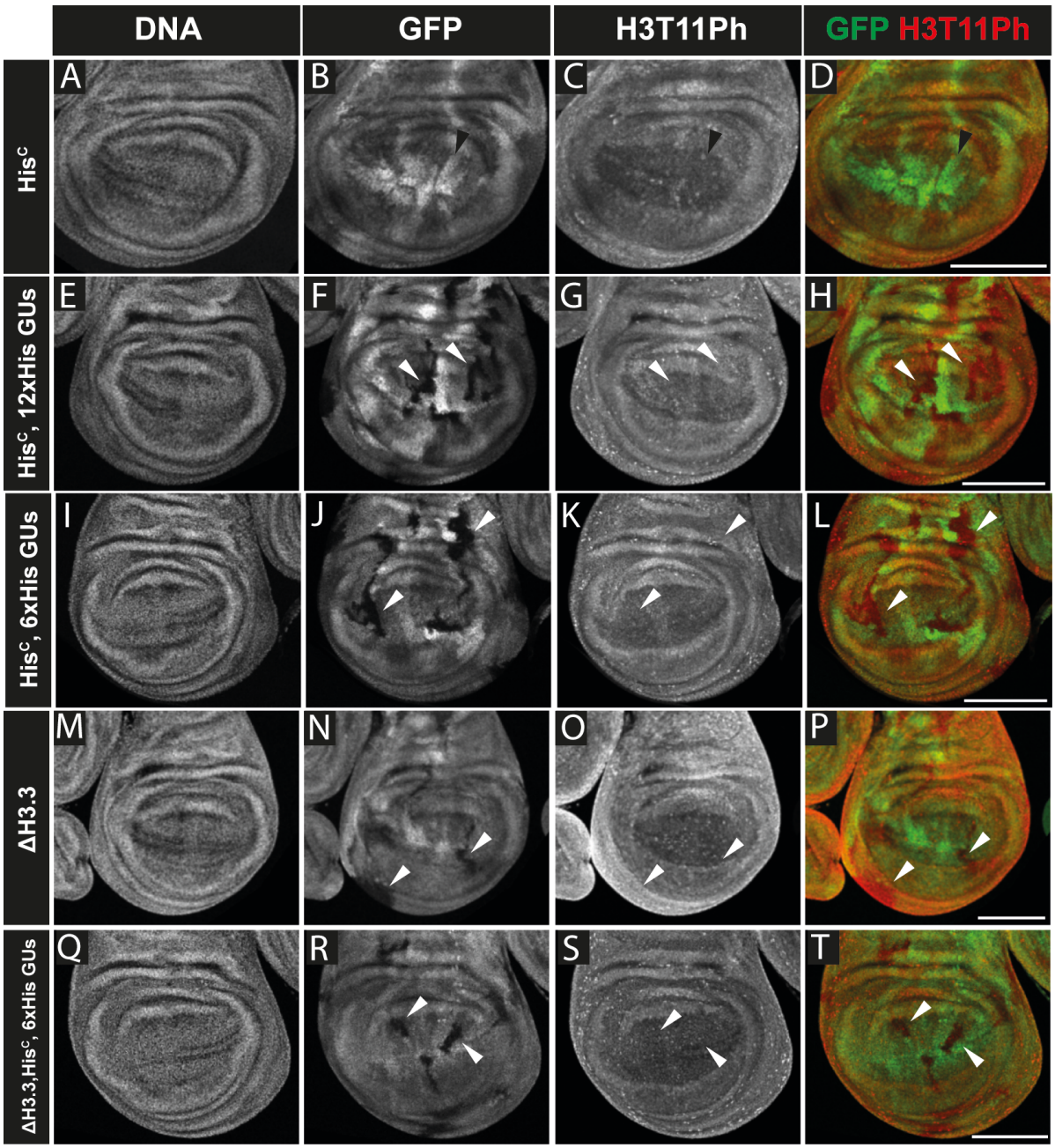

Figure 27: Rescue of *ΔH3.3; His^C* and *His^C* mutant cell clones with wild type histone gene units in wing imaginal discs.

The wing imaginal discs were dissected from late wandering 3rd instar larvae. Mutant cell clones were identified by the absence of GFP fluorescence. Clones were marked by white asterisks. The discs were stained with a H3T11ph antibody and DAPI (DNA). In all stainings made for H3T11ph there is no visible effect on the signal intensity of H3T11ph. (A-D) In animals without any His-GUs the wing imaginal discs have no *His^C* homozygous clones. However twin clones, which are homozygous for GFP and appear brighter, can be identified (black arrowheads). (E-H) *His^C; 12xHis-GUs* mutant cell clones in wing imaginal discs are detectable and are quite big. (I-L) The compensation of the homozygous *His^C* deletion with 6xHis-GUs results in cell clones that are comparable to *His^C; 12xHis-GUs* cell clones in size and frequency. (M-P) Homozygous *ΔH3.3* cell clones without any transgenes are found. The clones are small compared to *His^C; 6xHis-GUs* cell clones. (Q-T) *ΔH3.3; His^C; 6xHis-GUs* cell clones were found but they are smaller compared to *His^C; 6xHis-GUs* cell clones. Scale bars represent 100 µm.

4.6.3 Characterization of *ΔH3.3; His^C; 6xT11A* and *His^C; 6xT11A* cell clones in wing imaginal discs

Next, wing imaginal discs with transgenic His-GUs carrying the T11A mutation were examined (Figure 28).

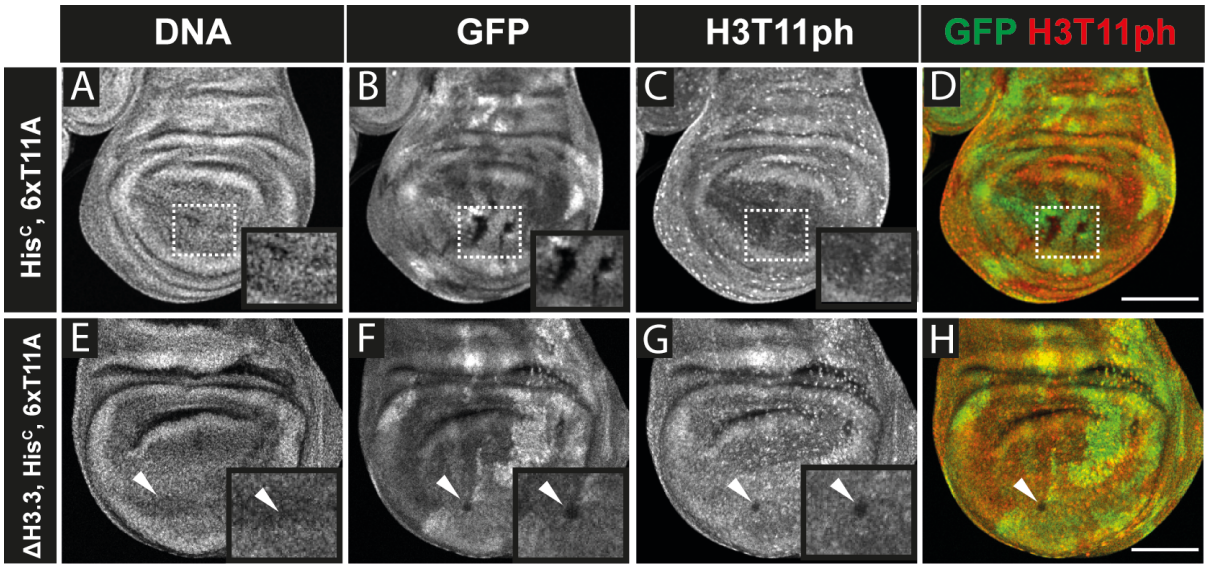

Figure 28: Distribution of H3T11ph in *ΔH3.3; His^C;6xT11A* and *His^C;6xT11A* cell clones.

Regions containing clones in A-D were marked by dashed white boxes and magnified in the insets. Clones in E-H were marked by white arrowheads. (A-D) The compensation of the homozygous *His^C* deletion with 6xT11A results in small cell clones. The signal for H3T11ph is unchanged in *His^C; 6xT11A* cell clones. (E-H) In *ΔH3.3; His^C; 6xT11A* mutant cell clones in wing imaginal discs are even smaller and less frequent compared to *His^C; 6xT11A* cell clones. The signal for H3T11ph is absent in these cell clones. Scale bars represent 100 µm.

In *His^{C}; 6x T11A* mutant cell clones in wing imaginal discs small cell clones were found (Figure 28 B, D; regions containing clones were marked by dashed white boxes and magnified in the insets) compared to wildtype His-GUs (Figure 27 J, L). The signal for H3T11ph is still present and unchanged in *His^{C}; 6x T11A* mutant cell clones compared to non-mutant cells. This resembles the results from follicle cells of the ovaries (see chapter 4.4.4). To clarify if an additional deletion of the histone variant H3.3 results in a reduction of H3T11ph, *ΔH3.3; His^{C}; 6xT11A* cell clones were induced in wing imaginal discs and investigated (Figure 28 E-H). *ΔH3.3; His^{C}; 6xT11A* cell clones are very small (Figure 28 F, H; marked by white arrowheads) showing that these cells clearly have a proliferation deficit. Nevertheless in *ΔH3.3; His^{C}; 6xT11A* cell clones the signal for H3T11ph is completely absent (Figure 28 G).

The distribution of H3K27me3 in *ΔH3.3; His^{C}; 6xT11A* cell clones was investigated as well and appeared not to be altered compared to the surrounding non-mutant cells (Figure 29).

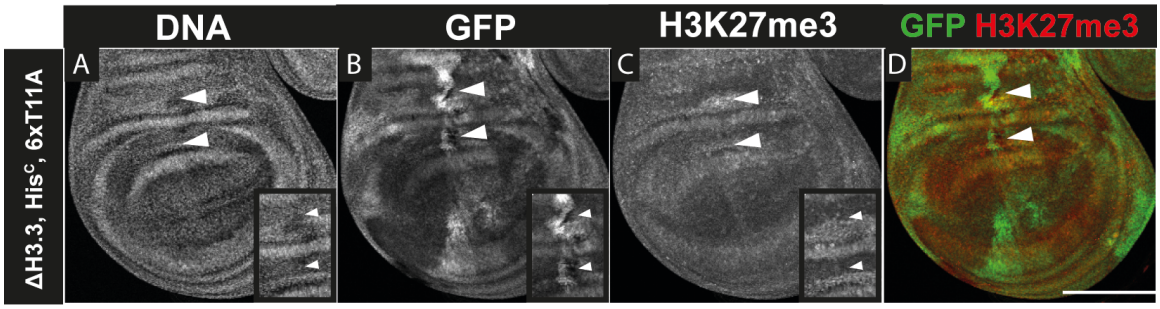

Figure 29: Distribution of H3K27me3 in *ΔH3.3; His^{C}; 6xT11A* cell clones.

The wing imaginal discs were dissected from late wandering 3rd instar larvae. Mutant cell clones were identified by the absence of GFP fluorescence (B). Clones were marked by white arrowheads. The discs were stained with a H3K27me3 antibody (C) and DAPI for staining of the DNA (A). (A-D) In *ΔH3.3; His^{C}; 6xT11A* cell clones the signal for H3K27me3 is not altered compared to the surrounding non-mutant cells.

4.6.4 Characterization of *ΔH3.3; His^{C}; 6xK27R* and *His^{C}; 6xK27R* cell clones in wing imaginal discs

Next, the distribution of H3K27me3 in *His^{C}; 6xK27R* cell clones was investigated (Figure 30). In *His^{C}; 6xK27R* cell clones in wing imaginal discs many big cell clones were obtained (Figure 30 B, D). In these cell clones the signal for H3K27me3 is completely absent (Figure 30 C, white arrowhead).

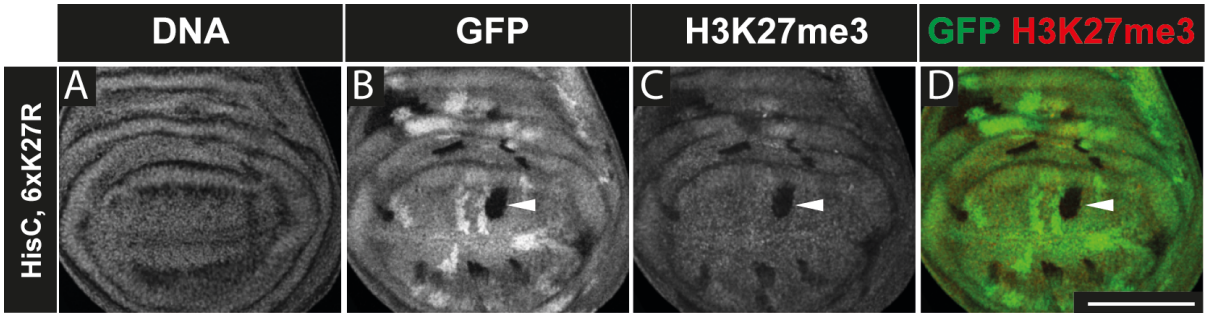

Figure 30: Distribution of H3K27me3 in *His^{C}; 6xK27R* cell clones.

The wing imaginal discs were dissected from late wandering 3rd instar larvae. Mutant cell clones were identified by the absence of GFP fluorescence (B). A Clone was marked by a white arrowhead. The discs were stained with a H3K27me3 antibody (C) and DAPI (A). The compensation of the homozygous *His^{C}* deletion with 6xK27R transgenes resulted in many big cell clones. The signal for H3K27me3 is absent in *His^{C}; 6xK27R* cell clones. The scale bar represent 100 µm.

The distribution of H3K27me3 and H3T11ph was investigated in *ΔH3.3; His^{C}; 6xK27R* cell clones. The signal for H3K27me3 is absent in these cell clones as well (Figure 31 E, F, insets marked by dashed white box) and the signal for H3T11ph is not changed in *ΔH3.3; His^{C}; 6xK27R* cell clones (Figure 31 A, B). *ΔH3.3; His^{C}; 6xK27R* cell clones are small compared to *ΔH3.3; His^{C}; 6xHis-GUs* cell clones (Figure 27 R, T) indicating that *ΔH3.3; His^{C}; 6xK27R* cell clones also have a proliferation deficit.

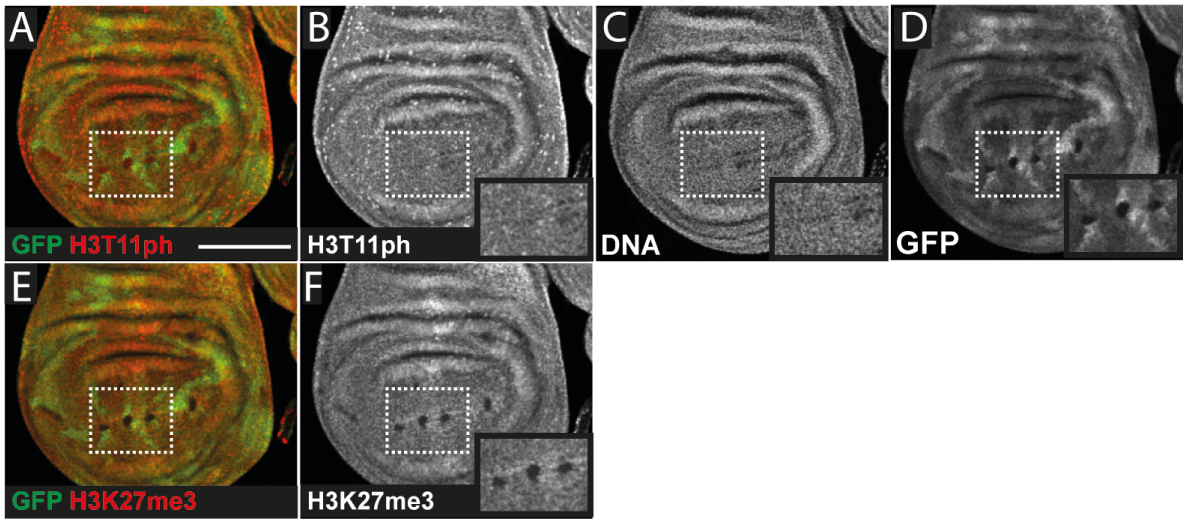

Figure 31: Distribution of H3K27me3 and H3T11ph in *ΔH3.3; His^{C}; 6xK27R* cell clones.

The wing imaginal discs were dissected from late wandering 3rd instar larvae. Mutant cell clones were identified by the absence of GFP fluorescence. Regions containing clones were marked by dashed white boxes and magnified in the insets. The discs were stained with a H3K27me3 and H3T11ph antibody and with DAPI (DNA). In *ΔH3.3; His^{C}; 6xK27R* mutant cell clones in wing imaginal discs are smaller compared to *His^{C}; 6xK27R* cell clones. The signal for H3K27me3 is completely absent in these cell clones (E, F) whereas the staining for H3T11ph revealed that the signal for H3T11ph remains unchanged (A, B). The scale bar represents 100 µm.

Next the distribution of H3K27ac in *ΔH3.3; His^{C}; 6xK27R* cell clones was investigated as well. In *ΔH3.3; His^{C}; 6xK27R* cell clones of wing imaginal discs the signal for H3K27ac is downregulated compared to the surrounding non-mutant cells (Figure 32 C).

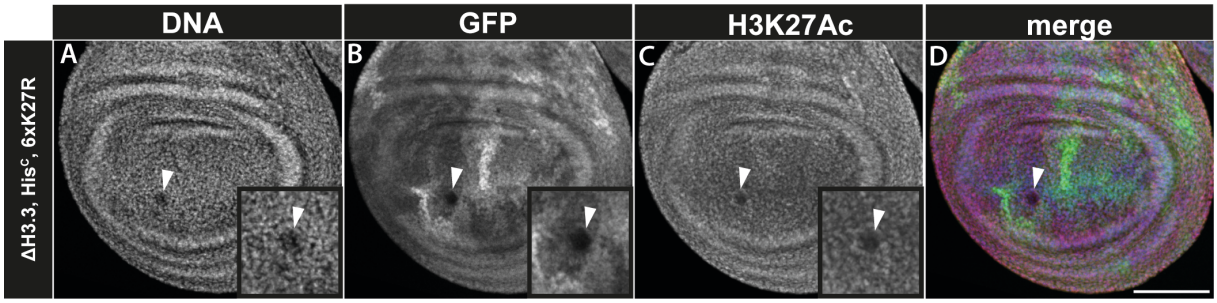

Figure 32: Distribution of H3K27ac in *ΔH3.3; His^{C}; 6xK27R* cell clones.
Mutant cell clones were identified by the absence of GFP fluorescence (B). A mutant cell clone was marked by a white arrowhead. The discs were stained with a H3K27ac antibody (C) and DAPI (A). The signal for H3K27ac is downregulated in *His^{C}; 6xK27R* cell clones. The scale bar represent 100 µm.

4.6.5 Influence of *ΔH3.3; His^{C}; 6xT11A* on the expression of Hox genes

The next step was to test whether the mark H3T11ph is linked to the regulation of Hox gene expression. It was already published that *His^{C}; 6xK27R* and E(z) mutant clones in anterior body segments show misexpression of posterior Hox genes resulting in a classical Polycomb phenotype (Pengelly et al., 2013). This data was reproducible in wing imaginal discs with our *His^{C}; 6xK27R* transgenic fly line as well as with *ΔH3.3; His^{C}; 6xK27R* transgenic fly lines (data not shown). *ΔH3.3; His^{C}; 6xT11A* cell clones were induced in 3rd instar larvae and stained for Sex-comb reduced (Scr), Ultrabithorax (Ubx), Abdominal-B (Abd-B) and Antennapedia (Antp) (Figure 33). Ubx, Scr and Abd-B are normally repressed in wing imaginal discs (Busturia & Morata, 1988). The Antp protein is normally observed in the part of the wing disc that will give rise to thoracic structures of the prescutum (Wirz, Fessler, & Gehring, 1986). In none of the stainings in wing imaginal discs carrying *ΔH3.3; His^{C}; 6xT11A* mutant cell clones is misexpression of Hox genes detected. At the same time haltere discs were also dissected and stained for Scr, Ubx, Abd-B and Antp to examine a potential change of Hox gene expression resulting in a Trithorax phenotype. In none of the

stainings in haltere discs is misexpression of Hox genes detected (data not shown). Thus, the H3T11A mutation does not result in any alteration of the expression of known Polycomb target genes.

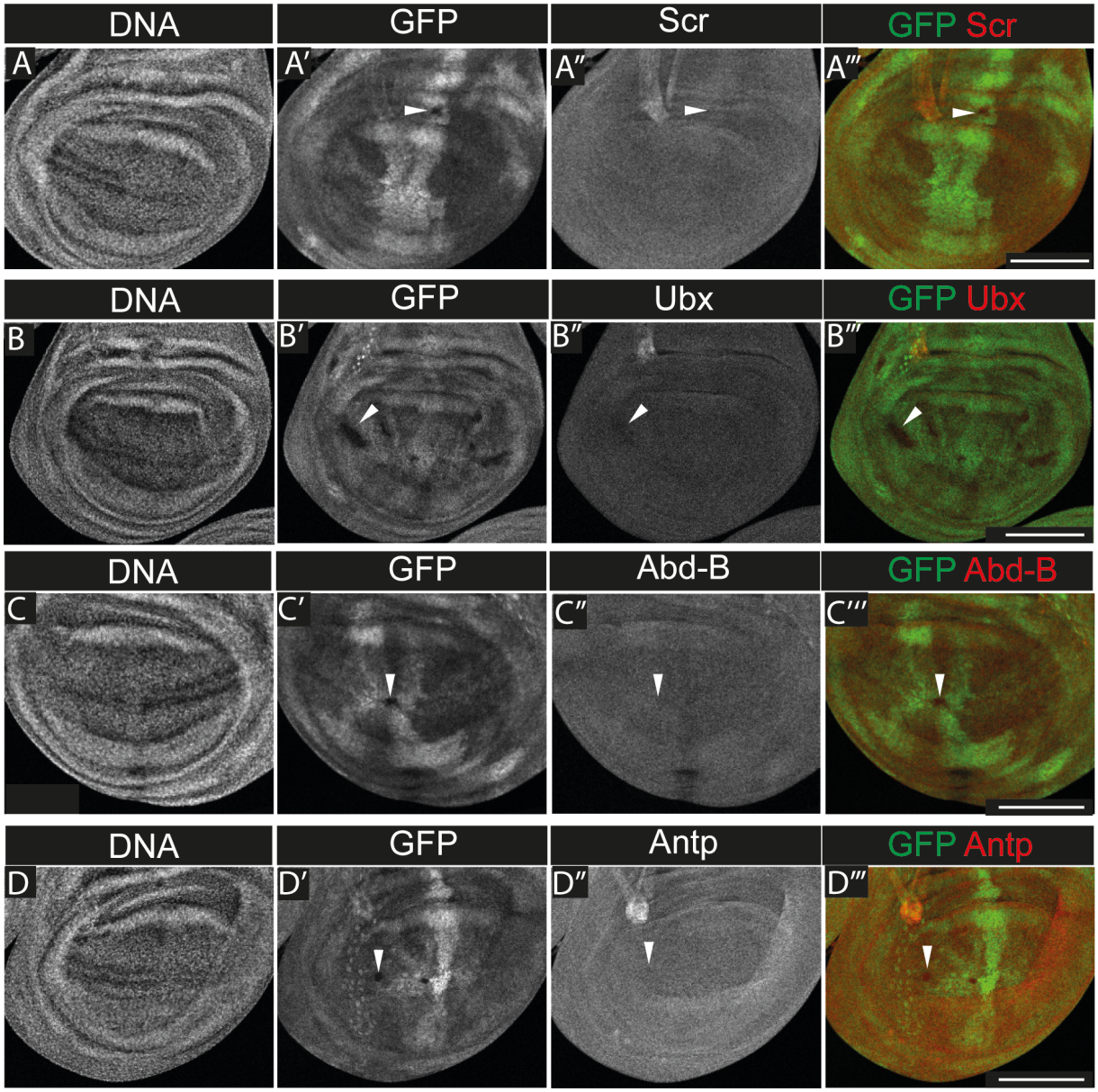

Figure 33: In *ΔH3.3; His^{C}; 6xT11A* mutant cell clones Hox genes are expressed normally.
The wing discs were dissected from late wandering 3rd instar larvae. Mutant cell clones were identified by the absence of GFP fluorescence (A', B', C' and D') and were marked by white arrowheads. The discs were stained for Scr (A''), Ubx (B''), Abd-B (C'') and Antp (D''). The DNA was stained with Dapi (A''', B''', C''' and D'''). (A-A''') Stainings with a Scr antibody revealed no change in *ΔH3.3; His^{C}; 6xT11A* cell clones compared to the surrounding non-mutant cells. (B-B''') In *ΔH3.3; His^{C}; 6xT11A* cell clones misexpression of Ubx is not detected. (C-C''') Stainings with an Abd-B antibody showed no difference in *ΔH3.3; His^{C}; 6xT11A* cell clones compared to the surrounding non-mutant cells. (D-D''') In *ΔH3.3; His^{C}; 6xT11A* cell clones a change of the signal for Ubx is not detected. Scale bars represent 100 µm.

4.7 Genome wide distribution of H3K27me3 and H3T11ph in S2R+ cells using the ChIP-seq technique

Chromatin immunoprecipitation (ChIP) followed by high-throughput DNA sequencing (ChIP-seq) has become a valuable and widely used approach for mapping the genomic location of transcription-factor binding and histone modifications in living cells (Barski et al., 2007; Johnson, Mortazavi, Myers, & Wold, 2007; Robertson et al., 2007). In brief, the DNA-associated protein is crosslinked to DNA *in vivo* by treating cells with formaldehyde and then the chromatin is sheared by sonication into small fragments, generally in the 200–600 bp range. Then an antibody specific to the protein of interest is used to immunoprecipitate the DNA-protein complex. Finally, the crosslinks are reversed and the released DNA is assayed to determine the sequences bound by the protein. During the construction of a sequencing library, the immunoprecipitated DNA is subjected to size selection (typically in the ~150–300 bp range). Then the library is sequenced using a next-generation sequencing platform, in this case the NextSeq 500 Illumina platform (Bonn, Zinzen, Perez-Gonzalez, et al., 2012). To obtain a clearer view in which chromatin domains H3T11ph is located and at which genes H3T11ph is enriched and depleted, Chip-Seq experiments were performed. Simultaneously the genome wide distribution of H3K27me3 was also examined by ChIP-Seq experiments to compare the distribution of both modifications in relation to each other.

4.7.1 Distribution of H3K27me3 and H3T11ph in S2R+ cells

The ModENCODE (Model organism Encyclopedia of DNA Elements) project is a consortium which aims to define all of the functional elements in the human, worm and fly genomes. The modENCODE project is run as an open consortium and its database provides access to already generated data to unravel the epigenome of the mentioned model organisms (Landt et al., 2012). For generation of the genome wide high resolution profile of H3K27me3 and H3T11ph the modENCODE cell line S2R+ was used (Yanagawa, Lee, & Ishimoto, 1998). Initially, the distribution of H3K27me3 and H3T11ph in S2R+ were analyzed by immunofluorescence. Both histone modifications are highly abundant in S2R+ cells as shown in figure 34.

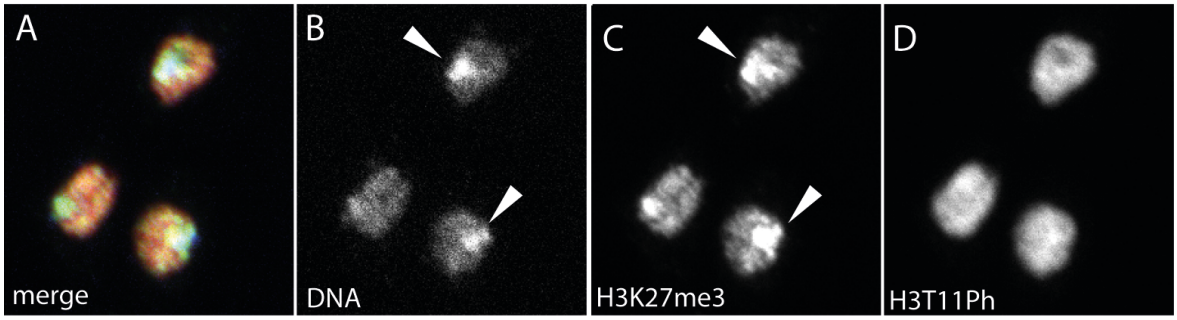

Figure 34: Occurence of H3K27me3 and H3T11ph investigated by Immunofluorescence.
S2R+ cells were grown to confluency and then stained with antibodies against H3K27me3 (C) and H3T11ph (D). The DNA was stained with Dapi (B). H3K27me3 is enriched in heterochromatic regions of the chromatin (see white asterisks). H3T11ph is broadly distributed all over the chromatin.

As the mutation of E(z) shows an effect in both the germline and wing imaginal discs of *D. melanogaster*, the question was whether the correlation between E(z) and H3T11ph is also present in S2R+ cells. Thus, dsRNA against exon 6 of E(z) and against exon 2 of Su(z)12 was generated. The cells were treated for 5 d with the corresponding dsRNA as described in chapter 3.3.6. Simultaneously untreated cells were also grown to examine the normal level of H3K27me3 and H3T11ph in S2R+ cells via western analysis. The treatment of S2R+ cells with dsRNA against E(z) and Su(z)12 both result in a decrease for the signal of H3K27me3 (Figure 35). The signal of H3T11ph decreases in cells treated with dsRNA against E(z) but remains the same in cells treated with dsRNA against Su(z)12 compared to untreated cells (Figure 35 B).

Thus, a knockdown of E(z) in S2R+ cells results in a decrease of H3T11ph and the knockdown of Su(z)12 has no influence on the level of H3T11ph. This resembles the phenotype found *in vivo* indicating that the correlation between E(z) and H3T11ph exists in general.

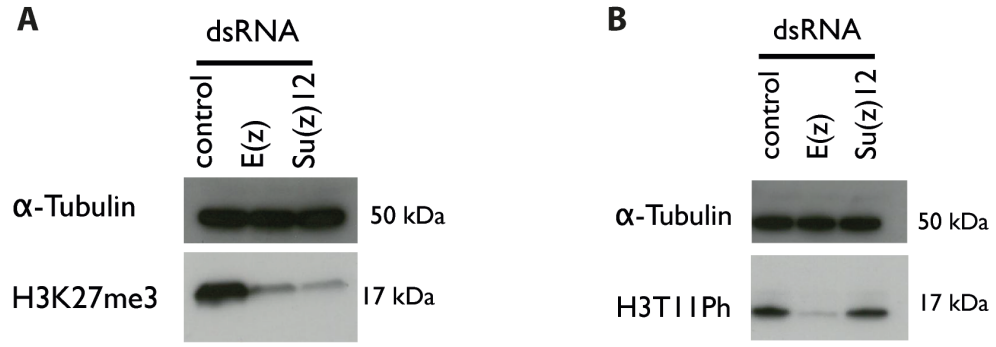

Figure 35: H3T11ph is downregulated in E(z) knockdowns in S2R+ cells.

Western Blots of whole S2R+ cell extracts after 5-days treatment with E(z) or Su(z)12 dsRNAs (lanes 2 and 3 respectively). Untreated S2R+ cells in lane 1 serves as a general control for the presence of the histone modifications. ß-tubulin served as loading controls. (A) Untreated cells show the normal enrichment of H3K27me3. S2R+ cells treated with E(z) and Su(z)12 dsRNA results in a decrease of H3K27me3. (B) Untreated cells show the normal enrichment of H3T11ph in S2R+ cells. S2R+ cells treated with E(z) dsRNA results in a decrease of H3T11ph, whereas S2R+ cells treated with Su(z)12 dsRNA does not change the signal of H3T11ph.

4.7.2 Optimization of the conditions for ChIP

The ChIP conditions are highly dependent on the quality of the antibody and the abundance and accessibility of the target protein epitope. Before starting to optimize the condition for the ChIP both antibodies were subjected to histone peptide arrays to validate the cross-reactivity of the H3K27me3 and H3T11ph antibodies with other PTMs (Figure 36). Each peptide array contains 384 unique histone modification combinations in duplicate. Both antibodies show only a little cross-reactivity with other histone modifications.

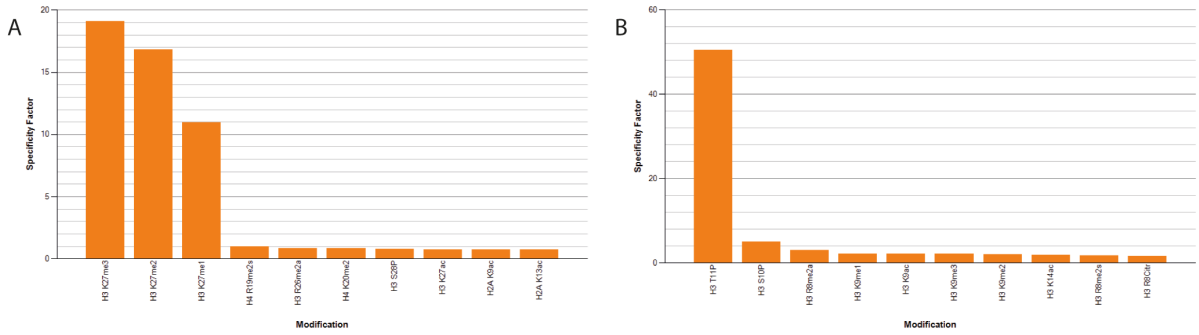

Figure 36: Results of Histone Peptide Arrays for validation of the specificity of the H3K27me3 and H3T11ph antibodies respectively.

Spot densitometry was used to analyze spot intensity from the ECL camera image. Results were compared to the provided reference grid to determine the associated peptide content. The results were graphed as a specificity factor, which is the ratio of the average intensity of all spots containing the mark divided by the ratio of the average intensity of all spots not containing the mark. The results for the H3K27me3 antibody is shown in (A) and for H3T11ph in (B). The results show that both antibodies have little cross-reactivity with other histone modifications.

The optimal amount of chromatin, antibody and magnetic beads are the main aspects that have to be considered for a successful ChIP experiment (Bonn, Zinzen, Perez-Gonzalez, et al., 2012). A sensitive yet specific antibody will give a high level of enrichment compared to the background, making it easier to detect binding events. The conditions of the ChIP for H3K27me3 were chosen as published before (Bonn, Zinzen, Girardot, et al., 2012). However, currently there is no published ChIP-Seq data from *D. melanogaster* cells available for H3T11ph as this histone modification is a less well characterized histone mark. Therefore, the first task to accomplish the Chromatin Immunoprecipitation was to set up the conditions of the ChIP for this antibody. To control the success of a ChIP experiment one has to keep two considerati-

ons in mind, the enrichment and the recovery. Enrichment provides an indication of the specificity of the ChIP and can be monitored by qPCRs of expected enriched regions over suspected negative regions. The enrichment determined serves as a guide in finding which antibody, chromatin and bead amounts allow for the best enrichment (Bonn, Zinzen, Perez-Gonzalez, et al., 2012). For H3K27me3 there is publicly available ChIP-seq data provided by ModENCODE. Thus, according to this data set, primer pairs to control for positive and negative genomic regions were chosen. As there is no genomic data available for the distribution of H3T11ph, the same primers were used as a hint to investigate the enrichment of H3T11ph. Recovery provides an indication of the efficiency of the ChIP and is especially important for subsequent library generation. In total 5 ng material from the ChIP is needed for library generation. The results for the determination of the efficiency of six performed ChIPs are illustrated in figure 37. For IP1-IP3 the H3K27me3 antibody was used in different amounts (0.5 µg, 1 µg, 2 µg). The same was done in IP4-IP6 using the H3T11ph antibody in different amounts (0.5 µg, 1 µg, 2 µg). The results of the qPCRs for three positive regions (Abd-A, Ubx, Opa) and one negative region (Gapdh1) are shown for IPs using both antibodies respectively (Figure 37 A, B). The negative region clearly shows a depletion of all IPs using the H3K27me3 antibody as well as for IPs using the H3T11ph antibody. The enrichment is finally obtained by calculating the ratio of the qPCR result of the positive region versus the negative region (see chapter 3.2.6). Values 5-fold over input are considered as specific (Figure 37 C). Thus, IP2 (H3K27me3) and IP5 (H3T11ph) were chosen for library generation as they showed the highest enrichment.

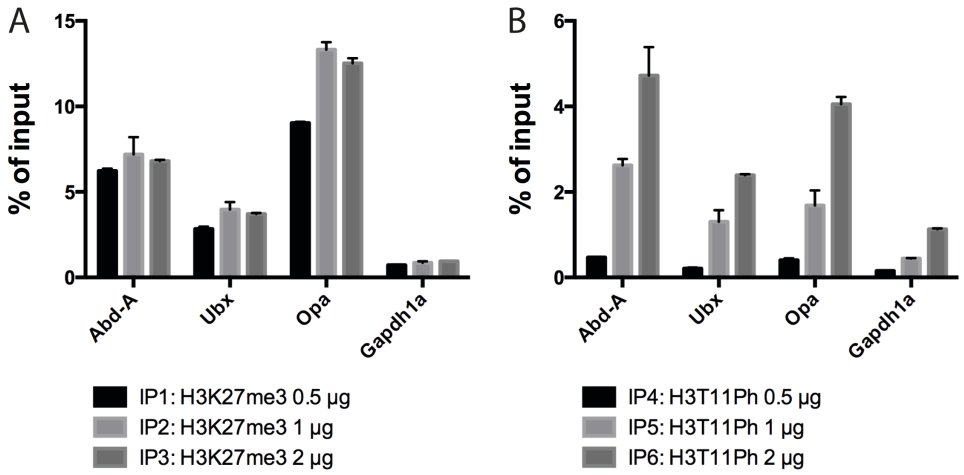

C

	Abd-A/Gapdh1	Ubx/Gapdh1	Opa/Gapdh1
IP1	8,67	3,94	12,57
IP2	8,35	4,61	15,44
IP3	7,18	3,91	13,21
IP4	3,1	1,37	2,69
IP5	5,94	2,95	3,82
IP6	4,18	2,12	3,59

Figure 37: Results of the ChIP optimization.

(A, B) Chromatin IPs were performed using sheared S2R+ chromatin (8 x 10^6 cells per ChIP) and different amounts of the indicated antibody respectively. qPCR was performed on DNA purified from each of the ChIP reactions using primer pairs specific for the indicated genes. The data is presented as % of input calculated from the ChIP antibody signal normalized to the input sample. (A) The positive gene regions Abdominal-A (Abd-A), Ultrabithorax (Ubx) and Odd-paired (Opa) are enriched in all IPs. The values for the negative region Gapdh1 are very low. (B) Using 0.5 µg of the H3T11ph antibody results in no enrichment in any of the tested regions. The values for the positive regions using the DNA from IP5 and IP6 show a clear enrichment and for the negative regions a depletion. (C) The final enrichment is obtained by calculating the ratio of the qPCR results of the positive regions versus negative regions. IP2 and IP5 show the highest enrichment and are used for subsequent library preparation.

After library generation the samples were committed to the sequencing core facility of the Max Planck Institute for Molecular Genetics in Berlin. For sequencing the NextSeq 500 Illumina platform was used.

4.7.3 Genome wide distribution of H3K27me3 and H3T11ph

The bioinformatic analysis of the obtained data from the sequencing facility was performed in collaboration with Dr. Alisa Fuchs from the research group „Computational Epigenomics“ from the MPI for Molecular Genetics in Berlin. All bioinformatics analysis was run on a server at the MPI for Molecular Genetics and operated by using a locally installed version of the GALAXY platform (Blankenberg et al., 2010; Giardine et al., 2005; Goecks et al., 2010). Effective analysis of ChIP-seq data requires sufficient coverage by sequencing reads (sequencing depth). The required depth depends mainly on the size of the genome and the number and size of the binding sites of the protein (Bailey et al., 2013). For the input sample 73.8 million reads were acquired, for H3K27me3 99.1 million reads and for H3T11ph 82.3 million reads. This sequencing depth is very deep indicating that the whole genome is covered by multiple reads. The reads were then mapped to the *D. melanogaster* genome Dm 2006 - BDGP R5/dm3 which was provided by the Berkeley *Drosophila* Genome Project (BDGP) using the short read aligner Bowtie (Langmead et al., 2009). After mapping, a peak calling analysis was conducted to predict the regions of the genome where the ChIPed protein is bound by finding regions with significant numbers of mapped reads (peaks) (Bailey et al., 2013). A fine balance between sensitivity and specificity depends on choosing an appropriate peak-calling algorithm and normalization method based on the type of protein ChIPed: point-source factors such as most transcription factors or broadly enriched factors such as histone marks. For both H3K27me3, as it is known to be a broadly distributed mark, and H3T11ph the peak calling algorithm MACS (Model-based Analysis of ChIP-Seq) was used (Feng, Liu, Qin, Zhang, & Liu, 2012; Feng, Liu, & Zhang, 2011; Zhang et al., 2008). All peaks were called against input controls with low stringency using the MACS2 program (Diaz, Park, Lim, & Song, 2012). It corrects mainly for bias related to the variable solubility of different regions, shearing of the DNA, and amplification. The peak caller also eliminates peaks that are not significant with respect to local background.

Next, the data was uploaded to the UCSC Genome Browser to visualize and compare the data sets (Figure 38).

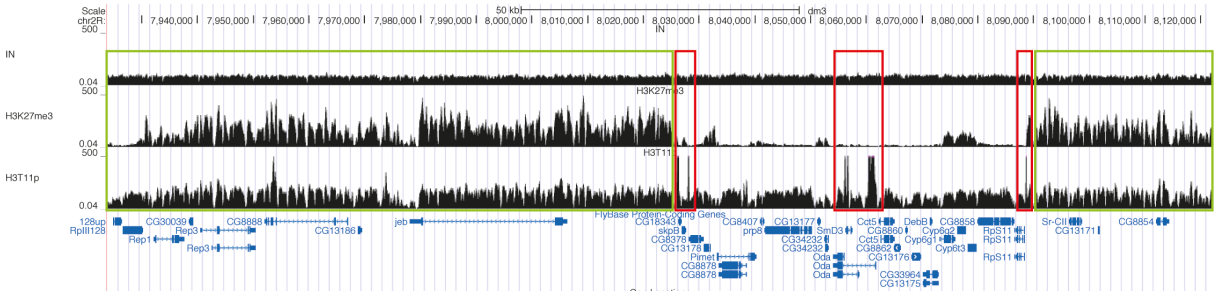

Figure 38: Representative genomic region of chromosome 2 showing the distribution of H3K27me3 and H3T11ph peaks.

The distribution of H3K27me3 and H3T11ph is shown in a genomic region of 180 kbp length. In some parts of the genome the peaks of H3T11ph are overlapping with peaks of H3K27me3 showing approximately the same shape of the peaks (green squares). In other parts H3T11ph is highly enriched in genomic regions resulting in very high peaks where H3K27me3 is depleted (red squares). IN: input sample

The height of the peaks represents the number of reads obtained in each region scaled to the total number of reads. The distribution of H3T11ph shows two different kinds of peaks. On the one side H3T11ph seems to be a broadly enriched factor covering a big part of the genome with a medium high peak enrichment (green boxes, Figure 38). From now on these peaks are called ’H3T11ph low peaks’. On the other side there are genomic regions where H3T11ph is highly enriched resulting in very high, sharp peaks as expected from point-source factors (red boxes, Figure 38). From now on these peaks are called ’H3T11ph high peaks’.

H3T11ph low peaks show a big overlap with H3K27me3, indicating that these histone modifications are co-localized and enriched in similiar genomic regions (Figure 39 A). For quantification of the overlap of the peaks of H3K27me3 and H3T11ph low peaks a Venn diagram was generated (Figure 39 B).

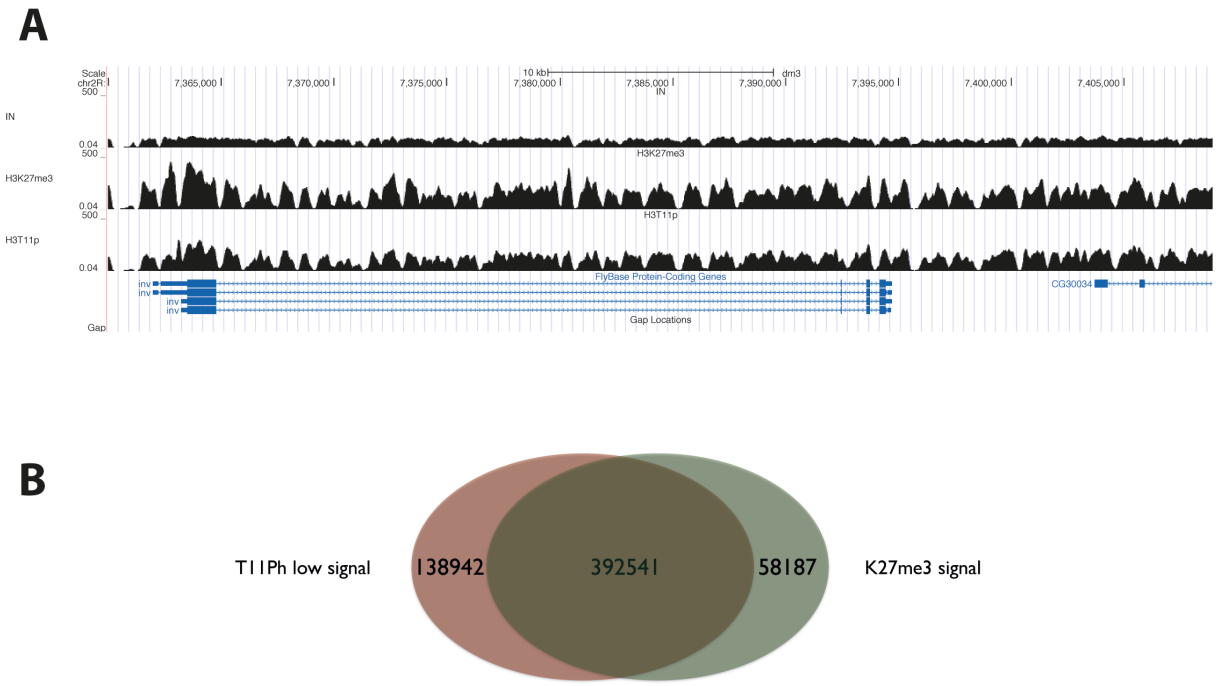

Figure 39: H3T11ph low peaks are highly overlapping with H3K27me3 peaks.
(A) A representative genomic region of approximately 40 kbp on chromosome 2 R shows that the peaks of H3K27me3 and H3T11ph low peaks are overlapping and that the shape of the peaks appears to be very similiar to each other. (B) A Venn diagram is shown comparing the datasets for H3K27me3 and H3T11ph low peaks. 73,85 % of all H3T11ph low peaks overlap with H3K27me3 and 87.09 % of all H3K27me3 peaks overlap with H3T11ph low peaks.

73.8 % of all H3T11ph low peaks overlap with H3K27me3 peaks and 87,09 % of all H3K27me3 peaks overlap with H3T11ph low peaks. Thus, H3K27me3 and H3T11ph low peaks are overlapping, indicating that they are enriched in the same genomic regions.

4.7.4 Distribution of H3T11ph high peaks and H3K27me3

At genomic regions where H3T11ph high peaks are located the signal for H3K27me3 is depleted (red boxes, Figure 40). Furthermore, H3T11ph high peaks seem to be located at borders of H3K27me3 domains as many of the H3T11ph high peaks are located at genomic regions where H3K27me3 is enriched on one side of the peak and depleted at the other side of the peak. H3T11ph high peaks furthermore appear to be primarily enriched at promotors and transcription start sites (TSS).

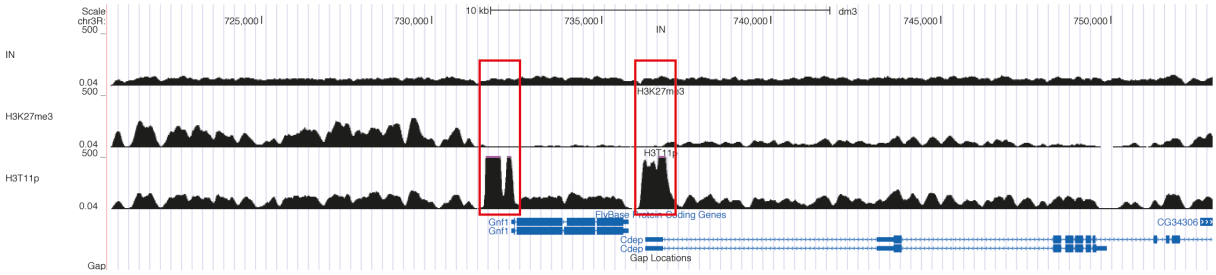

Figure 40: H3T11ph high peaks are enriched at promotors and transcription start sites (TSS).
A representative genomic region of 10 kbp shows that H3T11ph high peaks are enriched at promotors and TSS of genes. H3K27me3 is depleted at H3T11ph high peaks (red boxes). H3T11ph high peaks also appear to be located at borders of H3K27me3 domains indicated by the enrichment of H3K27me3 peaks at one side of H3T11ph high peaks and the depletion on the other side.

To further characterize and quantify the distribution of H3T11ph high peaks in regard to H3K27me3 domains, heatmaps were generated to investigate the overall distribution of H3K27me3 around H3T11ph high peaks (Figure 41). First, all genomic H3T11ph high peaks were aligned with the high peaks in the center. The regions 3 kbp upstream and downstream of the center are plotted. The peaks of H3K27me3 were then sorted according to the H3T11ph high peaks. Over the heatmaps a line plot of the averaged strength of reads is also shown (Figure 41 A). The line plot in figure 41 A shows the depletion of the H3K27me3 signal at sites of H3T11ph high peaks.

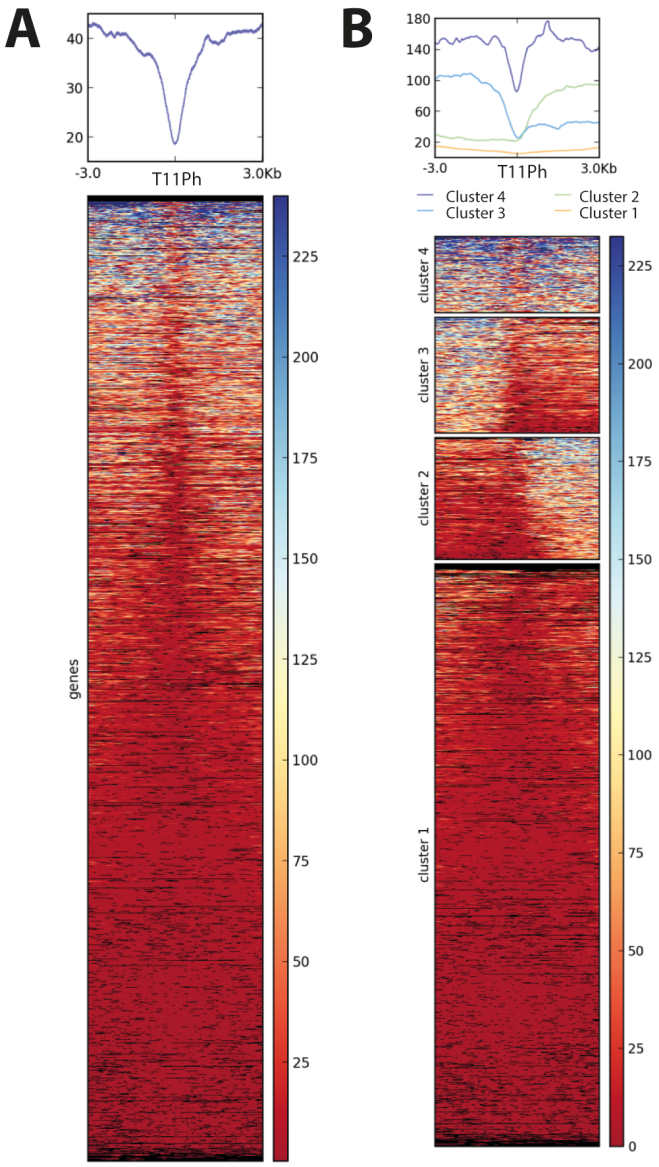

Figure 41: Line plots and heatmaps of H3K27me3 signal sorted according to H3T11ph high peaks and split into 4 clusters.

The signal intensity is shown as a spectogram with blue reflecting a high enrichment signal and red reflecting no signal. All genomic regions were scaled to have the same length (3 kbp upstream and downstream of H3T11ph high peaks). The center represents the aligned H3T11ph high peaks. Over the heatmaps a line plot of the averaged strength of reads is also shown. (A) The heatmap of H3K27me3 sorted according to H3T11ph high peaks is shown. The line plot shows a depletion of H3K27me3 around H3T11ph high peaks and an averaged signal on both sides of H3T11ph high peaks of about 40. (B) The signal for H3K27me3 sorted according to H3T11ph was split into four clusters. Cluster 1: Depletion of H3K27me3 of both sites of H3T11ph high peaks. Cluster 2: Enrichment of H3K27me3 downstream of H3T11ph high peaks. Cluster 3: Enrichment of H3K27me3 upstream of H3T11ph high peaks. Cluster 4: Enrichment of H3T11ph at both sites of H3T11ph high peaks. The line plot summarizes the results of the heatmap showing the averaged peak signal of H3K27me3 around H3T11ph high peaks for each cluster.

The signals for H3K27me3 sorted according to H3T11ph was split into 4 clusters (Figure 41 B). In regions of cluster 1 H3K27me3 is depleted upstream and downstream of H3T11ph high peaks. This represents the majority of the distribution of H3K27me3 around H3T11ph high peaks. In regions of cluster 2 H3K27me3 is depleted upstream of H3T11ph high peaks and enriched downstream of H3T11ph high peaks. In regions of cluster 3 the distribution of H3K27me3 is exactly reversed namely H3K27me3 is depleted downstream of H3T11ph high peaks and enriched upstream. Regions of cluster 4 shows genomic areas where H3K27me3 is enriched at both sites of H3T11ph high peaks. This pattern of H3K27me3 around H3T11ph high peaks indicates that H3T11ph high peaks might be a mark acting as a barrier for the H3K27me3 signal setting up borders to prevent the H3K27me3 signal from spreading in regions of actively transcribed genes. Therefore, the distribution of H3K27me3 and H3T11ph peaks were compared to the distribution of a histone modification which correlates with actively transcribed genes, namely H3K36me3 (Bannister et al., 2005).

4.7.5 Distribution of H3K36me3 around H3T11ph high peaks

The ChIP-seq data for H3K36me3 was an external data set derived from a recently published paper (Lhoumaud et al., 2014). This data-set was compared to H3K27me3 and H3T11ph, especially around H3T11ph high peaks (Figure 42).

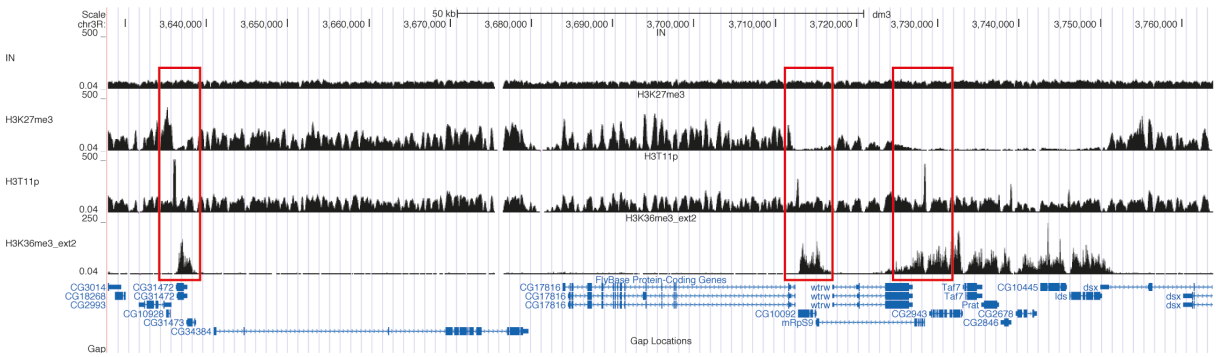

Figure 42: Distribution of H3K36me3 and H3K27me3 around H3T11ph high peaks.

The distribution of H3K27me3, H3T11ph and an external data set for H3K36me3 is shown in a representative genomic region of approximately 12 kbp. Around some H3T11ph high peaks the signal for H3K27me3 decreases (marked by red boxes) on one side and the signal for H3K36me3 increases on the other side.The data set for H3K36me3 was derived from a recently published paper (Lhoumaud et al., 2014).

It appears that H3T11ph high peaks function as a mark for the transition between H3K27me3 and H3K36me3 as H3T11ph high peaks seem to determine the decline of H3K27me3 on the one side and the increase of H3K36me3 on the other side. This most likely marks the transition from silenced gene regions to actively transcribed gene regions. In general the eukaryotic genome is structured into domains, which serve different functions. One of these functions is to group euchromatic and heterochromatic genomic regions into separate domains. The definition of a domain border is the switch from repressive marks to active marks on the chromatin landscape. Insulators functionally separate and demarcate these domains from each other to ensure the proper maintenance of their corresponding activity status (Ghirlando et al., 2012; Kyrchanova & Georgiev, 2014) and the spreading of H3K27me3 into neighbouring domains respectively (Bowman et al., 2014). To further investigate a potential role of H3T11ph in setting up borders, the interplay between H3T11ph high peaks and insulator proteins was examined.

4.7.6 H3T11ph high peaks overlap with insulator proteins

Classically, insulators are meant to have two major functions. One function is to block the propagation of heterochromatic structures into adjacent euchromatin and the second is to block the interaction between an enhancer and promoter when placed between them (Gurudatta & Corces, 2009). Insulators are DNA-protein complexes and many protein components of insulator elements have been characterized (Gerasimova & Corces, 1998). Their distribution across the genome of *D. melanogaster* was published before (Cuddapah et al., 2009; Negre et al., 2010). At least 5 subclasses of insulators are described in *D. melanogaster*. Each subclass contains a different DNA binding protein (Beaf, dCTCF, Su(Hw), Gaf, Zw5) that may define the specific function of the corresponding subclass. Most insulators share the common cofactor CP190, which is required for the functional activity of insulator proteins and is involved in the aggregation of the insulator proteins into specific structures named nuclear speckles (Oliver, Sheehan, South, Akbari, & Pai, 2010). In addition, all subclasses may also have one Mod(mdg4) isoform which is also necessary for homo-multimerization (Bushey, Dorman, & Corces, 2008; Gurudatta & Corces, 2009). To further investigate the question of whether H3T11ph high peaks coincide with insulators, a combinatorial track of 5 insulator proteins obtained by multiple Chip-Seq expe-

riments was compared to H3T11ph high peaks. A representative genomic region of about 65 kbp is shown in figure 43 A combining the tracks for H3K27me3, H3T11ph and the insulator track. The insulator track was obtained from experiments performed by Dr. Alisa Fuchs and shows the overlap of the peaks of the five individual single insulator tracks. The insulator track combines individual tracks for the insulator proteins CP190, CTCF, Mod(mdg4), Beaf and Su(Hw). The insulator peaks appear to coincide with H3T11ph high peaks (Figure 43 A, red boxes). This indicates that H3T11ph high peaks are indeed located at genomic positions where insulator proteins are also enriched. To further charaterize the overlap of H3T11ph high peaks and insulator proteins a Venn diagram was generated (Figure 43 B). The combined insulator track consists of 2407 peaks, the H3T11ph track has 3452 high peaks in total. 22.7 % of all H3T11ph high peaks overlap with the insulator peaks and 32.6 % of the combined insulator peaks overlap with H3T11ph high peaks.

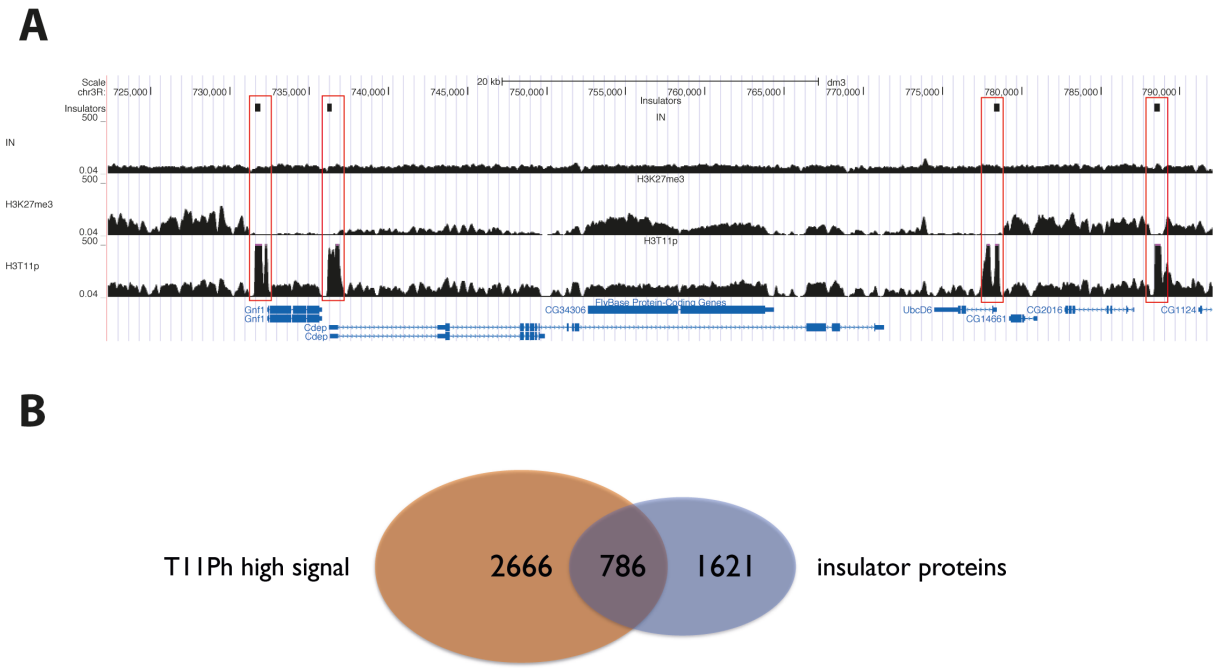

Figure 43: H3T11ph high peaks are overlapping with boundary proteins.

(A) A representative genomic region of approximately 65 kbp on chromosome 3 R shows that H3T11ph high peaks are overlapping with insulator peaks of a combined Chip-Seq track of 5 individual insulator protein tracks (red boxes). Both H3T11ph high peaks and the insulator track are enriched at H3K27me3 borders meaning the boundary of enrichment and depletion of H3K27me3.

(B) Shown is a Venn diagram comparing the datasets for H3T11ph high peaks and insulator peaks. In total there are 2407 peaks in the insulator track and 3452 peaks of H3T11ph high peaks. 22.7 % of all H3T11ph high peaks overlap with insulators and 32.6 % of the insulator peaks overlap with H3T11ph high peaks.

The overlap of H3T11ph high peaks and insulator peaks was further visualized by generation of a heatmap. Firstly, the insulator peaks were sorted with all peaks in the center of the heatmap and then the H3T11ph high peaks were aligned accordingly (Figure 44).

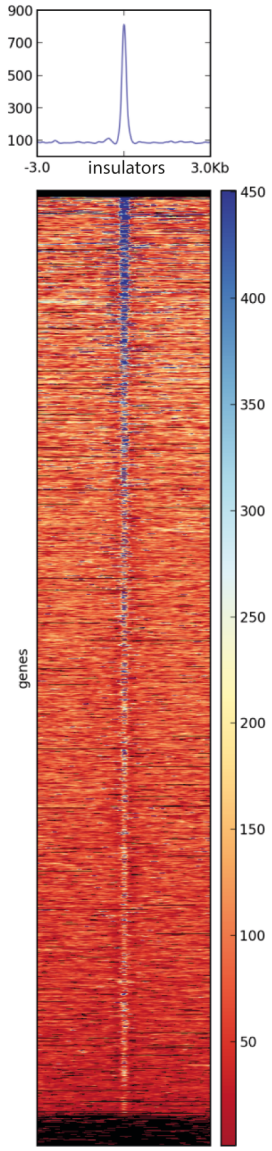

Figure 44: Line plot and heatmap showing the overlap of H3T11ph high peaks with boundary proteins.

The signal intensity is shown as a spectogram with blue reflecting a high enrichment signal and red reflecting no signal. All genomic regions were scaled to have the same length (3 kbp upstream and downstream of insulator proteins). The sorted insulator protein peaks are located in the middle of the heatmap. The heatmap of H3T11ph high peaks over insulator peaks in *D. melanogaster* S2R+ cells shows a big overlap of their high peaks.

The genomic regions 3 kbp upstream and downstream of the center are plotted. The two tracks overlap very well, which is also indicated by the line plot over the heatmap in figure 44. The line plot shows a big enrichment of H3T11ph high peaks with the peaks of insulator proteins sorted in the center of the heatmap. As the insulator track is a combination of 5 individual tracks derived from independent ChIP-Seq experiments, the single tracks were also analyzed regarding their overlap with H3T11ph high peaks respectively. In figure 45 the tracks for Beaf, CP190, CTCF, Mod(mdg4), Su(Hw), H3K27me3, H3T11ph and the combinatorial insulator track are plotted in a representative genomic region of 10 kbp. In this region the H3T11ph high peak does not overlap with the combinatorial insulator track as indicated by the blue arrow and the red box. Nevertheless the H3T11ph high peak overlaps with CP190 and Mod(mdg4) indicating that the H3T11ph high peaks might not overlap with the combinatorial track but with a smaller subset of insulator proteins.

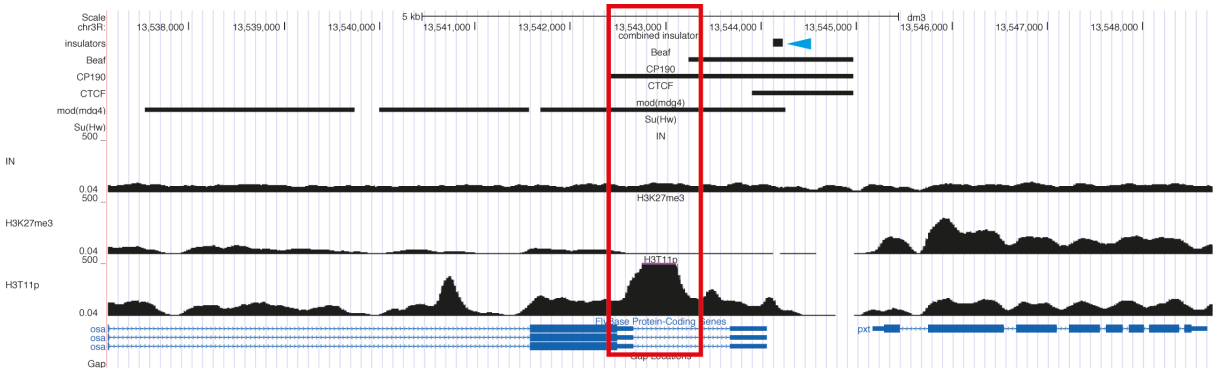

Figure 45: H3T11ph high peaks are overlapping with boundary proteins.

A representative genomic region of 10 kbp is shown. Tracks for H3T11ph, H3K27me3, input, Su(Hw), Mod(mdg4), CTCF, Cp190, Beaf and the combinatorial insulator track are plotted. The combinatorial track summarizes the highest overlap of the individual tracks here marked by a blue arrow. In this case the combinatorial track does not coincide with the H3T11ph high peak. Nevertheless, the H3T11ph high peak situated a little bit upstream of the insulator peak overlaps with CP190 and Mod(mdg4).

All H3T11ph high peaks, in total 3452 peaks, were analyzed for their overlap with single insulator proteins (table 8).

	number of peaks	peak overlap	% of overlap
H3T11Ph_high	3452		
insulator track	2407	786	22.7%
CP190	9019	1519	44.1%
mod(mdg4)	7417	1441	41.7%
Su(Hw)	7798	1419	41.1%
CTCF	5456	1189	34.4%
Beaf	5968	836	24.2%
Rad 21	3611	815	23.6%
Chromator	4944	713	20.6%
L3mbt	3213	698	20.2%
TF3C	2081	598	17.3%
Dref	2127	539	15.6%
Caph2	3280	539	15.6%

Table 8: Overlap of different boundary proteins with H3T11ph high peaks.

The overlap of H3T11ph high peaks with peaks of 11 insulator proteins was calculated. The insulator proteins are indicated on the left side. The total amount of peaks for each track is indicated under number of peaks. Next the overlap of peaks of each insulator track with H3T11ph high peaks is listed. Under % of overlap the proportion of each insulator protein overlapping with H3T11ph high peaks, referring to the total amount of H3T11ph high peaks, is indicated.

The highest overlap of H3T11ph high peaks was found for CP190 with 44.1 % overlap. The overlap of all H3T11ph high peaks with Mod(mdg4) was 41.7 % and with Su(Hw) 41.1 %. For CTCF the percentage of all H3T11ph high peaks overlapping with the CTCF peaks is 34.4 %. All other analyzed boundary proteins show an overlap of approximately 20 %. Thus, the H3T11ph high peaks appear to be located at genomic regions preferentially where CP190, Mod(mdg4) and Su(Hw) are located.

5 Discussion

Genomes of all eukaryotes are characterized by the assembly of chromatin composed of DNA and a variety of histone proteins (Marzluff & Duronio, 2002). Histones carry posttranslational modifications on their tails. These epigenetic marks in the context of the histone code hypothesis are thought to have regulatory potential for the transcription of target genes (Jenuwein & Allis, 2001). In the present work the interplay of epigenetic regulators and histone modifications was characterized *in vivo* and *in vitro* using the *D. melanogaster* Polycomb system as a model. The loss of the activity of E(z) and Su(z)12 leads to the loss of two different stem cell types in the ovary of *D. melanogaster* indicating that H3K27me3 is an epigenetic mark required for the maintenance of undifferentiated cells. Furthermore the loss of the enzymatic activity of E(z) leads to a reduction of H3T11ph. I could show that in *E(z)* mutant cells the signal for H3T11ph is reduced, whereas in Su(z)12 mutant cells the signal for H3T11ph remains unchanged indicating that E(z) has a PRC2 independent function in mediating the phosphorylation of H3T11ph. Furthermore, I successfully generated transgenic flies with 6 His-GUs carrying the H3T11A mutation. I was able to show that the histone 3 variant H3.3 and the cannonical histone H3 can redundantly act as substrates for T11 phosphorylation *in vivo*. Cells that solely depend on the expression of a H3 T11A mutant protein show a severe proliferation defect when they are simultaneously mutant for H3.3. Furthermore, I found that the H3K27me3 modification dramatically increases in ΔH3.3; His^{C}; 6xT11A follicle cells in late egg chambers. In ChIP-seq experiments I was able to unravel the genomic distribution of H3T11ph and H3K27me3 in S2R+ cells. H3T11ph overlaps with a significant portion of H3K27me3 and furthermore overlaps with the binding sites for insulator proteins.

5.1 E(z) and Su(z)12 are regulators of pluripotency

All cells of an organism share the same genome but exhibit different phenotypes and carry out diverse functions. Individual cell types, characterized by distinct gene expression patterns, are generated during development and then stably maintained. The chromatin state, characterized by the combinatorial presence or absence of specific histone modifications, shows a profound correlation with gene expression and is believed to contribute to the establishment and maintenance of cell identities. Genome-wide profiling of pluripotent cells and differentiated cells suggests global chromatin remodeling during differentiation, resulting in progressive transition from a relatively open chromatin configuration to a more compact state (T. Chen & Dent, 2014).
My approach to characterize histone modifications and their regulators that are involved in the regulation of cellular differentiation was to identify PTMs as candidates for regulating the undifferentiated state of tissue specific stem cells in *D. melanogaster*. In an antibody screen for histone modifications specifically enriched in germline stem cells of the ovary of *D. melanogaster,* I found that H3K27me3 is highly abundant in these undifferentiated, pluripotent cells. Upon differentiation it appears that H3K27me3 and most likely PcG activity gets restricted to domains of highly compacted heterochromatin. In the karyosome the signal of H3K27me3 is also highly abundant all over the chromatin. Enrichment of H3K27me3 in the karyosome may be due to the fact that upon fertilisation, the oocyte would regain the potential to form the whole organism as a zygote. Hence H3K27me3 might be an epigenetic mark needed to maintain pluripotency. In mammalian embryonic stem (ES) cells it was shown that there is a large cohort of developmental gene promoters that are simultaneously marked by both activating H3K4me3 and repressive H3K27me3 modifications. These patterns of seemingly opposing histone marks on the same promoter are referred to as “bivalent” domains (Bernstein et al., 2006; Boyer et al., 2006). Bivalent domains appear to silence developmental genes in ES cells while keeping them poised for activation until developmental cues lead to their expression. It was shown in ES cells that bivalent domains consist of large regions of H3K27me3 harboring smaller regions of H3K4me3 (Bernstein et al., 2006). This is consistent with the finding that H3K27me3 is found broadly distributed all over the chromatin of GSCs and that H3K4me3 is enriched in smaller regions of the chromatin (data not shown, result from antibody screen in chapter 4.1.1) in these cells. Nevertheless it is not yet proven

that bivalent domains containing both H3K4me3 and H3K27me3 do exist in *D. melanogaster*. Analysis of *D. melanogaster* embryos and testis-derived stem cells did not yield evidence for significant coexistence of both marks (Gan et al., 2010; Schuettengruber et al., 2009). Instead RNA polymerase II pausing may constitute an alternative means to coordinate the expression of early developmental genes in *D. melanogaster* (Muse et al., 2007; Zeitlinger et al., 2007). Stalled Pol II is particularly associated with developmental genes that are repressed and poised for activation. Maybe Pol II stalling allows genes to rapidly respond to developmental signals and thus facilitates the dynamic temporal and spatial expression patterns of developmental control genes. It might be that the local action of PRC1 in causing H2AK119ub at transcription start sites might block efficient clearing of Pol II from the preinitiation complex and prevents transcription elongation (X. Chen, Lu, Morillo Prado, Eun, & Fuller, 2011; H. Wang et al., 2004).

It was shown recently that during postembryonic neurogenesis in *D. melanogaster,* null mutations in E(z) and Su(z)12 lead to a dramatically reduced proliferation of neuroblasts, which are pluripotent cells that divide and give rise to differentiated neuronal cells. Moreover proliferating neuroblasts are absent in most of these mutant clones due to apoptosis and posterior Hox genes are ectopically expressed in the postembryonic neuroblast lineages (Bello, Holbro, & Reichert, 2007). The quantification of clonal E(z)- and Su(z)12-deficient stem cells in the germarium revealed that both factors are indispensable for the maintenance of germline stem cells as well as for follicle stem cells. Apparently these cells are forced to undergo differentiation as no apoptotic GSCs or FSCs were found. Most likely the corresponding non-mutant GSCs/FSCs are competing to replace the proliferation deficient mutant GSC/FSC. Cell competition is an important mechanism to eliminate cells that are potentially dangerous for the tissue, including those with insufficient growth or aberrant fates or cells with damage (de Beco, Ziosi, & Johnston, 2012). For homeostasis of the whole tissue and for continuous egg production it is indispensable that fitter cells compete and replace handicapped weaker stem cells.

It seems that the loss of GSCs/FSCs in the ovary due to the E(z) null mutation is a cell autonomous effect. A knockdown of E(z) in neighbouring somatic gonadal cells in the testis of *D. melanogaster* resulted in the upregulation of the somatic cell marker Zfh-1 in germline cells. This suggests that stem cell fate maintenance in testes of

adult males depends on the presence of an enzymatically intact E(z) protein in niche cells (Eun, Shi, Cui, Zhao, & Chen, 2014). This might also be true in the female germline and needs to be investigated by knockdowns of E(z) or other PRC2 subunits in cap cells, terminal filament cells and escort cells.

The causality for the disadvantage of E(z)/Su(z)12 mutant stem cells towards non-mutant stem cells in the ovary is still unknown. Inducing E(z) mutant oocytes abolished spatial and temporal control of the cell cycle and caused sterility via transdetermination of the oocyte into a nurse-like cell (Iovino, Ciabrelli, & Cavalli, 2013). This fate switch depends on loss of silencing of two PRC2 target genes, Cyclin E and dacapo which prevent the oocyte to undergo a fate switch into an endoreplicative program. Stainings for Hox genes in E(z)/Su(z)12 deficient cell clones showed no misexpression in GSCs or FSCs and stainings for known differentiation marker as well as pluripotency marker also showed no effect. For identification of genes that are misexpressed upon E(z)/Su(z)12 knockout in stem cells it might be possible in a broader approach to isolate mutant GFP negative germline cells from the ovary by dissection, FACS sorting and subsequent microscopical analysis for proper identification of GSCs. A microarray might then reveal the differences of gene expression of mutant versus non-mutant GSCs. This approach might be followed up in the future.

5.2 PRC2 independent function of E(z)

The analysis of the signal intensity of H3T11ph in $E(z)^{731}$ mutant follicle cells revealed a significant reduction of H3T11ph, whereas the H3T11ph level remained unchanged in $Su(z)12^{4}$ mutant follicle cells. These results indicate that E(z) is independent of the PRC2 complex mediating the phosphorylation of H3T11 and/or the maintenance of this phosphorylation mark. Traditionally, the main function of Polycomb group proteins is the maintenance of gene silencing which has been thought to involve recruitment of the PRC1 by PRC2-mediated trimethylation of K27 on histone H3. Biochemical *in vitro* assays identified H3K27 as the major site of methylation by E(z) in complex with the other PRC2 components (Muller et al., 2002) and recently it was demonstrated that H3K27 methylation directly mediates the function of PRC1 (Pengelly et al., 2013). The quantification of H3T11ph in His^{c}*; 6xK27R* mutant follcile cells however revealed that the absence of the H3K27me3 mark has no influence on the level of H3T11ph, suggesting again that E(z) independent of the PRC2 complex

might be necessary for the phosphorylation of H3T11 and/or the maintenance of this phosphorylation mark. There is in fact evidence for PRC2 independent functions of E(z). One recent study in mammalian prostate cancer cells showed that EZH2 has an PRC2 independent function (Xu et al., 2012). This study demonstrated that phosphorylation of EZH2 at Ser^{21}, mediated directly or indirectly by the PI3K-Akt pathway, can switch its function from a Polycomb repressor to a transcriptional coactivator of the androgen receptor (and potentially other factors). Rescue experiments and the lack of correlation with H3K27me3 levels support a role for EZH2-directed methylation of substrates other than H3K27, including potential nonhistone proteins. This PRC2 independent function also requires an intact methyltransferase domain (Xu et al., 2012). Therefore, it might also be possible that E(z) dependent methylation of non histone targets could be involved in the establishment of H3T11ph. In cells of *D. melanogaster,* E(z) likely leaves the canonical PRC2 complex and on its own or together with other components leads to the methylation of a H3T11ph kinase or its regulator and thereby activating it. How the balance of histone and non-histone methylation activity by E(z) is determined still remains to be solved. As E(z) itself can be phosphorylated at different positions (Zhai, Villen, Beausoleil, Mintseris, & Gygi, 2008), it is very likely that the histone and non-histone methylation activity of E(z) is regulated by a kinase as shown before in mammalian cells (Xu et al., 2012). Interestingly, it was shown that H3T11ph is also highly enriched in mammalian prostate cancer cells upon ligand-dependent recruitment to androgen receptor target genes by the Protein Kinase C-related Kinase 1 (Pkn1) leading to the activation of androgen receptor-dependent transcription (Metzger et al., 2008), which indicates a potential link between EZH2 and H3T11ph in mammalian cancer cells. Furthermore, in mammalian prostate cancer cells it was also shown that Pkn1 and H3T11ph facilitate the recruitment of WD repeat-containing protein 5 (WDR5) and the associated MLL1 complex, which leads to subsequent trimethylation of H3K4 and acetylation of H4K16 at androgen receptor target genes (Kim et al., 2014). This indicates that H3T11ph plays a role in the maintenance of activating marks or removal of repressing marks respectively. However, until now the functions of H3T11ph in *D. melanogaster* are uncharacterized and recent publications only hint at the functions of H3T11ph.

5.3 H3T11ph potentially restricts spreading of H3K27me3

The recruitment of PcG proteins to PREs leads to the establishment of a core of H3K27me3 modification at specific target sites. From there the H3K27me3 mark spreads along chromatin in a process that involves the PRC1 complex (Talbert & Henikoff, 2006). The PRC2 subunit ESC was shown to bind already existing H3K27me3 which leads to an allosteric stimulation of the PRC2 complex and propagation of the H3K27me3 mark (Hansen et al., 2008; Margueron et al., 2009). The exact mechanism of H3K27me3 spreading is still not entirely known, but it has been suggested that spreading is achieved by local diffusion of PRC2 or by the formation of chromosome loops (Y. B. Schwartz & Pirrotta, 2007; Talbert & Henikoff, 2006). Whereas mechanisms that lead to the spread of H3K27me3 are at least partially understood, much less is known about how this spread is limited. One proposed mechanism for regulating the spreading of the H3K27me3 mark is the incorporation of the histone variant H3.3 into chromatin at insulator regions thereby removing the H3K27me3 mark (Weth et al., 2014). Most likely the lack of the H3K27me3 mark interferes with ESC binding, leading to the release of the PRC2 complex from the chromatin and in the end to the establishment of a demarcated chromatin domain. Classically insulator proteins are thought to have one major role in blocking the spreading of heterochromatin into euchromatin. The mode of action of distinct insulator proteins is still not completely solved. It was suggested before that insulators are required to mediate long-range interactions important for PcG repression (Comet, Schuettengruber, Sexton, & Cavalli, 2011), and the recent identification of CTCF in transcription factories (Melnik et al., 2011) suggests that insulators may direct the localization of specific genomic loci to discrete nuclear subcompartments for gene regulation (Pirrotta & Li, 2012). In *D. melanogaster* S2 cells the distribution of CP190 and CTCF, which are two main insulator proteins in *D. melanogaster*, showed an enrichment of both factors at the borders of many PcG chromatin domains. RNAi knockdowns of CP190 and CTCF in *D. melanogaster* S2 cells results in an upregulation of H3K27me3 around many „H3K27me3 islands“ (Bartkuhn et al., 2009) indicating that the presence of insulator proteins indeed blocks the spreading of H3K27me3 directly. However, surprisingly it was also shown in a more recent study that the knockdown of CTCF in *D. melanogaster* Kc cells does not lead to an increase of H3K27me3 around insulator regions by spreading into flanking domains

(Van Bortle et al., 2012). In this study the down-regulation of *D. melanogaster* insulators by RNAi, individually or in combination, resulted in a decrease of H3K27me3 levels within the domain and no clear spreading of the modification. Interestingly, expression of genes within repressive H3K27me3 domains was not significantly affected by depletion of insulator proteins, suggesting that PcG mediated gene silencing was not abrogated or that additional steps are required to activate these developmental genes (Van Bortle et al., 2012). These controversial results indicate that barriers are complex genomic elements that require combinatorial action of multiple proteins and chromatin modifications with distinct roles. The primary role for insulators in these modular elements may be to mediate intra- or inter-chromosomal interactions that form the topological basis of barrier function, whereas other proteins and epigenetic modifications have the causal responsibility of preventing the spread of the repressive chromatin mark. A potential function of H3T11ph might be in contributing to the maintenance of H3K27me3 chromatin domains via regulation of certain boundary elements. In ChIP-seq experiments I could show that the H3T11ph peaks colocalize with a distinct set of insulator proteins and are localized at borders of H3K27me3. In *ΔH3.3; His^{C};6xT11A* mutant follicle cell clones of late egg chambers the chromatin appeared to be highly compacted compared to the non-mutant neighbouring cells. Moreover, the signal for H3K27me3 was highly enriched indicating that the loss of H3T11ph leads to the spreading of H3K27me3 which subsequently causes a higher compaction of the chromatin. As discussed above the signal for H3K27me3 seems to be broadly distributed in stem cell and becomes more restricted to smaller heterochromatic regions as the cells undergo differentiation. Most likely H3T11ph has different functions in distinct cell types. In postmitotic cells, which are terminally differentiated, H3T11ph appears to be indispensable for the maintenance of H3K27me3 domains and might be involved in setting up distinct types of insulators. In early follicle cells, where H3K27me3 is still broadly distributed all over the chromatin and is about to become restricted to heterochromatin, the loss of H3T11 does not show any effect towards H3K27me3. This resembles what was found for knockdowns of different insulators in Kc cells in which some knockdowns had no effect on the overall level of H3K27me3 (Van Bortle et al., 2012). In *ΔH3.3; His^{C};6xT11A* cell clones of wing imaginal discs the depletion of T11ph does not lead to any misexpression of Hox genes which are classically silenced Polycomb target genes in wing imaginal discs. These genes are expressed in a tightly spatial and temporal manner for esta-

lishment of the anterior-posterior axis (Schuettengruber et al., 2007). This indicates that an abrogation of T11ph does not affect PcG mediated gene silencing but rather other target genes which still remain to be elucidated. Interestingly, the expression of genes within repressive H3K27me3 domains was not significantly affected by depletion of insulator proteins in Kc cells suggesting that PcG mediated gene silencing was not abrogated or that additional steps are required to activate these developmental genes (Van Bortle et al., 2012), which might be also the case for the loss of T11ph.

5.4 H3.3 can compensate for the loss of H3K27ac and H3T11ph

The variant histone H3.3 is synthesized in a replication-independent manner and has been shown to replace canonical H3 at actively transcribed genes in *D. melanogaster* (Ahmad & Henikoff, 2002; B. E. Schwartz & Ahmad, 2005). Remarkably, this replacement variant H3.3 is one of the most conserved proteins present in all eukaryotes (Goldberg et al., 2010). H3.3 is associated with euchromatin and enriched in active histone modifications such as H3K4me2/3, H3K9Ac, and H3K14Ac (Chow et al., 2005; McKittrick et al., 2004). In *His^{C};6xT11A* mutant cell clones in the ovary and wing imaginal discs the signal for H3T11ph was still detectable at a level similiar to non-mutant cells. Analogous the same result was obtained for *His^{C}; 6xK27R* mutant cell clones for H3K27ac. In *His^{C}; 6xK27R* mutant cell clones the signal for H3K27me3 is completely abolished whereas the signal for H3K27ac is still detectable at normal non-mutant levels. In both cases an additional deletion of both genes encoding for H3.3 leads to the depletion of H3T11ph and H3K27ac respectively. This shows that H3.3 carries a substantial fraction of H3K27ac and H3T11ph in case canonical histone H3 is mutated at the respective sites. This suggests the H3T11ph modification is enriched in actively transcribed gene regions much like H3K27ac. If T11ph is enriched predominantly on the canonical histone one would expect the signal for T11ph to decrease in *His^{C}; 6xT11A* cell clones at least to some degree. Thus, it would be important to validate the signal of T11ph in *H3.3T11A* mutant cell clones in the presence of the canonical histone complex. This might help to answer the question if T11ph is predominantly found on the canonical H3 or the histone variant H3.3.

In recent studies investigating the composition of histone modifications on H3.3, no modifications were found to be exclusively found on H3.3 (McKittrick et al., 2004). All sites of known modification are shared between the two variants. Thus, it is also possible that T11ph is present on both the canonical H3 and the variant H3.3. Potentially the T11ph low peaks found in ChIP-seq experiments could be on the canonical histone H3. The phosphorylation of H3T11 in these low peaks is most likely linked to the activity of E(z) as H3T11ph appears to follow the genomic distribution of H3K27me3. The high peaks might be due to phosphorylation of the histone variant H3.3 marking borders of H3K27me3 regions as H3.3 was shown to replace H3 at insulator regions (Weth et al., 2014). This would also explain why the null mutation of E(z) in follicle cell clones does not lead to a complete loss of T11ph but to a reduction of about 50 %. The remaining signal most likely can be traced back to the T11ph signal enriched on H3.3 in insulator regions.

5.5 Disruption of T11ph leads to a proliferation deficit

The analysis of cell clones in follicle cells and wing imaginal disc cells indicates a clear proliferation deficit in the absence of functional H3T11ph and H3.3T11ph. This indicates that the deposition of T11ph is important for the regulation of the cell cycle and/or metabolism. In a recent publication it was shown in *S. cerevisiae* that H3T11ph is phosphorylated by a kinase called Pyk1, which is a key enzyme for glycolysis, catalyzing the conversion of phosphoenolpyruvate to pyruvate generating ATP (S. Li et al., 2015). Pyk1 was shown to be a part of a multi enzyme complex called SESAME which also harbors the SET1 H3K4 methyltransferase complex. The SESAME complex seems to regulate a crosstalk between H3K4 methylation and H3T11ph by regulating gene expression, responding to cellular metabolism via chromatin modifications. A link between H3T11ph and the metabolism in *D. melanogaster* might also be plausible as H3T11A mutant cells show a severe proliferation deficit. Nevertheless it appears that H3T11ph in *S.cerevisiae* is linked to H3K4 methylation which is in contrast to what was found in this present work linking H3T11ph to H3K27 methylation. The kinase responsible for H3T11ph in the fly is not known yet, but as a homolog of Pyk1 also exists in *D. melanogaster* it might be interesting to assess whether RNAi knockdown of this kinase in S2R+ leads to a reduction of H3T11ph levels.

5.6 H3T11ph coincides with boundary elements

ChIP-seq experiments in *D. melanogaster* S2R+ cells revealed that H3K27me3 and H3T11ph are overlapping in major parts of the genome. Additionally, high enrichment sites of H3T11ph (H3T11ph high peaks) were found, which are regions depleted of H3K27me3. Systematically generated heatmaps revealed that in two clusters H3K27me3 is enriched at one side of a H3T11ph high peak and depleted on the other side. The pattern of H3K27me3 around H3T11ph high peaks indicates that H3T11ph high peaks might be involved in the formation of chromatin boundaries. It was published before that chromatin in *D. melanogaster* as well as in humans can be sub-divided into specific chromatin regions (de Wit, Braunschweig, Greil, Bussemaker, & van Steensel, 2008; Filion et al., 2010; Guelen et al., 2008; Kharchenko et al., 2011). In *D. melanogaster* five principal chromatin types were characterized where ‚Polycomb chromatin' is characterized by the presence of H3K27me3 and the presence of PcG proteins covering chromatin (Filion et al., 2010). The other chromatin types are chromatin regions covered by various combinations of specific repressive or activating marks and proteins, respectively. As H3T11ph high peaks appear to be enriched at border regions of H3K27me3 domains the arising question is, if H3T11ph might be a histone modification which demarcates silenced chromatin from actively transcribed chromatin. Indeed an overlap of enrichment sites on the genome for H3T11ph high peaks with different insulator proteins was found. H3T11ph high peaks appear to be preferentially located at genomic regions where CP190, mod(mdg4), Su(Hw) and CTCF are localized. Chromatin conformation capture studies have revealed that the genomes of higher eukaryotes are divided into megabase size chromatin domains, within which smaller sub-domains are formed by local interactions at kilobase scale (Matharu & Ahanger, 2015). The large Mb scale domains are termed topologically associated domains (TADs). Within TADs, chromatin is organized into chromatin loops, via locus-specific interactions, and this organization is tightly related to genome function (Sexton et al., 2012). CTCF together with CP190, Mod(mdg4), Rad21 and other factors was shown to be frequently associated with TAD boundaries (Ghavi-Helm et al., 2014). Su(Hw), on the other hand, was generally absent from TAD borders and mostly localized within TADs (Van Bortle et al., 2014). Most likely H3T11Ph is a common factor at boundaries depending on the specific state of the cells.

The question is, how do insulator complexes mechanistically prevent the spreading of chromatin marks beyond a boundary? The boundary regions themselves are depleted for the repressive mark H3K27me3 and are enriched for active marks (Dixon et al., 2012). This matches with the sequencing results which showed a complete depletion of H3K27me3 at T11ph high peak sites on the genome. It was shown recently that histone demethylation at genomic insulator sites is accompanied by transient incorporation of the histone variant H3.3, suggesting that histone exchange is the mechanism for histone demethylation, and that this might be the mechanism to prevent spreading of histone marks from one domain through the insulator into the neighbouring domain (Jin et al., 2009; Weth et al., 2014). H3.3 is enriched in histone modifications associated with transcriptional activity and deficient in H3K27me3 and H3K9me3 (McKittrick et al., 2004). As H3T11ph high peaks are found to be enriched at promotor regions and TSS, thus correlating with actively transcribed gene regions, and enriched at insulator regions, it might be that T11ph high peak are enriched at nucleosomes carrying H3.3. This also matches the previously discussed findings that the loss of the canonical histone gene complex does not result in a loss of T11ph in T11A mutant cells. A complete loss of the T11ph signal is only achieved in cell carrying a double knockout of H3.3 and the canonical H3 together with the T11A mutation. The enrichment of T11ph high peaks at insulator sites also supports the findings that a complete loss of H3.3T11ph/H3T11ph results in an upregulation of H3K27me3 in mutant follicle cells indicating a functional role of H3T11ph in limiting the spreading of H3K27me3.

Summarizing the previously discussed data a putative model for the distribution of H3K27me3 and H3/H3.3T11ph can be seen in figure 46.

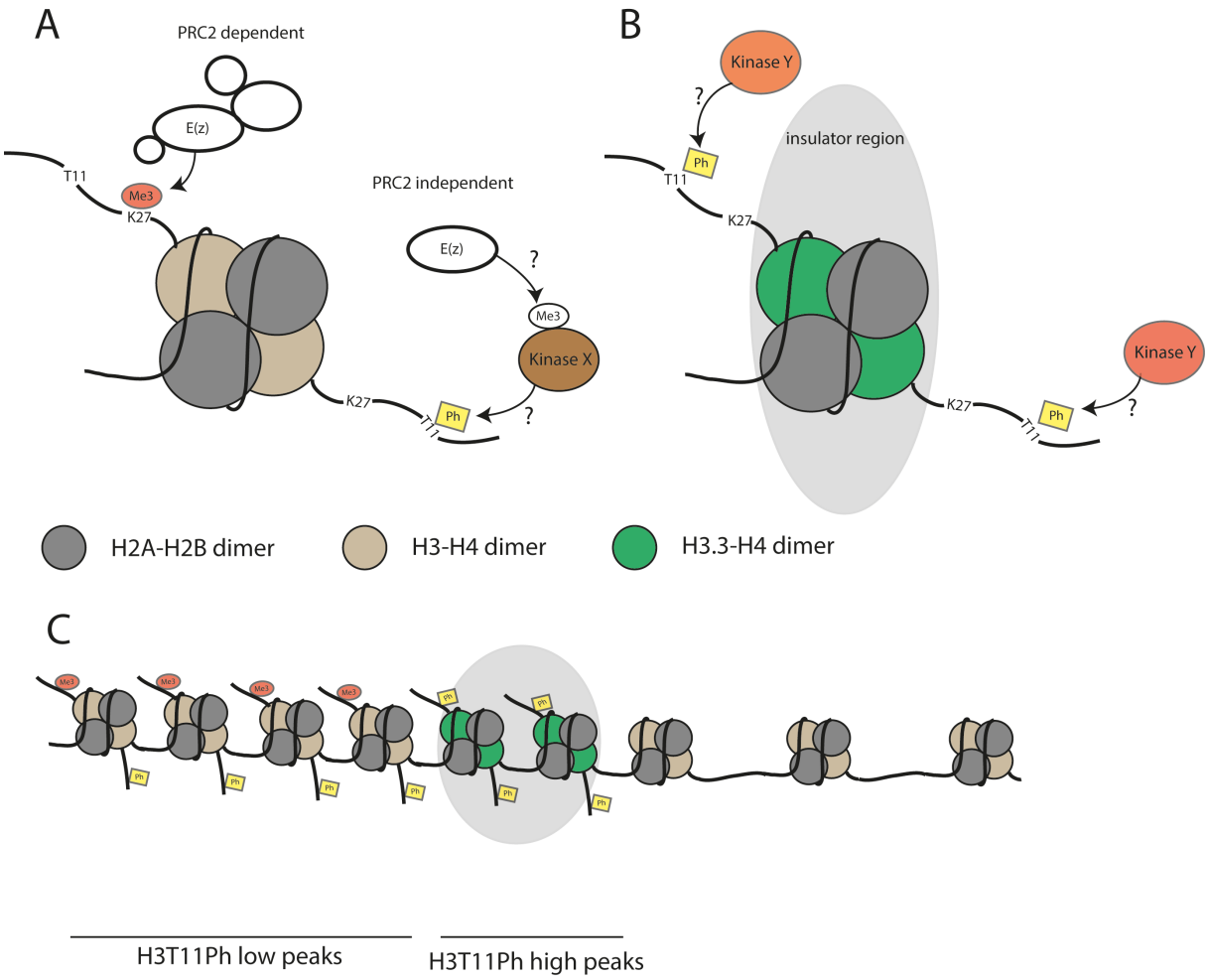

Figure 46: Summary model for a potential barrier function of H3T11ph.
In heterochromatic regions H3K27me3 and H3T11ph overlap which is reflected by the occurence of H3K27me3 and H3T11ph *in trans* on the two histone H3 of one nucleosome. In a PRC2 dependent manner E(z) leads to the trimethylation of H3K27. In a PRC2 independent manner E(z) leads to the activation of a so far unknow Kinase X which leads to the phosphorylation of H3T11. This leads to the overlap of H3K27me3 peaks and H3T11ph low peaks found via ChIP-seq experiments. In border regions of Polycomb chromatin domains the histone variant H3.3 is incorporated into the chromatin thereby replacing the canonical H3. This leads to the depletion of H3K27me3 in insulator regions. Most likely a Kinase Y is recruited to these insulator regions which leads then to the phosphorylation of both H3.3 molecules in a nucleosome establishing a functional barrier for H3K27me3 spreading.

At genomic regions, where H3K27me3 is enriched for the silencing of Polycomb target genes and establishment of heterochromatin, H3T11ph might be enriched only on one of the H3 tails of the nucleosome, which would explain the lower signal inten-

sities (low peaks). It might be possible that E(z) itself is phophorylated and therefore leaves the classical PRC2 complex. E(z) together with other components or on its own then leads to the methylation of a so far unkown kinase (Kinase X in figure 45) which then phosphorylates H3T11ph. This might explain the big overlap of H3T11ph and H3K27me3 peaks and the similarity of their peak shapes. Recently the PRC2 complex purified from human sfh cells was shown to be present in these cells as a dimer (Davidovich, Goodrich, Gooding, & Cech, 2014). It is also possible that the PRC2 complex is present in *D. melanogaster* cells as a dimer. One PRC2 complex might methylate H3K27 and the second PRC2 complex might methylate a kinase that leads then to the phosphorylation of H3T11ph. For a putative methylation of a H3T11 kinase, E(z) does not require the other PRC2 subunits to be functional as a mutation in Su(z)12 does not lead to a reduction of H3T11ph.

At T11ph high peaks this situation appears be different. T11ph high peaks colocalize with a variety of different insulator proteins and is enriched at chromatin borders where H3K27me3 is depleted. It has previously been shown that the canonical histone H3 is displaced by H3.3 at insulator regions providing an explanation for the depletion of H3K27me3 at these genomic areas. T11ph high peaks are most likely enriched on the histone variant H3.3. The kinase for H3.3T11ph gets recruited to these regions via a so far unknown mechanism leading to the phosphorylation of both H3.3 molecules in a nucleosome. It is conceivable that H3.3T11ph at these insulator regions limits the spreading of H3K27me3 through a so far unknown mechanism.

6 References

Ahmad, K., & Henikoff, S. (2002). The histone variant H3.3 marks active chromatin by replication-independent nucleosome assembly. *Mol Cell, 9*(6), 1191-1200.

Akhmanova, A. S., Bindels, P. C., Xu, J., Miedema, K., Kremer, H., & Hennig, W. (1995). Structure and expression of histone H3.3 genes in Drosophila melanogaster and Drosophila hydei. *Genome, 38*(3), 586-600.

Allis. (2007). *Epigenetics*. Cold Spring Harbor, New York: Cold Spring Harbor Laboratory Press.

Ashburner, M. (1989). *Drosophila: A Laboratory Handbook and Manual.* . Cold Spring Harbor: Cold Spring Harbor Laboratory Press.

Ausubel, F. M., R. Brent, R. E. Kingston, D. D. Moore, J. G. Seidman, J. A. Smith, and K. Struhl. (1990). *Current protocols in molecular biology.* New York: Greene Publishing and Wiley-Qnterscience.

Bailey, T., Krajewski, P., Ladunga, I., Lefebvre, C., Li, Q., Liu, T., . . . Zhang, J. (2013). Practical guidelines for the comprehensive analysis of ChIP-seq data. *PLoS Comput Biol, 9*(11), e1003326. doi: 10.1371/journal.pcbi.1003326

Bannister, A. J., & Kouzarides, T. (2011). Regulation of chromatin by histone modifications. *Cell Res, 21*(3), 381-395. doi: 10.1038/cr.2011.22

Bannister, A. J., Schneider, R., Myers, F. A., Thorne, A. W., Crane-Robinson, C., & Kouzarides, T. (2005). Spatial distribution of di- and tri-methyl lysine 36 of histone H3 at active genes. *J Biol Chem, 280*(18), 17732-17736. doi: 10.1074/jbc.M500796200

Bannister, A. J., Zegerman, P., Partridge, J. F., Miska, E. A., Thomas, J. O., Allshire, R. C., & Kouzarides, T. (2001). Selective recognition of methylated lysine 9 on histone H3 by the HP1 chromo domain. *Nature, 410*(6824), 120-124. doi: 10.1038/35065138

Barski, A., Cuddapah, S., Cui, K., Roh, T. Y., Schones, D. E., Wang, Z., . . . Zhao, K. (2007). High-resolution profiling of histone methylations in the human genome. *Cell, 129*(4), 823-837. doi: 10.1016/j.cell.2007.05.009

Bartkuhn, M., Straub, T., Herold, M., Herrmann, M., Rathke, C., Saumweber, H., . . . Renkawitz, R. (2009). Active promoters and insulators are marked by the centrosomal protein 190. *EMBO J, 28*(7), 877-888. doi: 10.1038/emboj.2009.34

Beachy, P. A., Helfand, S. L., & Hogness, D. S. (1985). Segmental distribution of bithorax complex proteins during Drosophila development. *Nature, 313*(6003), 545-551.

Bello, B., Holbro, N., & Reichert, H. (2007). Polycomb group genes are required for neural stem cell survival in postembryonic neurogenesis of Drosophila. *Development, 134*(6), 1091-1099. doi: 10.1242/dev.02793

Berger, S. L. (2007). The complex language of chromatin regulation during transcription. *Nature, 447*(7143), 407-412. doi: 10.1038/nature05915

Bernstein, B. E., Mikkelsen, T. S., Xie, X., Kamal, M., Huebert, D. J., Cuff, J., . . . Lander, E. S. (2006). A bivalent chromatin structure marks key developmental genes in embryonic stem cells. *Cell, 125*(2), 315-326. doi: 10.1016/j.cell.2006.02.041

Birve, A., Sengupta, A. K., Beuchle, D., Larsson, J., Kennison, J. A., Rasmuson-Lestander, A., & Muller, J. (2001). Su(z)12, a novel Drosophila Polycomb

group gene that is conserved in vertebrates and plants. *Development, 128*(17), 3371-3379.

Bischof, J., Maeda, R. K., Hediger, M., Karch, F., & Basler, K. (2007). An optimized transgenesis system for Drosophila using germ-line-specific phiC31 integrases. *Proc Natl Acad Sci U S A, 104*(9), 3312-3317. doi: 10.1073/pnas.0611511104

Bischoff, F. R., Maier, G., Tilz, G., & Ponstingl, H. (1990). A 47-kDa human nuclear protein recognized by antikinetochore autoimmune sera is homologous with the protein encoded by RCC1, a gene implicated in onset of chromosome condensation. *Proc Natl Acad Sci U S A, 87*(21), 8617-8621.

Blankenberg, D., Von Kuster, G., Coraor, N., Ananda, G., Lazarus, R., Mangan, M., . . . Taylor, J. (2010). Galaxy: a web-based genome analysis tool for experimentalists. *Curr Protoc Mol Biol, Chapter 19*, Unit 19 10 11-21. doi: 10.1002/0471142727.mb1910s89

Bonn, S., Zinzen, R. P., Girardot, C., Gustafson, E. H., Perez-Gonzalez, A., Delhomme, N., . . . Furlong, E. E. (2012). Tissue-specific analysis of chromatin state identifies temporal signatures of enhancer activity during embryonic development. *Nat Genet, 44*(2), 148-156. doi: 10.1038/ng.1064

Bonn, S., Zinzen, R. P., Perez-Gonzalez, A., Riddell, A., Gavin, A. C., & Furlong, E. E. (2012). Cell type-specific chromatin immunoprecipitation from multicellular complex samples using BiTS-ChIP. *Nat Protoc, 7*(5), 978-994. doi: 10.1038/nprot.2012.049

Bowman, S. K., Deaton, A. M., Domingues, H., Wang, P. I., Sadreyev, R. I., Kingston, R. E., & Bender, W. (2014). H3K27 modifications define segmental regulatory domains in the Drosophila bithorax complex. *Elife, 3*, e02833. doi: 10.7554/eLife.02833

Boyer, L. A., Plath, K., Zeitlinger, J., Brambrink, T., Medeiros, L. A., Lee, T. I., . . . Jaenisch, R. (2006). Polycomb complexes repress developmental regulators in murine embryonic stem cells. *Nature, 441*(7091), 349-353. doi: 10.1038/nature04733

Bushey, A. M., Dorman, E. R., & Corces, V. G. (2008). Chromatin insulators: regulatory mechanisms and epigenetic inheritance. *Mol Cell, 32*(1), 1-9. doi: 10.1016/j.molcel.2008.08.017

Busturia, A., & Morata, G. (1988). Ectopic expression of homeotic genes caused by the elimination of the Polycomb gene in Drosophila imaginal epidermis. *Development, 104*(4), 713-720.

Cao, R., Wang, L., Wang, H., Xia, L., Erdjument-Bromage, H., Tempst, P., . . . Zhang, Y. (2002). Role of histone H3 lysine 27 methylation in Polycomb-group silencing. *Science, 298*(5595), 1039-1043. doi: 10.1126/science.1076997

Cao, R., & Zhang, Y. (2004a). The functions of E(Z)/EZH2-mediated methylation of lysine 27 in histone H3. *Curr Opin Genet Dev, 14*(2), 155-164. doi: 10.1016/j.gde.2004.02.001

Cao, R., & Zhang, Y. (2004b). SUZ12 is required for both the histone methyltransferase activity and the silencing function of the EED-EZH2 complex. *Mol Cell, 15*(1), 57-67. doi: 10.1016/j.molcel.2004.06.020

Capelson, M., & Corces, V. G. (2004). Boundary elements and nuclear organization. *Biol Cell, 96*(8), 617-629. doi: 10.1016/j.biolcel.2004.06.004

Casanova, J., Sanchez-Herrero, E., & Morata, G. (1985). Contrabithorax and the control of spatial expression of the bithorax complex genes of Drosophila. *J Embryol Exp Morphol, 90*, 179-196.

Chen, S., Birve, A., & Rasmuson-Lestander, A. (2008). In vivo analysis of Drosophila SU(Z)12 function. *Mol Genet Genomics, 279*(2), 159-170. doi: 10.1007/s00438-007-0304-3

Chen, T., & Dent, S. Y. (2014). Chromatin modifiers and remodellers: regulators of cellular differentiation. *Nat Rev Genet, 15*(2), 93-106. doi: 10.1038/nrg3607

Chen, X., Lu, C., Morillo Prado, J. R., Eun, S. H., & Fuller, M. T. (2011). Sequential changes at differentiation gene promoters as they become active in a stem cell lineage. *Development, 138*(12), 2441-2450. doi: 10.1242/dev.056572

Chou, T. B., & Perrimon, N. (1992). Use of a yeast site-specific recombinase to produce female germline chimeras in Drosophila. *Genetics, 131*(3), 643-653.

Chow, C. M., Georgiou, A., Szutorisz, H., Maia e Silva, A., Pombo, A., Barahona, I., . . . Dillon, N. (2005). Variant histone H3.3 marks promoters of transcriptionally active genes during mammalian cell division. *EMBO Rep, 6*(4), 354-360. doi: 10.1038/sj.embor.7400366

Comet, I., Schuettengruber, B., Sexton, T., & Cavalli, G. (2011). A chromatin insulator driving three-dimensional Polycomb response element (PRE) contacts and Polycomb association with the chromatin fiber. *Proc Natl Acad Sci U S A, 108*(6), 2294-2299. doi: 10.1073/pnas.1002059108

Cuddapah, S., Jothi, R., Schones, D. E., Roh, T. Y., Cui, K., & Zhao, K. (2009). Global analysis of the insulator binding protein CTCF in chromatin barrier regions reveals demarcation of active and repressive domains. *Genome Res, 19*(1), 24-32. doi: 10.1101/gr.082800.108

Czermin, B., Melfi, R., McCabe, D., Seitz, V., Imhof, A., & Pirrotta, V. (2002). Drosophila enhancer of Zeste/ESC complexes have a histone H3 methyltransferase activity that marks chromosomal Polycomb sites. *Cell, 111*(2), 185-196.

Davidovich, C., Goodrich, K. J., Gooding, A. R., & Cech, T. R. (2014). A dimeric state for PRC2. *Nucleic Acids Res, 42*(14), 9236-9248. doi: 10.1093/nar/gku540

de Beco, S., Ziosi, M., & Johnston, L. A. (2012). New frontiers in cell competition. *Dev Dyn, 241*(5), 831-841. doi: 10.1002/dvdy.23783

de Cuevas, M., Lilly, M. A., & Spradling, A. C. (1997). Germline cyst formation in Drosophila. *Annu Rev Genet, 31*, 405-428. doi: 10.1146/annurev.genet.31.1.405

de Wit, E., Braunschweig, U., Greil, F., Bussemaker, H. J., & van Steensel, B. (2008). Global chromatin domain organization of the Drosophila genome. *PLoS Genet, 4*(3), e1000045. doi: 10.1371/journal.pgen.1000045

Diaz, A., Park, K., Lim, D. A., & Song, J. S. (2012). Normalization, bias correction, and peak calling for ChIP-seq. *Stat Appl Genet Mol Biol, 11*(3), Article 9. doi: 10.1515/1544-6115.1750

Dillon, S. C., Zhang, X., Trievel, R. C., & Cheng, X. (2005). The SET-domain protein superfamily: protein lysine methyltransferases. *Genome Biol, 6*(8), 227. doi: 10.1186/gb-2005-6-8-227

Dixon, J. R., Selvaraj, S., Yue, F., Kim, A., Li, Y., Shen, Y., . . . Ren, B. (2012). Topological domains in mammalian genomes identified by analysis of chromatin interactions. *Nature, 485*(7398), 376-380. doi: 10.1038/nature11082

Duncan, I. M. (1982). Polycomblike: a gene that appears to be required for the normal expression of the bithorax and antennapedia gene complexes of Drosophila melanogaster. *Genetics, 102*(1), 49-70.

Eun, S. H., Shi, Z., Cui, K., Zhao, K., & Chen, X. (2014). A non-cell autonomous role of E(z) to prevent germ cells from turning on a somatic cell marker. *Science, 343*(6178), 1513-1516. doi: 10.1126/science.1246514

Faust, C., Schumacher, A., Holdener, B., & Magnuson, T. (1995). The eed mutation disrupts anterior mesoderm production in mice. *Development, 121*(2), 273-285.

Felsenfeld, G., & Groudine, M. (2003). Controlling the double helix. *Nature, 421*(6921), 448-453. doi: 10.1038/nature01411

Feng, J., Liu, T., Qin, B., Zhang, Y., & Liu, X. S. (2012). Identifying ChIP-seq enrichment using MACS. *Nat Protoc, 7*(9), 1728-1740. doi: 10.1038/nprot.2012.101

Feng, J., Liu, T., & Zhang, Y. (2011). Using MACS to identify peaks from ChIP-Seq data. *Curr Protoc Bioinformatics, Chapter 2*, Unit 2 14. doi: 10.1002/0471250953.bi0214s34

Filion, G. J., van Bemmel, J. G., Braunschweig, U., Talhout, W., Kind, J., Ward, L. D., . . . van Steensel, B. (2010). Systematic protein location mapping reveals five principal chromatin types in Drosophila cells. *Cell, 143*(2), 212-224. doi: 10.1016/j.cell.2010.09.009

Finch, J. T., & Klug, A. (1976). Solenoidal model for superstructure in chromatin. *Proc Natl Acad Sci U S A, 73*(6), 1897-1901.

Fretzin, S., Allan, B. D., van Daal, A., & Elgin, S. C. (1991). A Drosophila melanogaster H3.3 cDNA encodes a histone variant identical with the vertebrate H3.3. *Gene, 107*(2), 341-342.

Fuller, M. T., & Spradling, A. C. (2007). Male and female Drosophila germline stem cells: two versions of immortality. *Science, 316*(5823), 402-404. doi: 10.1126/science.1140861

Gan, Q., Schones, D. E., Ho Eun, S., Wei, G., Cui, K., Zhao, K., & Chen, X. (2010). Monovalent and unpoised status of most genes in undifferentiated cell-enriched Drosophila testis. *Genome Biol, 11*(4), R42. doi: 10.1186/gb-2010-11-4-r42

Garcia, B. A., Hake, S. B., Diaz, R. L., Kauer, M., Morris, S. A., Recht, J., . . . Hunt, D. F. (2007). Organismal differences in post-translational modifications in histones H3 and H4. *J Biol Chem, 282*(10), 7641-7655. doi: 10.1074/jbc.M607900200

Gerasimova, T. I., & Corces, V. G. (1998). Polycomb and trithorax group proteins mediate the function of a chromatin insulator. *Cell, 92*(4), 511-521.

Ghavi-Helm, Y., Klein, F. A., Pakozdi, T., Ciglar, L., Noordermeer, D., Huber, W., & Furlong, E. E. (2014). Enhancer loops appear stable during development and are associated with paused polymerase. *Nature, 512*(7512), 96-100. doi: 10.1038/nature13417

Ghirlando, R., Giles, K., Gowher, H., Xiao, T., Xu, Z., Yao, H., & Felsenfeld, G. (2012). Chromatin domains, insulators, and the regulation of gene expression. *Biochim Biophys Acta, 1819*(7), 644-651. doi: 10.1016/j.bbagrm.2012.01.016

Giardine, B., Riemer, C., Hardison, R. C., Burhans, R., Elnitski, L., Shah, P., . . . Nekrutenko, A. (2005). Galaxy: a platform for interactive large-scale genome analysis. *Genome Res, 15*(10), 1451-1455. doi: 10.1101/gr.4086505

Goecks, J., Nekrutenko, A., Taylor, J., & Galaxy, T. (2010). Galaxy: a comprehensive approach for supporting accessible, reproducible, and transparent computational research in the life sciences. *Genome Biol, 11*(8), R86. doi: 10.1186/gb-2010-11-8-r86

Goldberg, A. D., Banaszynski, L. A., Noh, K. M., Lewis, P. W., Elsaesser, S. J., Stadler, S., . . . Allis, C. D. (2010). Distinct factors control histone variant H3.3 localization at specific genomic regions. *Cell, 140*(5), 678-691. doi: 10.1016/j.cell.2010.01.003

Golic, K. G., & Lindquist, S. (1989). The FLP recombinase of yeast catalyzes site-specific recombination in the Drosophila genome. *Cell, 59*(3), 499-509.

Guelen, L., Pagie, L., Brasset, E., Meuleman, W., Faza, M. B., Talhout, W., . . . van Steensel, B. (2008). Domain organization of human chromosomes revealed by mapping of nuclear lamina interactions. *Nature, 453*(7197), 948-951. doi: 10.1038/nature06947

Gunesdogan, U., Jackle, H., & Herzig, A. (2010). A genetic system to assess in vivo the functions of histones and histone modifications in higher eukaryotes. *EMBO Rep, 11*(10), 772-776. doi: 10.1038/embor.2010.124

Gunesdogan, U., Jackle, H., & Herzig, A. (2014). Histone supply regulates S phase timing and cell cycle progression. *Elife, 3*, e02443. doi: 10.7554/eLife.02443

Gunjan, A., & Verreault, A. (2003). A Rad53 kinase-dependent surveillance mechanism that regulates histone protein levels in S. cerevisiae. *Cell, 115*(5), 537-549.

Gurudatta, B. V., & Corces, V. G. (2009). Chromatin insulators: lessons from the fly. *Brief Funct Genomic Proteomic, 8*(4), 276-282. doi: 10.1093/bfgp/elp032

Hake, S. B., Garcia, B. A., Duncan, E. M., Kauer, M., Dellaire, G., Shabanowitz, J., . . . Hunt, D. F. (2006). Expression patterns and post-translational modifications associated with mammalian histone H3 variants. *J Biol Chem, 281*(1), 559-568. doi: 10.1074/jbc.M509266200

Hansen, K. H., Bracken, A. P., Pasini, D., Dietrich, N., Gehani, S. S., Monrad, A., . . . Helin, K. (2008). A model for transmission of the H3K27me3 epigenetic mark. *Nat Cell Biol, 10*(11), 1291-1300. doi: 10.1038/ncb1787

Heintz, N., Sive, H. L., & Roeder, R. G. (1983). Regulation of human histone gene expression: kinetics of accumulation and changes in the rate of synthesis and in the half-lives of individual histone mRNAs during the HeLa cell cycle. *Mol Cell Biol, 3*(4), 539-550.

Henikoff, S., Furuyama, T., & Ahmad, K. (2004). Histone variants, nucleosome assembly and epigenetic inheritance. *Trends Genet, 20*(7), 320-326. doi: 10.1016/j.tig.2004.05.004

Hodl, M., & Basler, K. (2009). Transcription in the absence of histone H3.3. *Curr Biol, 19*(14), 1221-1226. doi: 10.1016/j.cub.2009.05.048

Hodl, M., & Basler, K. (2012). Transcription in the absence of histone H3.2 and H3K4 methylation. *Curr Biol, 22*(23), 2253-2257. doi: 10.1016/j.cub.2012.10.008

Hu, H., Yang, Y., Ji, Q., Zhao, W., Jiang, B., Liu, R., . . . Gong, Y. (2012). CRL4B catalyzes H2AK119 monoubiquitination and coordinates with PRC2 to promote tumorigenesis. *Cancer Cell, 22*(6), 781-795. doi: 10.1016/j.ccr.2012.10.024

Ingham, P. W. (1984). A gene that regulates the bithorax complex differentially in larval and adult cells of Drosophila. *Cell, 37*(3), 815-823.

Iovino, N., Ciabrelli, F., & Cavalli, G. (2013). PRC2 controls Drosophila oocyte cell fate by repressing cell cycle genes. *Dev Cell, 26*(4), 431-439. doi: 10.1016/j.devcel.2013.06.021

Jackson, V. (1978). Studies on histone organization in the nucleosome using formaldehyde as a reversible cross-linking agent. *Cell, 15*(3), 945-954.

Jenuwein, T., & Allis, C. D. (2001). Translating the histone code. *Science, 293*(5532), 1074-1080. doi: 10.1126/science.1063127

Jin, C., Zang, C., Wei, G., Cui, K., Peng, W., Zhao, K., & Felsenfeld, G. (2009). H3.3/H2A.Z double variant-containing nucleosomes mark 'nucleosome-free regions' of active promoters and other regulatory regions. *Nat Genet, 41*(8), 941-945. doi: 10.1038/ng.409

Johnson, D. S., Mortazavi, A., Myers, R. M., & Wold, B. (2007). Genome-wide mapping of in vivo protein-DNA interactions. *Science, 316*(5830), 1497-1502. doi: 10.1126/science.1141319

Jones, R. S., & Gelbart, W. M. (1993). The Drosophila Polycomb-group gene Enhancer of zeste contains a region with sequence similarity to trithorax. *Mol Cell Biol, 13*(10), 6357-6366.

Joshi, P., Carrington, E. A., Wang, L., Ketel, C. S., Miller, E. L., Jones, R. S., & Simon, J. A. (2008). Dominant alleles identify SET domain residues required for histone methyltransferase of Polycomb repressive complex 2. *J Biol Chem, 283*(41), 27757-27766. doi: 10.1074/jbc.M804442200

Kamakaka, R. T., & Biggins, S. (2005). Histone variants: deviants? *Genes Dev, 19*(3), 295-310. doi: 10.1101/gad.1272805

Kaygun, H., & Marzluff, W. F. (2005). Translation termination is involved in histone mRNA degradation when DNA replication is inhibited. *Mol Cell Biol, 25*(16), 6879-6888. doi: 10.1128/MCB.25.16.6879-6888.2005

Ketel, C. S., Andersen, E. F., Vargas, M. L., Suh, J., Strome, S., & Simon, J. A. (2005). Subunit contributions to histone methyltransferase activities of fly and worm polycomb group complexes. *Mol Cell Biol, 25*(16), 6857-6868. doi: 10.1128/MCB.25.16.6857-6868.2005

Kharchenko, P. V., Alekseyenko, A. A., Schwartz, Y. B., Minoda, A., Riddle, N. C., Ernst, J., . . . Park, P. J. (2011). Comprehensive analysis of the chromatin landscape in Drosophila melanogaster. *Nature, 471*(7339), 480-485. doi: 10.1038/nature09725

Kim, J. Y., Banerjee, T., Vinckevicius, A., Luo, Q., Parker, J. B., Baker, M. R., . . . Chakravarti, D. (2014). A role for WDR5 in integrating threonine 11 phosphorylation to lysine 4 methylation on histone H3 during androgen signaling and in prostate cancer. *Mol Cell, 54*(4), 613-625. doi: 10.1016/j.molcel.2014.03.043

Kirilly, D., & Xie, T. (2007). The Drosophila ovary: an active stem cell community. *Cell Res, 17*(1), 15-25. doi: 10.1038/sj.cr.7310123

Klein, T. (2001). Wing disc development in the fly: the early stages. *Curr Opin Genet Dev, 11*(4), 470-475.

Klymenko, T., Papp, B., Fischle, W., Kocher, T., Schelder, M., Fritsch, C., . . . Muller, J. (2006). A Polycomb group protein complex with sequence-specific DNA-binding and selective methyl-lysine-binding activities. *Genes Dev, 20*(9), 1110-1122. doi: 10.1101/gad.377406

Kornberg, R. D. (1974). Chromatin structure: a repeating unit of histones and DNA. *Science, 184*(4139), 868-871.

Kouzarides, T. (2007). Chromatin modifications and their function. *Cell, 128*(4), 693-705. doi: 10.1016/j.cell.2007.02.005

Kuzmichev, A., Nishioka, K., Erdjument-Bromage, H., Tempst, P., & Reinberg, D. (2002). Histone methyltransferase activity associated with a human multiprotein complex containing the Enhancer of Zeste protein. *Genes Dev, 16*(22), 2893-2905. doi: 10.1101/gad.1035902

Kyrchanova, O., & Georgiev, P. (2014). Chromatin insulators and long-distance interactions in Drosophila. *FEBS Lett, 588*(1), 8-14. doi: 10.1016/j.febslet.2013.10.039

Lachner, M., O'Carroll, D., Rea, S., Mechtler, K., & Jenuwein, T. (2001). Methylation of histone H3 lysine 9 creates a binding site for HP1 proteins. *Nature, 410*(6824), 116-120. doi: 10.1038/35065132

Lagarou, A., Mohd-Sarip, A., Moshkin, Y. M., Chalkley, G. E., Bezstarosti, K., Demmers, J. A., & Verrijzer, C. P. (2008). dKDM2 couples histone H2A ubiquitylation to histone H3 demethylation during Polycomb group silencing. *Genes Dev, 22*(20), 2799-2810. doi: 10.1101/gad.484208

Landt, S. G., Marinov, G. K., Kundaje, A., Kheradpour, P., Pauli, F., Batzoglou, S., . . . Snyder, M. (2012). ChIP-seq guidelines and practices of the ENCODE and modENCODE consortia. *Genome Res, 22*(9), 1813-1831. doi: 10.1101/gr.136184.111

Langmead, B., Trapnell, C., Pop, M., & Salzberg, S. L. (2009). Ultrafast and memory-efficient alignment of short DNA sequences to the human genome. *Genome Biol, 10*(3), R25. doi: 10.1186/gb-2009-10-3-r25

Lawrence, P. A., & Morata, G. (1977). The early development of mesothoracic compartments in Drosophila. An analysis of cell lineage and fate mapping and an assessment of methods. *Dev Biol, 56*(1), 40-51.

Lewis, E. B. (1978). A gene complex controlling segmentation in Drosophila. *Nature, 276*(5688), 565-570.

Lhoumaud, P., Hennion, M., Gamot, A., Cuddapah, S., Queille, S., Liang, J., . . . Cuvier, O. (2014). Insulators recruit histone methyltransferase dMes4 to regulate chromatin of flanking genes. *EMBO J, 33*(14), 1599-1613. doi: 10.15252/embj.201385965

Li, G., Sudlow, G., & Belmont, A. S. (1998). Interphase cell cycle dynamics of a late-replicating, heterochromatic homogeneously staining region: precise choreography of condensation/decondensation and nuclear positioning. *J Cell Biol, 140*(5), 975-989.

Li, S., Swanson, S. K., Gogol, M., Florens, L., Washburn, M. P., Workman, J. L., & Suganuma, T. (2015). Serine and SAM Responsive Complex SESAME Regulates Histone Modification Crosstalk by Sensing Cellular Metabolism. *Mol Cell, 60*(3), 408-421. doi: 10.1016/j.molcel.2015.09.024

Lin, H., & Spradling, A. C. (1993). Germline stem cell division and egg chamber development in transplanted Drosophila germaria. *Dev Biol, 159*(1), 140-152. doi: 10.1006/dbio.1993.1228

Lin, H., Yue, L., & Spradling, A. C. (1994). The Drosophila fusome, a germline-specific organelle, contains membrane skeletal proteins and functions in cyst formation. *Development, 120*(4), 947-956.

Liu, N., Han, H., & Lasko, P. (2009). Vasa promotes Drosophila germline stem cell differentiation by activating mei-P26 translation by directly interacting with a (U)-rich motif in its 3' UTR. *Genes Dev, 23*(23), 2742-2752. doi: 10.1101/gad.1820709

Luger, K., Rechsteiner, T. J., Flaus, A. J., Waye, M. M., & Richmond, T. J. (1997). Characterization of nucleosome core particles containing histone proteins made in bacteria. *J Mol Biol, 272*(3), 301-311. doi: 10.1006/jmbi.1997.1235

MacAlpine, H. K., Gordan, R., Powell, S. K., Hartemink, A. J., & MacAlpine, D. M. (2010). Drosophila ORC localizes to open chromatin and marks sites of

cohesin complex loading. *Genome Res, 20*(2), 201-211. doi: 10.1101/gr.097873.109

Malik, H. S., & Henikoff, S. (2003). Phylogenomics of the nucleosome. *Nat Struct Biol, 10*(11), 882-891. doi: 10.1038/nsb996

Margueron, R., Justin, N., Ohno, K., Sharpe, M. L., Son, J., Drury, W. J., 3rd, . . . Gamblin, S. J. (2009). Role of the polycomb protein EED in the propagation of repressive histone marks. *Nature, 461*(7265), 762-767. doi: 10.1038/nature08398

Margueron, R., & Reinberg, D. (2010). Chromatin structure and the inheritance of epigenetic information. *Nat Rev Genet, 11*(4), 285-296. doi: 10.1038/nrg2752

Martin, C., & Zhang, Y. (2005). The diverse functions of histone lysine methylation. *Nat Rev Mol Cell Biol, 6*(11), 838-849. doi: 10.1038/nrm1761

Marzluff, W. F., & Duronio, R. J. (2002). Histone mRNA expression: multiple levels of cell cycle regulation and important developmental consequences. *Curr Opin Cell Biol, 14*(6), 692-699.

Marzluff, W. F., Gongidi, P., Woods, K. R., Jin, J., & Maltais, L. J. (2002). The human and mouse replication-dependent histone genes. *Genomics, 80*(5), 487-498.

Marzluff, W. F., Wagner, E. J., & Duronio, R. J. (2008). Metabolism and regulation of canonical histone mRNAs: life without a poly(A) tail. *Nat Rev Genet, 9*(11), 843-854. doi: 10.1038/nrg2438

Matharu, N. K., & Ahanger, S. H. (2015). Chromatin Insulators and Topological Domains: Adding New Dimensions to 3D Genome Architecture. *Genes (Basel), 6*(3), 790-811. doi: 10.3390/genes6030790

McKittrick, E., Gafken, P. R., Ahmad, K., & Henikoff, S. (2004). Histone H3.3 is enriched in covalent modifications associated with active chromatin. *Proc Natl Acad Sci U S A, 101*(6), 1525-1530. doi: 10.1073/pnas.0308092100

Melnik, S., Deng, B., Papantonis, A., Baboo, S., Carr, I. M., & Cook, P. R. (2011). The proteomes of transcription factories containing RNA polymerases I, II or III. *Nat Methods, 8*(11), 963-968. doi: 10.1038/nmeth.1705

Metzger, E., Yin, N., Wissmann, M., Kunowska, N., Fischer, K., Friedrichs, N., . . . Schule, R. (2008). Phosphorylation of histone H3 at threonine 11 establishes a novel chromatin mark for transcriptional regulation. *Nat Cell Biol, 10*(1), 53-60. doi: 10.1038/ncb1668

Muller, J., & Bienz, M. (1991). Long range repression conferring boundaries of Ultrabithorax expression in the Drosophila embryo. *EMBO J, 10*(11), 3147-3155.

Muller, J., Hart, C. M., Francis, N. J., Vargas, M. L., Sengupta, A., Wild, B., . . . Simon, J. A. (2002). Histone methyltransferase activity of a Drosophila Polycomb group repressor complex. *Cell, 111*(2), 197-208.

Mullis, K., Faloona, F., Scharf, S., Saiki, R., Horn, G., & Erlich, H. (1986). Specific enzymatic amplification of DNA in vitro: the polymerase chain reaction. *Cold Spring Harb Symp Quant Biol, 51 Pt 1*, 263-273.

Muse, G. W., Gilchrist, D. A., Nechaev, S., Shah, R., Parker, J. S., Grissom, S. F., . . . Adelman, K. (2007). RNA polymerase is poised for activation across the genome. *Nat Genet, 39*(12), 1507-1511. doi: 10.1038/ng.2007.21

Nakanishi, S., Sanderson, B. W., Delventhal, K. M., Bradford, W. D., Staehling-Hampton, K., & Shilatifard, A. (2008). A comprehensive library of histone mutants identifies nucleosomal residues required for H3K4 methylation. *Nat Struct Mol Biol, 15*(8), 881-888. doi: 10.1038/nsmb.1454

Negre, N., Brown, C. D., Shah, P. K., Kheradpour, P., Morrison, C. A., Henikoff, J. G., . . . White, K. P. (2010). A comprehensive map of insulator elements for the Drosophila genome. *PLoS Genet, 6*(1), e1000814. doi: 10.1371/journal.pgen.1000814

Nekrasov, M., Wild, B., & Muller, J. (2005). Nucleosome binding and histone methyltransferase activity of Drosophila PRC2. *EMBO Rep, 6*(4), 348-353. doi: 10.1038/sj.embor.7400376

Nystul, T., & Spradling, A. (2007). An epithelial niche in the Drosophila ovary undergoes long-range stem cell replacement. *Cell Stem Cell, 1*(3), 277-285. doi: 10.1016/j.stem.2007.07.009

Nystul, T., & Spradling, A. (2010). Regulation of epithelial stem cell replacement and follicle formation in the Drosophila ovary. *Genetics, 184*(2), 503-515. doi: 10.1534/genetics.109.109538

O'Carroll, D., Erhardt, S., Pagani, M., Barton, S. C., Surani, M. A., & Jenuwein, T. (2001). The polycomb-group gene Ezh2 is required for early mouse development. *Mol Cell Biol, 21*(13), 4330-4336. doi: 10.1128/MCB.21.13.4330-4336.2001

O'Meara, M. M., & Simon, J. A. (2012). Inner workings and regulatory inputs that control Polycomb repressive complex 2. *Chromosoma, 121*(3), 221-234. doi: 10.1007/s00412-012-0361-1

Olins, D. E., & Olins, A. L. (2003). Chromatin history: our view from the bridge. *Nat Rev Mol Cell Biol, 4*(10), 809-814. doi: 10.1038/nrm1225

Oliver, D., Sheehan, B., South, H., Akbari, O., & Pai, C. Y. (2010). The chromosomal association/dissociation of the chromatin insulator protein Cp190 of Drosophila melanogaster is mediated by the BTB/POZ domain and two acidic regions. *BMC Cell Biol, 11*, 101. doi: 10.1186/1471-2121-11-101

Palmer, D. K., O'Day, K., Trong, H. L., Charbonneau, H., & Margolis, R. L. (1991). Purification of the centromere-specific protein CENP-A and demonstration that it is a distinctive histone. *Proc Natl Acad Sci U S A, 88*(9), 3734-3738.

Pasini, D., Bracken, A. P., Jensen, M. R., Lazzerini Denchi, E., & Helin, K. (2004). Suz12 is essential for mouse development and for EZH2 histone methyltransferase activity. *EMBO J, 23*(20), 4061-4071. doi: 10.1038/sj.emboj.7600402

Pengelly, A. R., Copur, O., Jackle, H., Herzig, A., & Muller, J. (2013). A histone mutant reproduces the phenotype caused by loss of histone-modifying factor Polycomb. *Science, 339*(6120), 698-699. doi: 10.1126/science.1231382

Pettitt, J., Crombie, C., Schumperli, D., & Muller, B. (2002). The Caenorhabditis elegans histone hairpin-binding protein is required for core histone gene expression and is essential for embryonic and postembryonic cell division. *J Cell Sci, 115*(Pt 4), 857-866.

Pirrotta, V., & Li, H. B. (2012). A view of nuclear Polycomb bodies. *Curr Opin Genet Dev, 22*(2), 101-109. doi: 10.1016/j.gde.2011.11.004

Plumb, M., Stein, J., & Stein, G. (1983). Coordinate regulation of multiple histone mRNAs during the cell cycle in HeLa cells. *Nucleic Acids Res, 11*(8), 2391-2410.

Ramakrishnan, V., Finch, J. T., Graziano, V., Lee, P. L., & Sweet, R. M. (1993). Crystal structure of globular domain of histone H5 and its implications for nucleosome binding. *Nature, 362*(6417), 219-223. doi: 10.1038/362219a0

Rea, S., Eisenhaber, F., O'Carroll, D., Strahl, B. D., Sun, Z. W., Schmid, M., . . . Jenuwein, T. (2000). Regulation of chromatin structure by site-specific histone H3 methyltransferases. *Nature, 406*(6796), 593-599. doi: 10.1038/35020506

Reik, W. (2007). Stability and flexibility of epigenetic gene regulation in mammalian development. *Nature, 447*(7143), 425-432. doi: 10.1038/nature05918

Robbins, E., & Borun, T. W. (1967). The cytoplasmic synthesis of histones in hela cells and its temporal relationship to DNA replication. *Proc Natl Acad Sci U S A, 57*(2), 409-416.

Robertson, G., Hirst, M., Bainbridge, M., Bilenky, M., Zhao, Y., Zeng, T., . . . Jones, S. (2007). Genome-wide profiles of STAT1 DNA association using chromatin immunoprecipitation and massively parallel sequencing. *Nat Methods, 4*(8), 651-657. doi: 10.1038/nmeth1068

Rozen, S., & Skaletsky, H. (2000). Primer3 on the WWW for general users and for biologist programmers. *Methods Mol Biol, 132*, 365-386.

Rugg-Gunn, P. J., Cox, B. J., Ralston, A., & Rossant, J. (2010). Distinct histone modifications in stem cell lines and tissue lineages from the early mouse embryo. *Proc Natl Acad Sci U S A, 107*(24), 10783-10790. doi: 10.1073/pnas.0914507107

Sakai, A., Schwartz, B. E., Goldstein, S., & Ahmad, K. (2009). Transcriptional and developmental functions of the H3.3 histone variant in Drosophila. *Curr Biol, 19*(21), 1816-1820. doi: 10.1016/j.cub.2009.09.021

Sarma, K., & Reinberg, D. (2005). Histone variants meet their match. *Nat Rev Mol Cell Biol, 6*(2), 139-149. doi: 10.1038/nrm1567

Saurin, A. J., Shao, Z., Erdjument-Bromage, H., Tempst, P., & Kingston, R. E. (2001). A Drosophila Polycomb group complex includes Zeste and dTAFII proteins. *Nature, 412*(6847), 655-660. doi: 10.1038/35088096

Schuettengruber, B., Chourrout, D., Vervoort, M., Leblanc, B., & Cavalli, G. (2007). Genome regulation by polycomb and trithorax proteins. *Cell, 128*(4), 735-745. doi: 10.1016/j.cell.2007.02.009

Schuettengruber, B., Ganapathi, M., Leblanc, B., Portoso, M., Jaschek, R., Tolhuis, B., . . . Cavalli, G. (2009). Functional anatomy of polycomb and trithorax chromatin landscapes in Drosophila embryos. *PLoS Biol, 7*(1), e13. doi: 10.1371/journal.pbio.1000013

Schulz, R. A., Cherbas, L., & Cherbas, P. (1986). Alternative splicing generates two distinct Eip28/29 gene transcripts in Drosophila Kc cells. *Proc Natl Acad Sci U S A, 83*(24), 9428-9432.

Schwartz, B. E., & Ahmad, K. (2005). Transcriptional activation triggers deposition and removal of the histone variant H3.3. *Genes Dev, 19*(7), 804-814. doi: 10.1101/gad.1259805

Schwartz, Y. B., & Pirrotta, V. (2007). Polycomb silencing mechanisms and the management of genomic programmes. *Nat Rev Genet, 8*(1), 9-22. doi: 10.1038/nrg1981

Sexton, T., Yaffe, E., Kenigsberg, E., Bantignies, F., Leblanc, B., Hoichman, M., . . . Cavalli, G. (2012). Three-dimensional folding and functional organization principles of the Drosophila genome. *Cell, 148*(3), 458-472. doi: 10.1016/j.cell.2012.01.010

Shogren-Knaak, M., Ishii, H., Sun, J. M., Pazin, M. J., Davie, J. R., & Peterson, C. L. (2006). Histone H4-K16 acetylation controls chromatin structure and protein interactions. *Science, 311*(5762), 844-847. doi: 10.1126/science.1124000

Simon, J., Chiang, A., Bender, W., Shimell, M. J., & O'Connor, M. (1993). Elements of the Drosophila bithorax complex that mediate repression by Polycomb group products. *Dev Biol, 158*(1), 131-144. doi: 10.1006/dbio.1993.1174

Simon, J. A., & Kingston, R. E. (2009). Mechanisms of polycomb gene silencing: knowns and unknowns. *Nat Rev Mol Cell Biol, 10*(10), 697-708. doi: 10.1038/nrm2763

Simpson, R. T. (1978). Structure of the chromatosome, a chromatin particle containing 160 base pairs of DNA and all the histones. *Biochemistry, 17*(25), 5524-5531.

Sittman, D. B., Graves, R. A., & Marzluff, W. F. (1983). Structure of a cluster of mouse histone genes. *Nucleic Acids Res, 11*(19), 6679-6697.

Snow, P. M., Bieber, A. J., & Goodman, C. S. (1989). Fasciclin III: a novel homophilic adhesion molecule in Drosophila. *Cell, 59*(2), 313-323.

Song, X., Wong, M. D., Kawase, E., Xi, R., Ding, B. C., McCarthy, J. J., & Xie, T. (2004). Bmp signals from niche cells directly repress transcription of a differentiation-promoting gene, bag of marbles, in germline stem cells in the Drosophila ovary. *Development, 131*(6), 1353-1364. doi: 10.1242/dev.01026

Struhl, G. (1981). A gene product required for correct initiation of segmental determination in Drosophila. *Nature, 293*(5827), 36-41.

Struhl, G., & Akam, M. (1985). Altered distributions of Ultrabithorax transcripts in extra sex combs mutant embryos of Drosophila. *EMBO J, 4*(12), 3259-3264.

Suka, N., Suka, Y., Carmen, A. A., Wu, J., & Grunstein, M. (2001). Highly specific antibodies determine histone acetylation site usage in yeast heterochromatin and euchromatin. *Mol Cell, 8*(2), 473-479.

Sun, F. L., & Elgin, S. C. (1999). Putting boundaries on silence. *Cell, 99*(5), 459-462.

Tagami, H., Ray-Gallet, D., Almouzni, G., & Nakatani, Y. (2004). Histone H3.1 and H3.3 complexes mediate nucleosome assembly pathways dependent or independent of DNA synthesis. *Cell, 116*(1), 51-61.

Talbert, P. B., & Henikoff, S. (2006). Spreading of silent chromatin: inaction at a distance. *Nat Rev Genet, 7*(10), 793-803. doi: 10.1038/nrg1920

Theodosiou, N. A., & Xu, T. (1998). Use of FLP/FRT system to study Drosophila development. *Methods, 14*(4), 355-365. doi: 10.1006/meth.1998.0591

Thoma, F., Koller, T., & Klug, A. (1979). Involvement of histone H1 in the organization of the nucleosome and of the salt-dependent superstructures of chromatin. *J Cell Biol, 83*(2 Pt 1), 403-427.

Tie, F., Banerjee, R., Stratton, C. A., Prasad-Sinha, J., Stepanik, V., Zlobin, A., . . . Harte, P. J. (2009). CBP-mediated acetylation of histone H3 lysine 27 antagonizes Drosophila Polycomb silencing. *Development, 136*(18), 3131-3141. doi: 10.1242/dev.037127

Tie, F., Furuyama, T., Prasad-Sinha, J., Jane, E., & Harte, P. J. (2001). The Drosophila Polycomb Group proteins ESC and E(Z) are present in a complex containing the histone-binding protein p55 and the histone deacetylase RPD3. *Development, 128*(2), 275-286.

Turner, B. M. (2000). Histone acetylation and an epigenetic code. *Bioessays, 22*(9), 836-845. doi: 10.1002/1521-1878(200009)22:9<836::AID-BIES9>3.0.CO;2-X

Van Bortle, K., Nichols, M. H., Li, L., Ong, C. T., Takenaka, N., Qin, Z. S., & Corces, V. G. (2014). Insulator function and topological domain border strength scale with architectural protein occupancy. *Genome Biol, 15*(6), R82. doi: 10.1186/gb-2014-15-5-r82

Van Bortle, K., Ramos, E., Takenaka, N., Yang, J., Wahi, J. E., & Corces, V. G. (2012). Drosophila CTCF tandemly aligns with other insulator proteins at the borders of H3K27me3 domains. *Genome Res, 22*(11), 2176-2187. doi: 10.1101/gr.136788.111

Van Holde, K. E., Sahasrabuddhe, C. G., & Shaw, B. R. (1974). A model for particulate structure in chromatin. *Nucleic Acids Res, 1*(11), 1579-1586.

Waddington, C. H. (2012). The epigenotype. 1942. *Int J Epidemiol, 41*(1), 10-13. doi: 10.1093/ije/dyr184

Wang, H., Wang, L., Erdjument-Bromage, H., Vidal, M., Tempst, P., Jones, R. S., & Zhang, Y. (2004). Role of histone H2A ubiquitination in Polycomb silencing. *Nature, 431*(7010), 873-878. doi: 10.1038/nature02985

Wang, Z., Zang, C., Rosenfeld, J. A., Schones, D. E., Barski, A., Cuddapah, S., . . . Zhao, K. (2008). Combinatorial patterns of histone acetylations and methylations in the human genome. *Nat Genet, 40*(7), 897-903. doi: 10.1038/ng.154

Wedeen, C., Harding, K., & Levine, M. (1986). Spatial regulation of Antennapedia and bithorax gene expression by the Polycomb locus in Drosophila. *Cell, 44*(5), 739-748.

Weth, O., Paprotka, C., Gunther, K., Schulte, A., Baierl, M., Leers, J., . . . Renkawitz, R. (2014). CTCF induces histone variant incorporation, erases the H3K27me3 histone mark and opens chromatin. *Nucleic Acids Res, 42*(19), 11941-11951. doi: 10.1093/nar/gku937

White, R. A., & Wilcox, M. (1985). Distribution of Ultrabithorax proteins in Drosophila. *EMBO J, 4*(8), 2035-2043.

Wirbelauer, C., Bell, O., & Schubeler, D. (2005). Variant histone H3.3 is deposited at sites of nucleosomal displacement throughout transcribed genes while active histone modifications show a promoter-proximal bias. *Genes Dev, 19*(15), 1761-1766. doi: 10.1101/gad.347705

Wirz, J., Fessler, L. I., & Gehring, W. J. (1986). Localization of the Antennapedia protein in Drosophila embryos and imaginal discs. *EMBO J, 5*(12), 3327-3334.

Wu, R. S., & Bonner, W. M. (1985). Mechanism for differential sensitivity of the chromosome and growth cycles of mammalian cells to the rate of protein synthesis. *Mol Cell Biol, 5*(11), 2959-2966.

Xie, T., & Spradling, A. C. (1998). decapentaplegic is essential for the maintenance and division of germline stem cells in the Drosophila ovary. *Cell, 94*(2), 251-260.

Xu, K., Wu, Z. J., Groner, A. C., He, H. H., Cai, C., Lis, R. T., . . . Brown, M. (2012). EZH2 oncogenic activity in castration-resistant prostate cancer cells is Polycomb-independent. *Science, 338*(6113), 1465-1469. doi: 10.1126/science.1227604

Yamashita, Y. M. (2010). Cell adhesion in regulation of asymmetric stem cell division. *Curr Opin Cell Biol, 22*(5), 605-610. doi: 10.1016/j.ceb.2010.07.009

Yanagawa, S., Lee, J. S., & Ishimoto, A. (1998). Identification and characterization of a novel line of Drosophila Schneider S2 cells that respond to wingless signaling. *J Biol Chem, 273*(48), 32353-32359.

Yung, P. Y., Stuetzer, A., Fischle, W., Martinez, A. M., & Cavalli, G. (2015). Histone H3 Serine 28 Is Essential for Efficient Polycomb-Mediated Gene Repression in Drosophila. *Cell Rep, 11*(9), 1437-1445. doi: 10.1016/j.celrep.2015.04.055

Zeitlinger, J., Stark, A., Kellis, M., Hong, J. W., Nechaev, S., Adelman, K., . . . Young, R. A. (2007). RNA polymerase stalling at developmental control genes in the

Drosophila melanogaster embryo. *Nat Genet, 39*(12), 1512-1516. doi: 10.1038/ng.2007.26

Zhai, B., Villen, J., Beausoleil, S. A., Mintseris, J., & Gygi, S. P. (2008). Phosphoproteome analysis of Drosophila melanogaster embryos. *J Proteome Res, 7*(4), 1675-1682. doi: 10.1021/pr700696a

Zhang, Y., Liu, T., Meyer, C. A., Eeckhoute, J., Johnson, D. S., Bernstein, B. E., . . . Liu, X. S. (2008). Model-based analysis of ChIP-Seq (MACS). *Genome Biol, 9*(9), R137. doi: 10.1186/gb-2008-9-9-r137

Zhou, Y. B., Gerchman, S. E., Ramakrishnan, V., Travers, A., & Muyldermans, S. (1998). Position and orientation of the globular domain of linker histone H5 on the nucleosome. *Nature, 395*(6700), 402-405. doi: 10.1038/26521

7 Appendix

Abbreviations

Δ	deletion
A	
Abd-A	Abdominal-A
Abd-B	Abdominal-B
Antp	Antennapedia
attB	attachment site B
attP	attachment site P
B	
BDGP	Berkeley Drosophila Genome Project
Beaf	Boundary element-associated factor
bp	base pairs
C	
Caf1	Chromatin assembly factor 1
CB	cystoblast
CC	cap cells
C.elegans	*Caenorhabditis elegans*
CENP-A	Centromere Protein A
CTCF	corrected total cell fluorescence
ChIP	Chromatin Immunoprecipitation
CP190	Centrosomal protein 190kD
D	
DAPI	4′,6-Diamidin-2-phenylindol
D. melanogaster	*Drosophila melanogaster*
DMSO	Dimethylsulfoxide
DNA	Desoxyribonuclein acid
dNTPs	Deoxynucleotide
dsRNA	double stranded RNA

E

E. coli	Escherichia *coli*
ES	embryonic stem cells
ESC	extra sex combs
E(z)	Enhancer of zeste

F

Fas-3	Fasciclin-3
FBS	fetal bovine serum
FSC	follicle stem cell
FC	follicle cell
Flp	flipase
FRT	flipase recognition target

G

Gapdh1	Glyceraldehyde 3 phosphate dehydrogenase 1
GC	guanine/cytosine
GFP	green fluorescent protein
GU	gene unit
GS	goat serum
GSC	germline stem cell

H

His^{C}	Histone complex deletion
His-GU	histone gene unit
HMTase	histone methyltransferase
HP1	heterochromatin protein 1
HRP	horseradish peroxidase
HTS	hu-li tai shao
H3K27	lysine 27 of histone H3
H3K27R	alteration of lysine at position 27 to arginine
H3T11	threonine 11 of histone H3
H3T11A	alteration of threonine at position 11 to alanine

I

IP	immunoprecipitation

M

MACS	Model-based Analysis of Chip Seq
MBT	malignant brain tumor
mRNA	messenger RNA
modENCODE	Model organism Encyclopedia of DNA Elements
Mod(mdg4)	modifier of mdg4
MPI	Max-Planck Institute

O

ON	over night
Opa	odd-paired
ORC	origin recognition complex

P

PAGE	Polyacrylamide gel electrophoresis
Pc	Polycomb
PcG	Polycomb-group
PCR	polymerase chain reaction
PFA	paraformaldehyde
Ph	Polyhomeotic
PhoRC	Pho repressive complex
PKN1	protein kinase C related kinase 1
PMSF	Phenylmethylsulfonyl fluoride
Pol II	Polymerase II
PRC1	Polycomb repressive complex 1
PRC2	Polycomb repressive complex 2
PRE	Polycomb response element
Psc	Posterior sex combs
PTMs	posttranslational modifications

Q

QC	quality control
qPCR	quantitative PCR

R

RNA	ribonucleic acid
RNase	ribonuclease
RT	room temperature

S

S2R+	Schneider's line 2
SAM	S-adenosyl-L-methionine
SAP	shrimp alkaline phosphatase
Scr	Sex combs reduced
SDS	sodium dodecyl sulphate
Su(Hw)	Suppressor of hairy wings
Su(z)12	Suppressor of zeste 12

T

TADs	Topologically associated domains
Taq	*Thermus aquaticus*
TF	terminal filament
trxG	Trithorax-group
TSS	transcription start site

U

Ubx	Ultrabithorax
UV	ultraviolet

W

WDR5	WD reapeat containing protein 5
Wt	wildtype

List of figures

List of tables

Danksagung

Zu allererst möchte ich mich für die Betreuung bei Dr. Alf Herzig bedanken. Alf, du hast in diesen fünf Jahren immer an mich und meine Fähigkeiten geglaubt und mich auf meinem Weg fortwährend motiviert. Ohne deine unzähligen Ratschläge und Tipps wäre diese Arbeit nie zustande gekommen. Dafür danke ich dir von ganzem Herzen.

Prof. Dr. Sigrist und Prof. Dr. Zychlinsky danke ich für die Begutachtung meiner Arbeit.

Dr. Ho-Ryun Chung und Dr. Alisa Fuchs möchte ich für die Unterstützung bei den ChIP-seq Experimenten danken.

Für das Korrekturlesen meiner Arbeit bedanke ich mich herzlich bei Dr. Holly Stephenson, Julia-Etterich Rätz und Dr. Alf Herzig.

Das erste Jahr meiner Doktorarbeit durfte ich in der Abteilung Molekulare Entwicklungsbiologie von Prof. Herbert Jäckle am MPI für biophysikalische Chemie in Göttingen verbringen. Dafür und für hilfreiche Ratschläge meine Arbeit betreffend möchte ich mich bei Prof. Herbert Jäckle herzlich bedanken.

In meinem Göttinger Labor möchte ich mich bei unserer TA Dajana Meinhardt für ihre Unterstützung und Hilfe bei Fliegenarbeiten und Klonierungen bedanken. Weiterhin gilt mein besonderer Dank Iris Bickmeyer, eine wirklich hilfsbereite Arbeitskollegin die über die Jahre zu einer meiner engsten Freunde geworden ist. Danke Iri, ich hab dich lieb!

Den Rest meiner Doktorarbeit habe ich am MPI für Infektionsbiologie in Berlin in der Abteilung Molekulare Mikrobiologie von Prof. Arturo Zychlinsky verbracht. Zunächst möchte ich mich bei Prof. Zychlinsky dafür bedanken, dass ich meine Arbeit in seinem Labor fortführen durfte. Ich wurde von ihm und seiner Arbeitsgruppe herzlich und interessiert empfangen. Dafür möchte ich euch allen danken. Besonderer Dank gilt Viola, Soo und Yvonne, die mir immer den Rücken freigehalten haben und bei allen Fragen und Wünschen für mich da sind.

Zuletzt möchte ich mich bei meiner Familie bedanken. Hier gilt ganz besonderer Dank meiner lieben Schwester. Sie ist der Mensch, auf den ich mich in jeder Lebenslage verlassen kann und die mich in allem was ich mache bedingungslos unterstützt. Danne, ich weiß wie besonders unsere Verbindung ist und ich bin jeden Tag dankbar dafür.

Der Lebenslauf ist in der Online-Version aus Gründen des Datenschutzes nicht enthalten

Der Lebenslauf ist in der Online-Version aus Gründen des Datenschutzes nicht enthalten

Eidesstattliche Erklärung

Hiermit erkläre ich, Katharina Kawall, die vorliegende Arbeit selbstständig und nur mit den angegebenen Quellen und Hilfsmitteln erstellt zu haben.

Berlin, den 26.01.2016